2011

DESIGN, SYNTHESIS AND CHARACTERIZATION OF PEPTIDE MIMICS OF HYALURONAN AS MOLECULAR IMAGING PROBES TARGETING RHAMM EXPRESSING CANCER CELLS

Kenneth Virgel N. Esguerra

DESIGN, SYNTHESIS AND CHARACTERIZATION OF PEPTIDE MIMICS OF HYALURONAN AS MOLECULAR IMAGING PROBES TARGETING RHAMM EXPRESSING CANCER CELLS

Spine title: Design, Synthesis and Characterization of Peptide Mimics of Hyaluronan

(Thesis format: Monograph)

By

Kenneth Virgel N. Esguerra

Graduate Program in Chemistry
In collaboration with Molecular Imaging

A thesis submitted in partial fulfillment
of the requirements for the degree of
Master of Science

The School of Graduate and Postdoctoral Studies
The University of Western Ontario
London, Ontario, Canada

THE UNIVERSITY OF WESTERN ONTARIO
SCHOOL OF GRADUATE AND POSTDOCTORAL STUDIES

CERTIFICATE OF EXAMINATION

Supervisor:	Examiners:
Dr. Leonard G. Luyt	Dr. Robert Hudson
	Dr. Mark Workentin
	Dr. Nathalie Bérubé

The thesis by

Kenneth Virgel N. Esguerra

entitled:

Design, Synthesis and Characterization of Peptide Mimics of Hyaluronan as Molecular Imaging Probes Targeting Rhamm Expressing Cancer Cells

is accepted in partial fulfilment of the
requirements for the degree of
Master of Science

Date_____

_____
Chair of the Thesis Examination Board

Abstract

Receptor for hyaluronan mediated motility (Rhamm), is a extracellular receptor for hyaluronan, which is over-expressed in breast cancer. To develop imaging probes for Rhamm, peptide mimics of hyaluronan (HA) were developed using: (1) screening of combinatorial peptide library, and (2) basic local alignment search tool (BLAST) to elucidate proteins high affinity ligands. Using combinatorial approach, a library consisting of D-peptides was screened and resulted in 15 novel peptides showing micromolar affinities. Through rational-based approach, 17 tubulin-derived peptides were screening using surface plasmon spectroscopy (SPR) and resulted in 6 high affinity ligands with nanomolar affinities. Using enzyme-linked immunosorbent assay (ELISA), candidate peptides from the two approaches showed specificity to the Rhamm's HA binding domain and were able to compete with HA for binding.

Rhenium (I) complexes containing the *fac*-$M(CO)_3^+$ moieties served as surrogates for *fac*-$^{99m}Tc(CO)_3^+$ complexes, which are fundamental in the development of radioactive products for diagnostic applications. Rhenium tricarbonyl complexes incorporating bi- and tridentate bis(1-methylbenzimidazol-2-yl) ligands were developed, synthesized and characterized spectroscopically.

Keywords: Receptor for hyaluronan mediated motility, tubulin carboxy terminal tails, hyaluronan, cancer, molecular imaging, probe design, technetium rhenium tricarbonyl, bis-benzimidazole, benzimidazole.

List of Abbreviations

$^{99m}Tc(CO)_3^+$	Technitium-99m tricarbonyl core
Ahx	Aminohexanoic acid
ANOVA	Analysis of variance
BLAST	Basic local alignment search tool
BSA	Bovine serum albumin
CTT	Carboxy terminal tail
DCM	Dichloromethane
DIPEA	*N,N*-diisopropylethylamine
DMF	Dimethylformide
DMSO	Dimethylsulfoxide
EDAC	1-Ethyl-3-(3-dimethylaminopropyl)carbodiimide
ELISA	Enzyme-linked immunosorbent assay
ER	Endoplasmic reticulum
ESI-MS	Electrospray ionization mass spectrometry
fac	Facial
FBS	Fetal bovine serum
FITC	Fluorescein isothiocynate
FluoSpheres	Fluorescent beads
Fmoc	Fluorenylmethyloxycarbonyl
GST	Glutathione S-transferase
GST	Gluthathione S-transferase
HA	Hyaluronan
HBTU	*O*-Benzotriazole-*N,N,N',N'*-tetramethyluroniumhexafluoro-phosphate
HRMS	High-resolution mass spectrometry
J	Coupling constant
K_D	Dissociation constant
K_{OFF}	Dissociation rate constant
K_{ON}	Association rate constant
LC-MS	Liquid chromatography – mass spectrometry
MALDI-TOF	Matrix-assisted laser desorption/ionization – time of flight
MAPs	Microtubule associated proteins
ModFluoSpheres	Peptide-modified fluorescent beads
nBuLi	*n*-butyllithium
NMR	Nuclear magnetic resonance
N-term	Amino terminus
ppm	Parts per million
Re	Rhenium
$Re(CO)_3^+$	Rhenium tricarbonyl core
Rhamm	Receptor for hyaluronan mediated motility

ROI	Region of interest
RP-HPLC	Reverse-phase high pressure liquid chromatography
SPR	Surface Plasmon Resonance
Sulfo-NHS	*N*-hydroxysulfosuccinimide
TBST	Tris-buffered saline tween-20
TFA	Trifluoroacetic acid
THF	Tetrahydrofuran
TIPS	Triisopropylsilane
UV-Vis	Ultraviolet-Visible
α	Alpha
β	Beta
γ	Gamma

Co-Authorship Statement

This project was completed in collaboration with the laboratories of Dr. Eva A. Turley and Dr. John D. Lewis in the London Regional Cancer Program at London Health Sciences Centre. ELISA binding and cellular fluorescence assays were done by Natalia Akentieva and Jing Zhang (Turley Lab); however all data processing and statistical analysis was done solely by me. Screening of peptides using Surface Plasmon Resonance Spectroscopy (SPR) was performed by BioRad Laboratory (Hamilton, Ontario, CA). SPR binding assay experiments were performed by the Lewis Laboratory (Choi-Fong Cho); however, I performed all reagent preparations, data processing and calculations. Finally, the concept of using synthetic tubulin carboxy terminal tails as ligands for Rhamm was my invention. I have synthesized all reported compounds and performed all serum stability studies.

Dedicated to

My father, *Arturo S. Esguerra*,

whose memory is always in my thoughts

Acknowledgement

I would like to thank my advisor, Dr. Leonard G. Luyt, whose help, inspiration and guidance while fostering independence of thought and freedom of individual action are instrumental for the completion of this project. His encouragement during times of self-doubt was greatly appreciated. I am also particularly thankful to Dr. Eva A. Turley for her helpful advice, suggestions and discussion throughout my graduate studies.

Special thanks for my fellow lab members, especially Dina Rosita and Babak Behnam Azad, as their input significantly influences my work and have always stood by me during the good times and the bad. I would like to thank my outstanding friends at the LRCP (Niamh, Fong, Hon, Gobi, Monica and Jenny) with whom I had many lengthy and memorable conversations. Finally, I would like to thank my mom Zaida, Rustan (brother) and Ariza (sister) for their unconditional love, encouragement and support.

I would like to acknowledge the financial support provided by the studentship from the Translational Breast Cancer Research Unit at the London Regional Cancer Program.

Table of Contents

List of Figures

List of Tables

List of Schemes

1. Introduction

1.1. Molecular Imaging

Molecular imaging is defined as a discipline aimed at visualization, characterization and measurement of biological processes noninvasively at the molecular and cellular levels in biological systems. Central to this discipline is the development of molecular imaging probes which are used to elucidate and quantify biological processes such as metabolic activity, cell proliferation, apoptosis, receptor occupancy, reporter gene expression, and/or disease progression. Molecular imaging probes are designed to target a particular site within the body and their concentration and/or spectral properties are altered by the specific biological process under investigation. Typically, disease states such as cancer accompany changes in receptor concentration, thus the use of a receptor-specific ligand as a targeting moiety creates a target-directed molecular imaging probe capable of selective imaging of a particular site within the body.

Figure 1: Components of a molecular imaging probe. The label provides a signal to be detected and denotes the type of imaging modality used. The linker distances the targeting entity from the label to allow proper receptor-ligand binding. The use of a spacer has been shown to reduce the steric hindrance that can occur when the targeting entity conjugates to its biological receptor. The targeting entity gives the probe specificity due to its high affinity to a particular biological receptor.

A molecular imaging probe (Figure 1) consists of two main components: (1) the "targeting entity", that is a chemical entity (e.g. small molecule, peptide, protein or

other bio-molecule) specifically tailored to recognize and bind with high affinity to a particular biological receptor and (2) the "label" whose function is to provide a signal for detection. The label can be a light- or near-infrared emitting molecule (e.g. a dye) or a radioisotope. A radioisotope is a molecule, possessing a relatively short half-life, which releases radiation of appropriate energy high enough for detection and low enough to avoid exposure to harmful ionizing radiation. Dyes (or fluorophores), another type of label, are molecules which fluoresce upon the absorption of light at a specific wavelength.

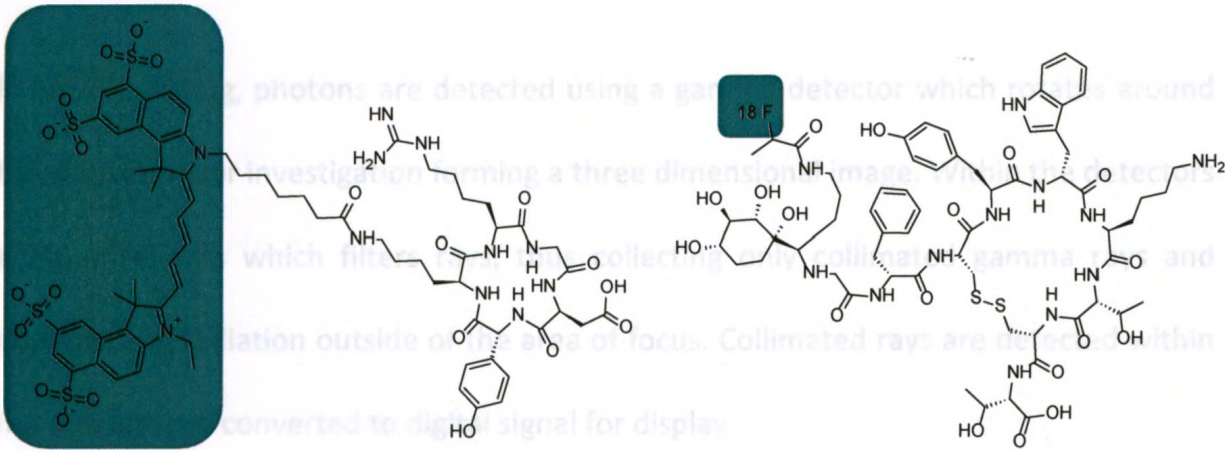

Figure 2: Examples of molecular imaging probes. (A) Structure of c(RGDyK) conjugated to Cy5.5 near-infrared dye. (B) Structure of octreotide labelled with 18F radionuclide, a common isotope for nuclear imaging. Molecular imaging probe labels are boxed in teal.

To date, a large variety of sophisticated imaging probes have been developed by combining various labels and targeting entities.[1] For instance, polypeptide domains containing the R-G-D peptide sequence has been shown to bind to $\alpha_V\beta_3$ receptor, an integrin receptor known to be over expressed on proliferating endothelial cells during angiogenesis and metastasis.[2,3] Cyclic-RGD peptides conjugated to Cy5.5 dye (a type of near-infrared dye) has been shown to image integrin-positive tumours *in vivo* (Figure

2A).[4] Also, octreotide imaging probes (Figure 2B) have been reported to target neuroendocrine tumours and somatostatin receptor positive cancer cells. [5,6]

1.2. Fluorescence and SPECT Imaging

Different imaging modalities are used to monitor molecular imaging probes in biological systems, and typically the label denotes the type of imaging modality used. For instance, probes which are conjugated to a dye generally use fluorescence imaging and probes that utilize radioisotopes uses nuclear imaging such as single photon emission computed tomography (SPECT).

In SPECT imaging, photons are detected using a gamma detector which rotates around the subject under investigation forming a three dimensional image. Within the detectors are parallel slits which filters rays, thus collecting only collimated gamma rays and excludes any radiation outside of the area of focus. Collimated rays are detected within the slits and are converted to digital signal for display.

Another type of imaging modality, called fluorescence imaging, uses fluorophores instead of radionuclides. Dyes are commercially available and come with a variety of activated groups (e.g. NHS-ester activated carboxylates) which are easily incorporated to a compatible prosthetic functional group (e.g. amines for this particular case) within the targeting entity. This type of imaging utilizes a tunable light of a particular wavelength to excite a dye, and detection of the emitted light of specific but longer wavelength.

1.3. Receptor for Hyaluronan Mediated Motility (Rhamm) and Cancer

Hyaluronan (HA), a polysaccharide consisting of dimeric repeats of D-glucuronic acid and *N*-acetylglucosamine, is a glycosaminoglycan essential for proper cell growth, organ structural stability and tissue organization.[7,8] HA affects cellular processes by interacting with receptors on the cell surface. In many cancers of epithelial origin, there is up-regulation of cell-surface HA receptors.[9,10] Furthermore, many of the downstream pathways (e.g. kinase-AKT pathways and Ras-MAPK signaling[11]) following the activation of these receptors are deregulated in cancers, leading to tumor growth, progression and metastasis.[12,13,14] The receptor for hyaluronan mediated motility (Rhamm) is a extracellular HA binding protein that regulates cell proliferation and promotes cell locomotion.[15,16] Rhamm is over-expressed in metastatic cancers (e.g. prostate and breast), and in both acute and chronic leukemia.[17,18,19,20] Rhamm has been implicated in tumour metastasis, in particular, the processes of cell motility and invasion.[21,22,23] Thus, Rhamm could potentially be used as a molecular target for cancer diagnosis.

The HA-binding motif of Rhamm has been identified near the carboxy-terminus, and consists of two basic amino acids flanking a seven amino acid stretch, $B(X)_7B$, in which B is either Lys or Arg and the X_7 contains no acidic residues.[24,25] Synthetic peptides representing this domain inhibit HA binding to full length Rhamm, while peptides representing other parts of the primary sequence fail to inhibit binding.[26] The interaction of HA with Rhamm is believed to be based on ionic contacts between positively charged residues in the protein and negatively charged carboxylate groups on

HA, as well as potential hydrophobic interactions involving lipophilic patches on Rhamm.[27]

1.4. Design of Hyaluronan Mimetic Peptides

Proteins which interact with carbohydrates are attractive drug/imaging probe targets in that they are involved in many biological processes.[28] Protein-sugar interactions can be inhibited by the administration of structurally related carbohydrates, but this approach is strongly hampered by the lack of robust methods for the synthesis of carbohydrates.[29] An alternative method is to use a non-carbohydrate-based scaffold to project the essential functionality that would enable structural resemblance to a particular type of carbohydrate.[27]

Recently, peptides have attracted increasing attention for their use in the design of drugs/targeting agents due to several advantages: (1) peptides show higher specificity for their target at nanomolar concentrations[30]; (2) low toxicity in animal systems; (3) peptides can be easily synthesized and modified structurally to improve their stability against proteolytic degradation, thus increasing half-life in biological systems[30]; and (4) compared to macromolecular targeting agents, peptides are low in molecular weight causing them to have higher tissue and cell permeability.[30]

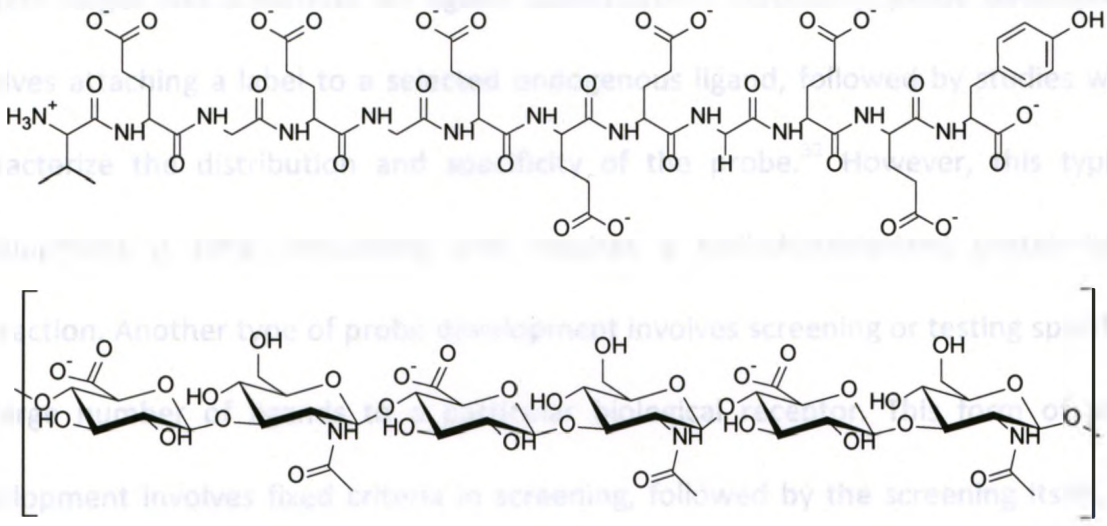

Figure 3: Chemical structure of hyaluronan (bottom) and a putative hyaluronan peptide mimic (top), indicating the carboxylates required for binding to Rhamm.

Carbohydrates display remarkable biological activities, but problems associated with synthesis, degradation and delivery hinders their potential to be used as molecular imaging probes.[31] Thus, identifying peptides that selectively bind to carbohydrate receptors using classical approaches of drug/probe design, could aid in development of chemical entities targeting protein-carbohydrate mediated disease states. In this study, peptides with the same structural features to that of HA, a type of carbohydrate, are created in order to mimic its physio-chemical properties towards Rhamm. For instance, it can be postulated that acidic residues, with the appropriate configurations, strategically placed within a peptide backbone could potentially mimic the carboxylates of HA (Figure 3).

The process of obtaining new targeting entities consists of several steps and may require different technologies for biological characterization (Scheme 1). Typically, designing targeting entities for molecular imaging probes requires a well characterized

protein target and a method for ligand identification. Classically, probe development involves attaching a label to a selected endogenous ligand, followed by studies which characterize the distribution and specificity of the probe.[32] However, this type of development is time consuming and requires a well-characterized protein-ligand interaction. Another type of probe development involves screening or testing specificity of large number of ligands to a particular biological receptor. This form of probe development involves fixed criteria in screening, followed by the screening itself, and then further validation to address potential issues associated with the screening.

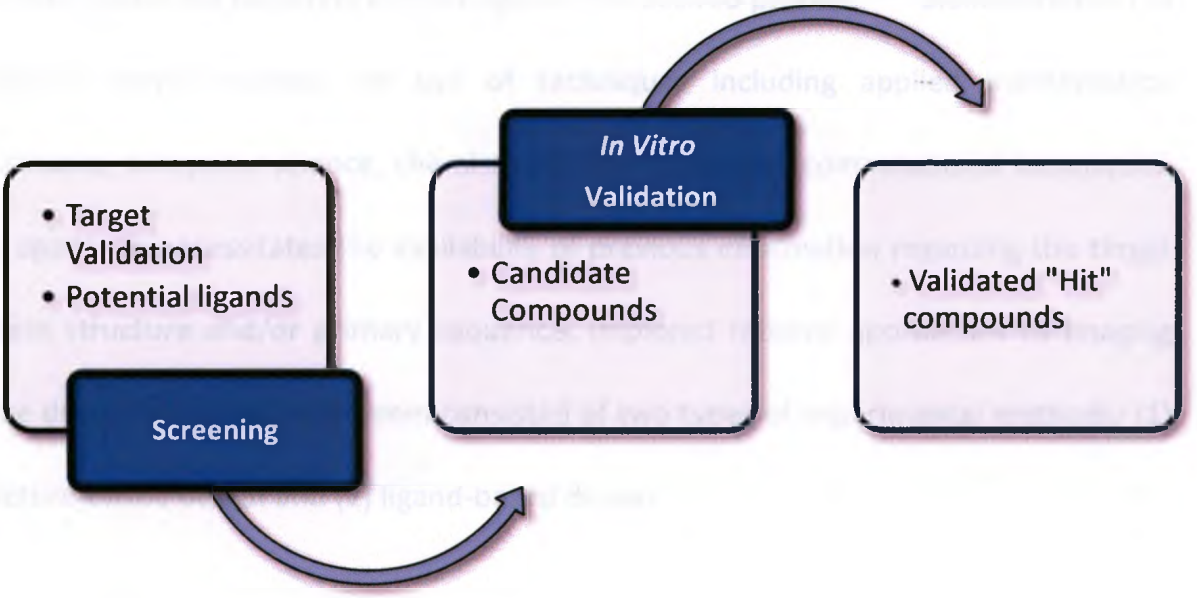

Scheme 1: Initial stages of Imaging probe development.

Despite improvement in the selection of imaging probes, false positives can still arise; and for this reason, those potential compounds identified by the initial screening needs to be confirmed and validated using *in vitro* assays before being considered as "hits". Finally after intensive probe characterization, one or several "hit" compounds showing activity over a certain threshold are obtained.

In designing peptides which mimics the binding of HA, two approaches were undertaken: (1) rational-based design which uses ligand-based and structural-based approaches; and (2) a method utilizing screening of a random combinatorial peptide library. The resulting "hits" from the different method were further characterized using *in vitro* assays.

1.4.1. Rational Approach

Some rational approaches for the design of imaging probe/drug utilizes bioinformatics to predict potential targeting entities against the desired protein.[33,34] Bioinformatics is a discipline which involves the use of techniques including applied mathematics, informatics, computer science, chemistry, biochemistry and computational techniques. This approach necessitates the availability of previous information regarding the target protein structure and/or primary sequence. Implored rational approaches to imaging probe design for targeting Rhamm consisted of two types of experimental methods: (1) structure-based design and (2) ligand-based design.

1.4.1.1. Structure-Based Design

Most structure-based approaches are based on docking calculations, which enables visual inspection of the results leading to a better understanding of the ligand-protein binding process.[35] Recent advances in methods for protein expression and production, computational biochemistry, NMR spectroscopy and X-ray crystallography have led to a significant rise in the number of protein structures solved.[36] Many of these structures are deposited and made publicly accessible in online databases such as Protein Data

Bank (PDB), and currently containing over 47,000 entries and its size is continually increasing annually.[37] Accordingly, using PDB data, it is now possible to generate models from protein cavities to profile similarities against multiple proteins,[38] and dock a single molecule against a many binding sites extracted from the PDB.[39]

However, despite the great number of data within the PDB, the application of structure-based methods in the design of targeting entities for molecular imaging is often limited by the relatively low experimentally-determined structures since most entries are unevenly distributed among the protein members of the main target families of interest. For instance, while enzymes (37%) and nuclear receptors (51%) constitutes most of PDB, membrane spanning receptors (trans-membrane proteins) and recently discovered proteins are almost devoid of structural information.[40]

Aside from having access to prior knowledge, designing imaging probes to a particular protein family requires a method of elucidating compounds with the right moiety which are complementary to the protein cavity of interest.[41] Computed-aided drug/probe design is a research discipline centered on bioinformatics which includes development of digital repositories for the study of chemical relationships, computer programs for designing compounds with interesting physiochemical characteristics, and tools for the systematic assessment of potential compounds.[42] Protein threading or side chain conformation search is a computational method for designing drugs/probes which allows for backbone modelling of a source structure and permits the modelled structure to be compared to structurally conserved proteins with reported crystal structure within

a database.[43,44,45] This could provide the foundation for probe design by providing data which can be modelled in 3D by modeling programs (such as SWISS-MODEL[46], COMPOSER[47], 3D-JIGSAW[48], SegMod/ENCAD[49]). Finally, ligands are placed within the active site and then modified to fill the space available.[50,51] Also, energies of binding, free energies of perturbation and other thermodynamic parameters could be performed using software tools such as DOCK.[52]

A peptide, containing the sequence YDSeYeSe, (NB lower case letters denote amino acids with D-configuration) which showed binding affinity to Rhamm was previously identified by Prestwich using rational based design of a peptide library.[53] Furthermore, Ziebell *et al.* characterized the binding of this molecule by computationally docking it onto a molecular model of Rhamm.[54] In Chapter 1, this model peptide was further developed via characterization by *in vitro* assays, and was conjugated to a metal to create a surrogate probe for nuclear imaging. To this end, the optimal placement of a metal chelator was elucidated, and a metal chelator in the form of *N,N*-bis(quinolinoyl)amine was incorporated to the peptide.

1.4.1.2. Ligand-Based Design

A ligand-based approach utilizes knowledge of the target protein structure and ligands which could potentially bind to the protein of interest. In other words, targeting entities could be developed using information regarding the biological target and what surrogate molecules bind to it; and this in turn may be used as a model to design new molecular entities that interact with the target.

With the advent of bioinformatics, protein function can be elucidated by matching the desired protein's primary sequence to previously reported proteins whose function has been established with experimental evidence. Sequence alignment tools such as BLAST[55] and PSI-BLAST[56] allows for protein sequences to be screened to large online databases (e.g. COGs[57], ProDom[58], Pfam[59], SMART[60], PRINTS[61]) to determine proteins which show high level of sequence similarity and allows evaluation the alignment using sequence comparison parameters (such as substitution matrices, gap penalties, and propensity scales).[62]

Using bioinformatics, functional classifications (i.e. sequence-based classification) of many protein families that share consensus protein sequences were created and had a profound influence on the way novel ligands are discovered. This method of classification allowed identification of conserved binding sites within protein families, which could then be translated into a conservation of architectures of binding sites that enables proper binding.[63] Since protein-protein contacts is mediated by interactions of corresponding binding sites within the two interacting proteins, ligand structures based on the primary sequence of the active site of one interacting protein could be elucidated.[64] This classification scheme implies that a particular class of compound which is active against a particular protein can potentially be active to the entire protein family, even though other family members have different biological function.[65] In other words, a ligand-based approach relies on the principal notion that similar conserved protein sequences (and by extension, similar molecules) exhibit more or less similar properties.[66]

In Chapter 2, ligand-based rational design was employed using sequence homology to a database of known proteins with reported ligands, using the basic local alignment search tool (BLAST) to discover peptides which show high affinity for Rhamm. Structural homology between proteins can be seen as a function of sequence similarities, thus proteins (and protein fragments) which bind to a characteristic sequence motif in another protein that show high homology to the HA binding domain sequence can be used as targeting moiety in probes designed to target Rhamm.

1.4.2. Library-Based Approach

In the past, potential ligands were identified individually using *in vitro* assays towards a single purified target. Now, the advent of combinatorial chemistry and high-throughput screening allows for rapid identification of potential ligands. Combinatorial chemistry allows for increased capacity for synthesizing compounds while high-throughput screening allows for rapid testing of compounds on *in vitro* target-based assay.

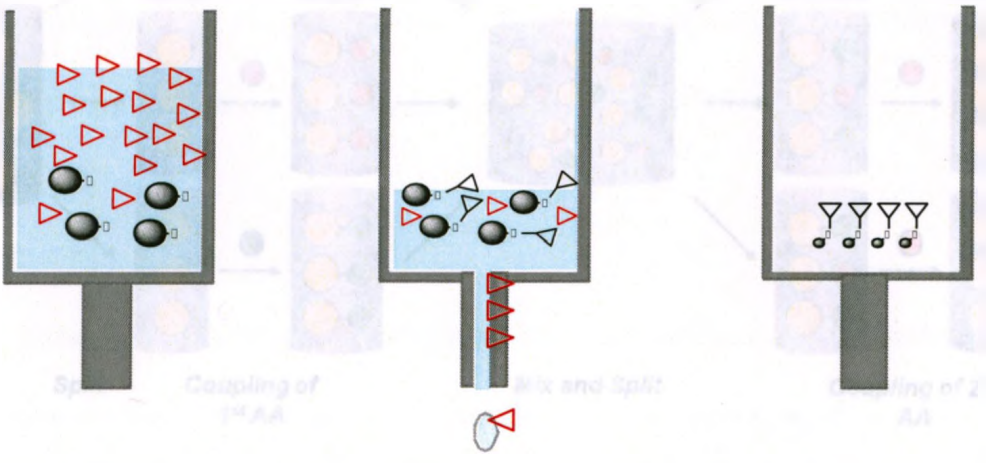

Figure 4: General schematic of solid phase synthesis. Solid supports (denoted by **S**) are allowed to react to large excess of reagents (denoted by ❑) in the first step. Purification of compounds bound to solid support from those in solution is accomplished by simple filtration and multiple washings.

Combinatorial chemistry utilizes parallel synthesis of a large number of compounds in a short amount of time on solid support (Figure 4). In this study, a combinatorial peptide library is utilized to create a pool of peptides. This peptide library is expected to contain a diverse set of small molecules, which have the potential to probe a selected targeted protein. Peptide-based targeting of tumour-associated proteins is particularly attractive in molecular imaging because high affinity sequences can easily be discovered *de novo* through screening of synthetic peptide libraries. A synthetic peptide library consists of beads each carrying a single species of covalently bound peptide.[67] Peptide libraries have two distinct advantages for ligand screening: (1) unnatural amino acids, D-amino acids and even non-peptide moieties can be incorporated in the construction of synthetic peptide library, (2) beads can be screened using diverse bioassays that uses purified proteins, cells and/or crude cellular extracts.[68,69]

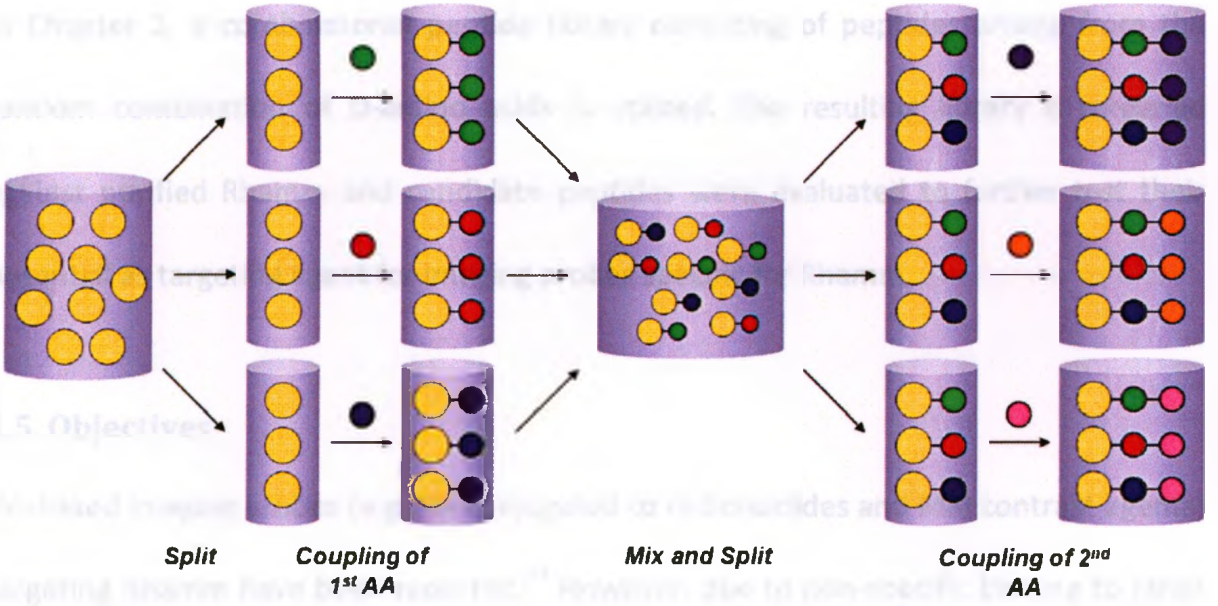

Figure 5: Split/Mix synthesis method for creating combinatorial peptide library. Yellow circles represent beads and coloured circles represent amino acids.

A random peptide library is created using split/mix synthesis method (Figure 5).[70] This synthesis method involves distribution of carrier beads (approximately 90 μm in diameter) into separate reaction vessels each containing a single amino acid. After the coupling of the first amino acids, the beads are re-pooled and the cycle is repeated several times to extend the peptide chain to the desired length. Following the creation of the library, it is screened against purified protein. To this end, beads are incubated with purified protein and bead-protein complex is identified via high-throughput screenings such as protein-charged magnetic bead screening assay[71] or enzyme-linked screening assay.[72] After screening, peptides identity contained within each isolated bead can be determined using methods such as automated Edman degradation,[73] MALDI deconvolution,[74] chromatography selection,[75] positional scanning synthetic combinatorial library.[76]

In Chapter 3, a combinatorial peptide library consisting of peptides arising from the random combination of D-amino acids is utilized. The resulting library is screened against purified Rhamm and candidate peptides were evaluated to further test their potential as targeting agent for imaging probes specific for Rhamm.

1.5. Objectives

HA-based imaging probes (e.g. HA conjugated to radionuclides and MRI contrast agents) targeting Rhamm have been reported.[77] However, due to non-specific binding to other extracellular surface receptors, high concentrations of HA-based probes are needed to image tumours.[78] Thus, peptides that mimic the binding properties of HA are proposed

as an alternative approach to HA-based probes. Furthermore, this project intends to develop a peptide-based imaging probe that shows significant uptake into Rhamm-expressing breast tumour cells while demonstrating variably low uptake in normal (non-Rhamm expressing) cells.

It was envisaged that these novel peptides will lead to the generation of a class of imaging agents with unique and superior biological properties to that of the natural ligand HA. These advantages include: (1) these peptides can be specifically tailored to bind to the HA binding domain of Rhamm, thus minimizing interaction to other hyaladerins (e.g. CD44) and providing a reagent for tumour subset specificity; (2) Tumour cells also express high levels of HA and hyaluronidase (a protein which rapidly degrades endogenous HA),[79] thus HA-based probes must not only compete with high levels of endogenous HA but are rapidly degraded at the tumour site; (3) Since HA is a polymer (approx. 350,000 Da), it is expected that these low molecular weight peptides will penetrate tumours to a greater extent than HA; and finally, (4) these peptides might not be recognized by the liver cell receptors involved in HA clearance from the bloodstream, thus increasing its concentration in tumours. In summary, this research aims to design, synthesize and *in vitro* characterize optical and metal conjugated peptides as HA mimics.

2. Structural Design: Design, synthesis and characterization of metal conjugated HA mimic as a surrogate for imaging probes for cancer.

2.1. Introduction

2.1.1. Hyaluronan-Binding Motif of Rhamm

Receptor for hyaluronan mediated motility (Rhamm) contains an HA-binding domain localized to a 62-amino acid segment (S1) at the carboxy terminus of the protein that is lacks structural similarities with traditional HA-binding motifs found in many HA surface receptors.[80] Circular dichroism experiments show that S1 is predominantly helical, which is comparatively different from the β-sheet dominated HA-binding region of other hyaladerins.[81] Although the crystal structure of Rhamm has not been elucidate to date, the structure of the aforementioned 62-amino acid segment along with HA has been elucidated in using a combination of solution phase NMR and molecular modelling.[81] This structural information regarding the HA-binding domain of Rhamm can then be used to reveal important information regarding the mechanism of HA binding and the regulatory role ligand binding might play in conformational changes of Rhamm. For instance, docking calculations of HA to Rhamm can provide data on the steric and energetic restraints necessary for optimal binding, which could then be applied to candidate ligands.

Compound **1**, previously elucidated by Ziebell et al,[82] was reported to bind to the HA-binding domain of Rhamm with an affinity of 2.1 nM (Figure 6). This compound was designed with the premise that alternating acidic residues within the peptidyl chain places the negative charges in a similar spatial manner to that of the carboxylates on HA.[82] Furthermore, data suggests that the inclusion of D-glutamates creates a 12-14 Å distance between two neighbouring carboxylate side chains, which is close enough to match the 10 Å separation of carboxylates on HA. However, it should be noted that using molecular dynamics simulation, we were not able to reproduce these results.

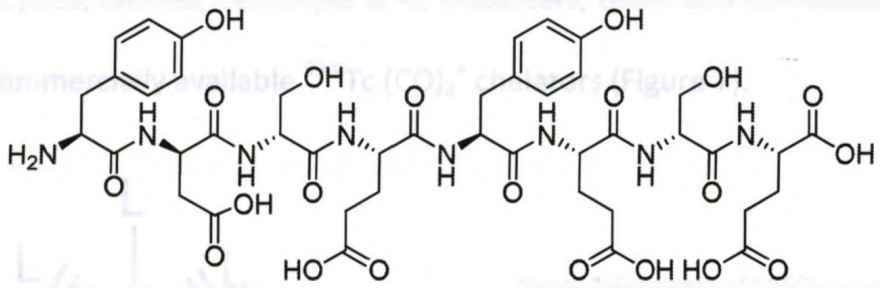

1

Figure 6: Chemical structure of candidate targeting entity containing the peptide sequence YDSeYeSe (Note: Upper case letters denote natural L-amino acids while lower case amino acids note unnatural D-amino acids).

As mentioned earlier, Rhamm-HA complex is mainly held by ionic interactions and thus it is expected that high affinity ligands should also contain the same degree of electrostatic interactions to Rhamm. HA interacts with residues Lys548, Lys553 and Lys560, while **1** interacts with residues Lys548, Arg555, and Lys560 on Rhamm. A common binding site in Rhamm for HA and **1** (i.e. Lys548 and Lys560) predicts potential competition between the two ligands; for this reason, it is believed that **1** could

potentially inhibit HA binding to Rhamm in physiological systems. Thus, compound **1** has the potential for further probe development.

2.1.2. Rhenium and Technetium

Technetium-99m (^{99m}Tc), which has a half-life of six hours and releases gamma rays upon decay, is one of the most widely used radionuclide due to its low cost and high availability. In imaging, new ^{99m}Tc based imaging probes use a $^{99m}Tc(CO)_3^+$ core. This core readily conjugates to molecules by complexing to a variety of ligand systems (such as N-heterocycles, amines, carboxylic acid, thioesters, thiols and combinations thereof) present in commercially available $^{99m}Tc(CO)_3^+$ chelators (Figure 7).

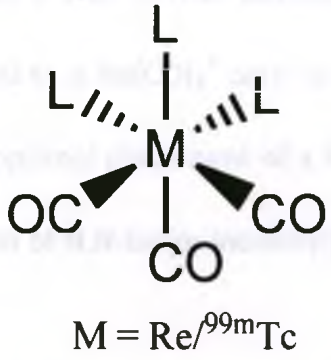

Figure 7: Schematic of $M(CO)_3L$ complex. M represents Re/^{99m}Tc while L represents any tridentate ligand donors

This core structure is particularly attractive because the low spin d^6 Tc (I) center is chemically inert and allows three facial positions for ligand substitution.[83] Rhenium (Re) is a non-radioactive element located one row beneath technetium in the periodic table, has two stable nuclei (^{185}Re (37.4%) and ^{187}Re (62.6%)) and is found to have similar size and formal charge as technetium.[84] Re complexes can serve as structural models for Tc complexes because homologous compounds have very similar coordination parameters. Thus, analogous Re and Tc complexes are nearly identical and are potentially

indistinguishable in biological systems. Thus, rhenium provides a suitable method for the structural characterization of compounds, while avoiding any radioactivity.

The Re/^{99m}Tc$(CO)_3^+$ core is relatively small and lipophilic, thus allowing it to be tightly bound by tridentate chelators in aqueous biological settings.[85] The facial carbonyl ligands have been known to make their *trans* positioned ligands to be more labile, allowing easy incorporation in chelation sites of an imaging probes. For instance, Re/^{99m}Tc $(CO)_3^+$ cores with halides (Cl^- or Br^-) defining the other face of the complex easily dissociates in water to produce *fac*-$[Re(CO)_3(OH_2)_3]^+$.[85] The facial arrangement of the carbonyls also makes fewer products upon complexation as it provides a limited variation in ligand configuration.

Compound **1** was further developed and characterized using *in vitro* assays, and was conjugated to a $Re(CO)_3^+$ core to create a surrogate probe for nuclear imaging. To this end, the optimal placement of a $Re(CO)_3^+$ chelator was elucidated, and a metal chelator in the form of N,N-bis(quinolinoyl)amine was incorporated to the peptide.

2.2. Results and Discussion

2.2.1. Initial Studies

To examine the potential of peptide **1** as a metal conjugated molecular imaging probe, the affinity of the peptide to Rhamm was first examined. The peptide was synthesized using solid phase peptide synthesis (SPPS), purified and conjugated to 0.2 µm aldehyde-sulphate charged fluorescent beads (FluoSpheres®) using reductive amination. The amino group of the peptide (compound **1**) was reacted with the aldehyde functionality

of the FluoSpheres in methanol, and the resulting imine was reduced using sodium cyanoborohydride. Non-conjugated peptides were removed via dialysis in water. FluoSpheres were chosen due to high dye equivalent per microsphere and increased resistance to photobeaching.[86] Figure 8A gives the pictograph representation of peptide-charged FluoSpheres (ModFluoSpheres).

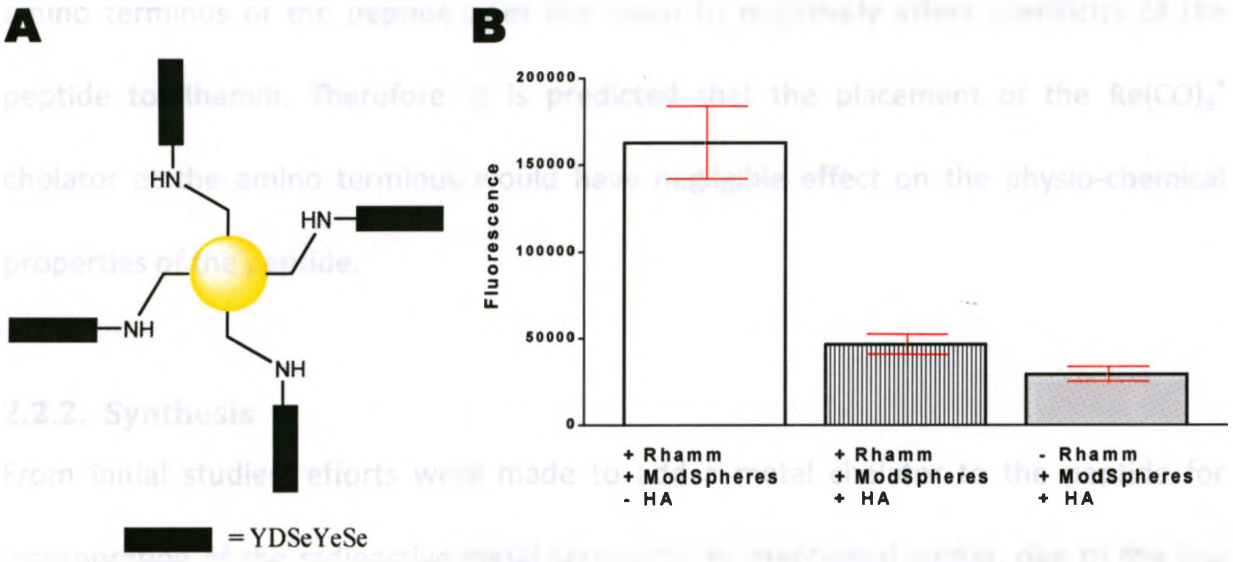

Figure 8: (A) Pictographic representation of ModFluoSpheres. (B) Binding of ModFluoSpheres to Rhamm using ELISA. In each assay, Rhamm bound to a 96-well plate was used as the primary protein. Fluorescent beads have maxima at 405 nm. Data are the mean of four experiments, analyzed using ANOVA, and error bars shown are the standard error of the mean. Background (no immobilized Rhamm) signal was subtracted for each treatment groups.

To assess specificity, the ability of ModFluoSpheres to compete with HA for the HA-binding domain of Rhamm was assessed using enzyme-linked immunosorbent assay or ELISA (Figure 8B). ELISA is a biomolecular technique used to detect the affinity of a ligand to a specific biological receptor. Initially in an ELISA, a biomolecule is immobilized to a plate. This step is followed by the addition of a known ligand which attaches to the functionalized surface if it displays a binding affinity to the immobilized substrate. In this assay, the observed fluorescence can be seen as a function of ModSpheres bound to

immobilized Rhamm. Results indicate that ModFluoSpheres are able to compete with HA, suggesting specificity to the HA-binding domain of Rhamm.

Previous reports on molecular docking experiments of Prestwich *et al.* suggest that the amino terminus of the peptide does not seem to participate in binding. Furthermore, experimental data suggests that functionalization (i.e. addition of FluoSpheres) at the amino terminus of the peptide does not seem to negatively affect specificity of the peptide to Rhamm. Therefore, it is predicted that the placement of the $Re(CO)_3^+$ chelator at the amino terminus would have negligible effect on the physio-chemical properties of the peptide.

2.2.2. Synthesis

From initial studies, efforts were made to add a metal chelator to the peptide for incorporation of the radioactive metal surrogate. As mentioned earlier, due to the low cost and high availability of ^{99m}Tc, it is one of the most used radionuclide in diagnostic imaging. Since ^{99m}Tc is radioactive, rhenium analogs which are non-radioactive surrogates of technetium-99m are typically used for characterization of complexes. To create a metal conjugated imaging probe (compound **2**), a $Re(CO)_3^+$ chelator in the form of N,N-bis(quinolinoyl)amine was utilized.[87] This chelator provides a tridentate donor set for chelation and an amine functionality for attachment to biomolecules (Figure 9). The rhenium coordination geometry is defined by three facial carbonyl groups thus orienting the quinolinoyl nitrogen donors and amine nitrogen to the other face.

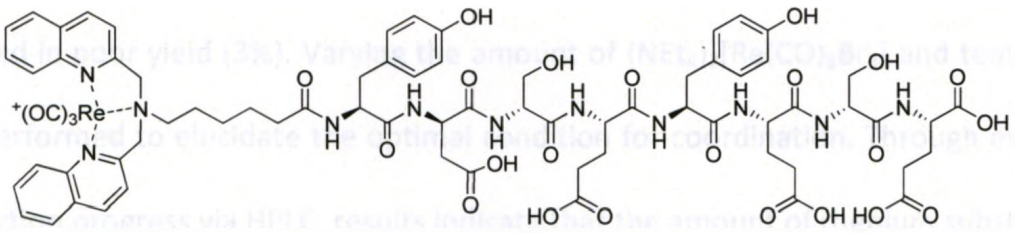

2

Figure 9: Proposed metal-conjugated probe for breast cancer.

Using SPPS, the amino acid corresponding to the desired sequence was added in succession starting from the carboxy terminal of the peptide (Scheme 2). Next, aminohexanoic acid linker was incorporated to the sequence to distance the targeting entity to the chelator. The employed chelator was created by coupling the two methylquinoline arms to the N-terminus of the peptide following Fmoc-deprotection. To this end, excess 2-(chloromethyl)quinoline was reacted to the amino group of the peptide on solid support at room temperature in DMF in the presence of a base for 24 hours. The resulting peptide was rhenium coordinated using $(NEt_4)_2[Re(CO)_3Br_3]$ in methanol via microwave irradiation.

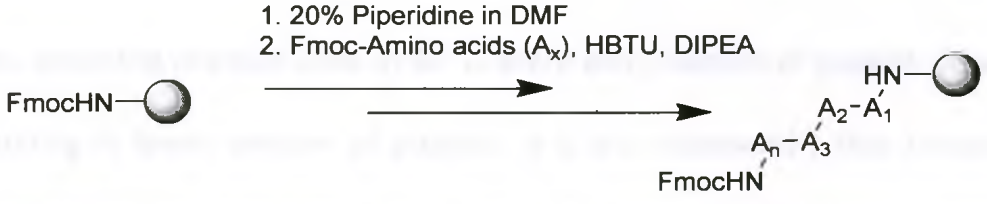

Scheme 2: Solid phase peptide synthesis using standard Fmoc protocols.

Prior to rhenium coordination, $(NEt_4)_2[Re(CO)_3Br_3]$ was synthesized from reaction between $Re(CO)_5Br$ and tetraethylammonium bromide in diglyme at 120^{O}C for eight hours (89% yield).[88,89] Unfortunately, rhenium coordination did not proceed readily and

resulted in poor yield (3%). Varying the amount of $(NEt_4)_2[Re(CO)_3Br_3]$ and temperature was performed to elucidate the optimal condition for coordination. Through evaluation of reaction progress via HPLC, results indicate that the amount of rhenium substrate had little or no effect on increasing product formation while temperature variations significantly increase the amount of rhenium bound peptides (**Error! Not a valid bookmark self-reference.**).

Table 1: % Rhenium-bound peptides with varying temperature and amounts of $(NEt_4)_2[Re(CO)_3Br_3]$. Reaction was heated using microwave irradiation for 15 minutes. % Rhenium-bound peptides were determined using LC-MS.

Temperature (^{O}C)	$(NEt_4)_2[Re(CO)_3Br_3]$ Equiv.	% Rhenium-bound Peptides
30	1	33
	3	37
	5	40
50	1	67
	3	64
	5	68
60	1	45
	3	38
	5	34

However, when the reaction done at 60^{O}C, there was evidence of peptide degradation, thus resulting in lower amount of product. It is also noteworthy that increasing the duration of the reaction had little or no effect on the formation of desired product. The resulting product was removed from solid support, purified via HPLC (89% purity) and characterized by mass spectrometry (Figure 10).

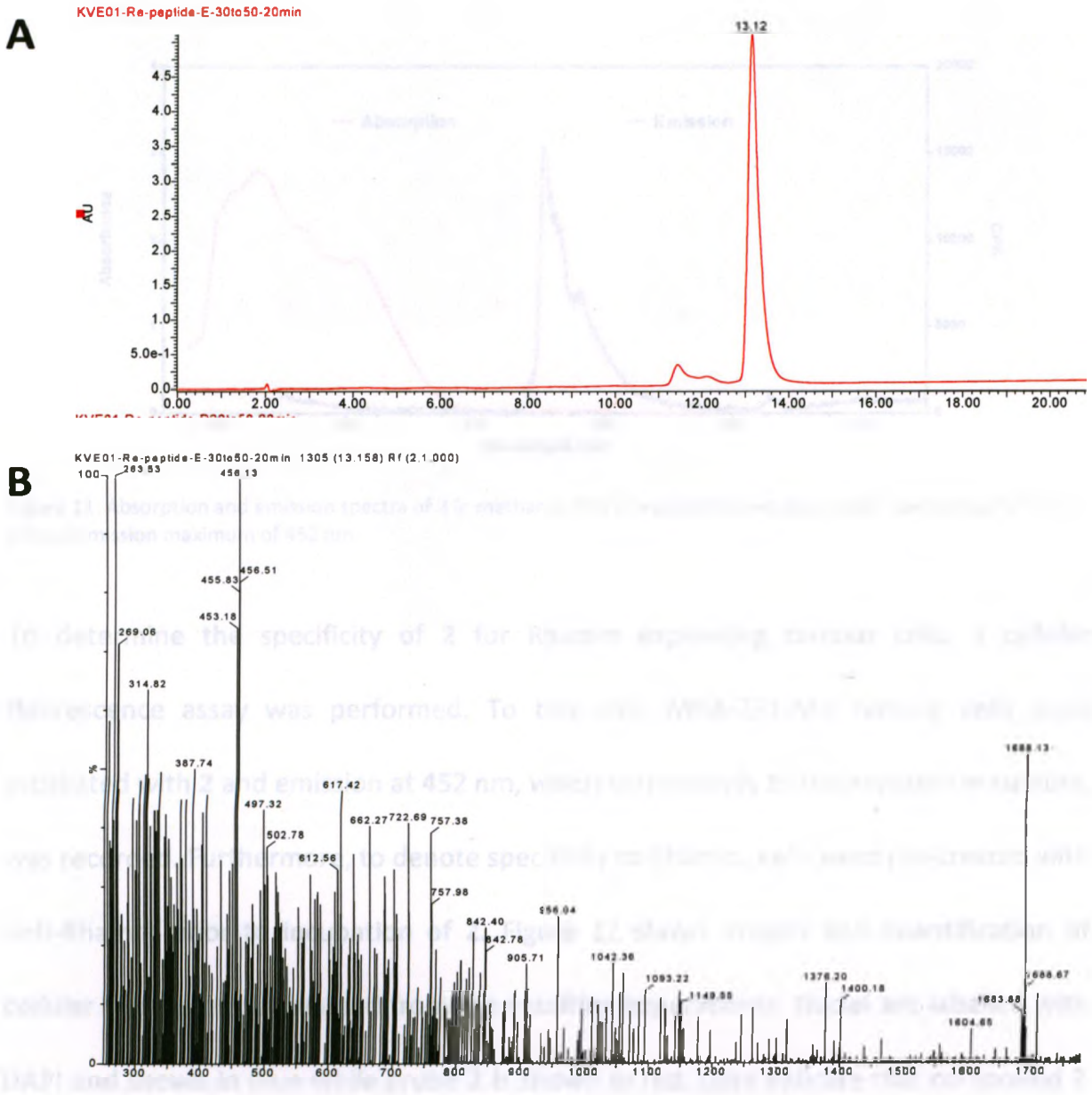

Figure 10: (A) HPLC trace of purified **2** with a retention time of 13.1 min displaying a purity of 89% in 12% yield. **(B)** ESI-MS showing observed $[M+H]^+$ = 1688.12 m/z (calculated 1688.74 m/z).

2.2.3. *In Vitro* Characterization

Rhenium tricarbonyl *N,N*-bis(quinolinoyl)amine complexes have been reported to have optical properties suitable for fluorescence imaging.[90] Thus, the absorption and emission maxima were determined to facilitate the further in vitro characterization of **2**. The probe was determined to have absorption maximum of 235 nm and an emission maximum of 452 nm in methanol (Figure 11).

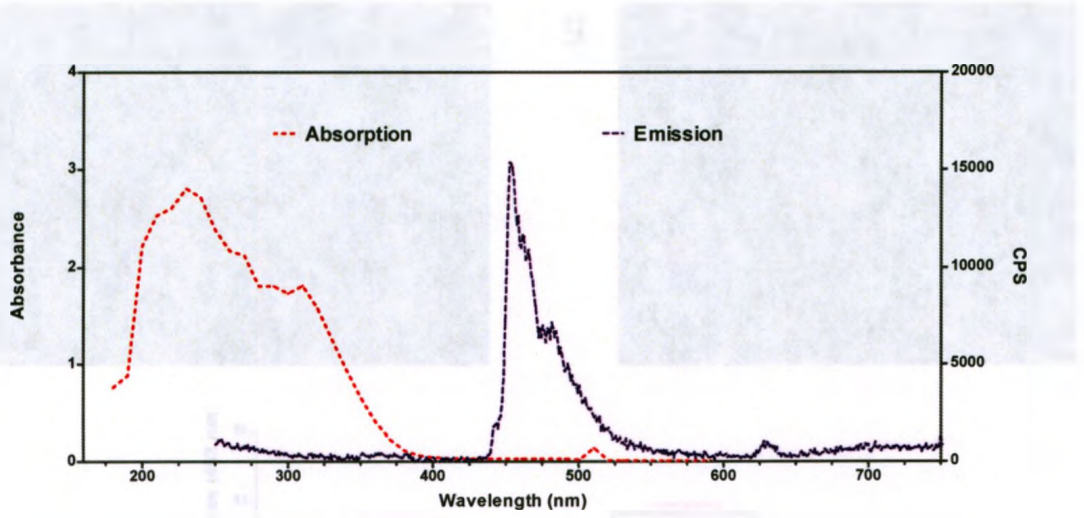

Figure 11: Absorption and emission spectra of **2** in methanol. The compound shows absorption maximum of 235 nm, and an emission maximum of 452 nm.

To determine the specificity of **2** for Rhamm expressing tumour cells, a cellular fluorescence assay was performed. To this end, MDA-231-MB tumour cells were incubated with **2** and emission at 452 nm, which corresponds to the emission maximum, was recorded. Furthermore, to denote specificity to Rhamm, cells were pre-treated with anti-Rhamm prior to incubation of **2.** Figure 12 shows images and quantification of cellular fluorescence obtained from the resulting experiments. Nuclei are labelled with DAPI and shown in blue while probe **2** is shown in red. Data indicate that compound **2** was taken up by MDA-231-MB; however, uptake is not decreased upon treatment of anti-Rhamm, indicating that this is non-specific uptake.

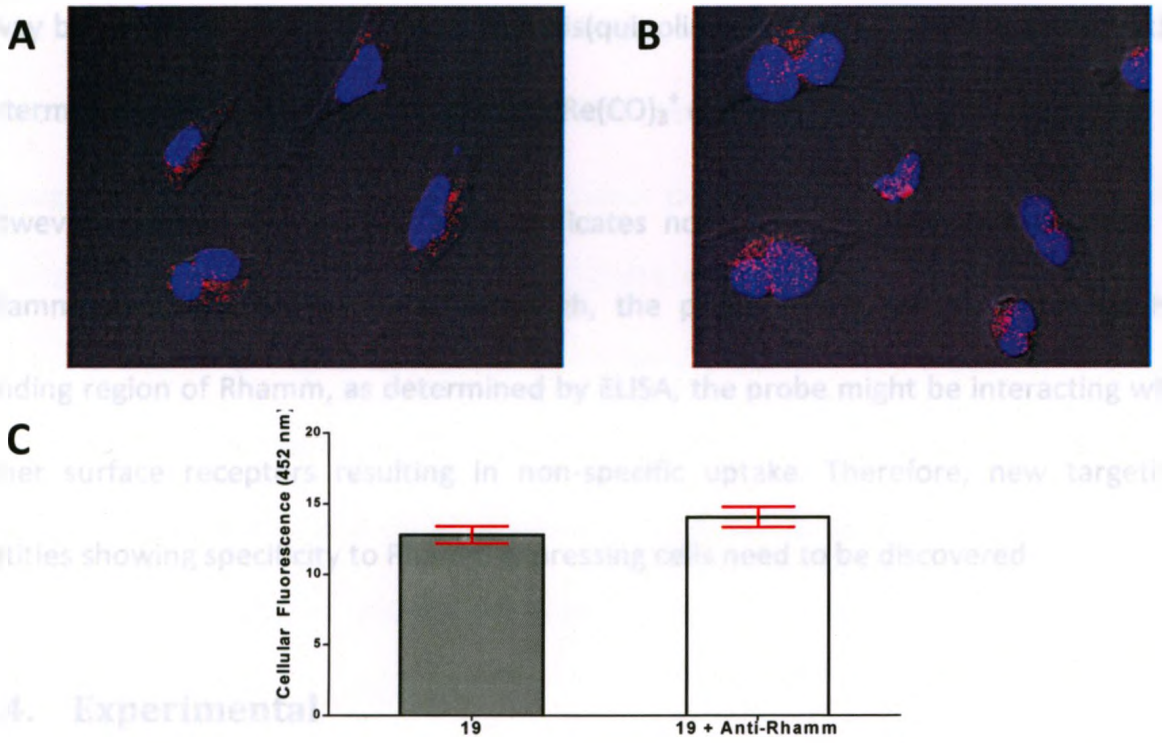

Figure 12: Cellular uptake studies and quantification of **2** in MDA-MB-231 cancer cell line. **(A)** Cells incubated with the probe. **(B)** Cells pre-treated with anti-Rhamm antibody and incubated with the probe. Nuclei (stained with DAPI) are shown in blue while metal- conjugated peptides are shown in red. **(C)** Quantification of cellular uptake (148 ROI for each treatment group, n = 2) showed no statistical significance between cells receiving anti-Rhamm and cells which receive no antibody treatment.

2.3. Conclusion

This study aims to create a metal-conjugated imaging probe as a surrogate for nuclear imaging. The peptide, containing the sequence YDSeYeSe, which was previously reported to have affinity to Rhamm, was examined using *in vitro* assays. To this end, peptides were conjugated to fluorescent beads (FluoSpheres) and their specificity to the HA binding domain of Rhamm was examined. Data indicate that the targeting entity was able to compete with HA suggesting specificity to the HA binding domain of Rhamm. Since direct conjugation of the amino terminus of the peptide to FluoSpheres does not seem to affect specificity, the metal chelator was placed along the N-terminus spaced

away by aminohexanoic acid linker. *N,N*-Bis(quinolinoyl)amine was incorporated to the N-terminus of the peptide and served as a $Re(CO)_3^+$ chelator.

However, cellular fluorescence assay indicates non-specific uptake of the probe in Rhamm-expressing tumour cells. Although, the probe shows specificity to the HA binding region of Rhamm, as determined by ELISA, the probe might be interacting with other surface receptors resulting in non-specific uptake. Therefore, new targeting entities showing specificity to Rhamm expressing cells need to be discovered.

2.4. Experimental

Solvents were used without further purification, and purchased either from VWR, Fisher Scientific, or Sigma Aldrich. Fmoc-dGlu preload Wang resin (100-200 mesh, 0.70 mmol/g), standard Fmoc amino acids, Fmoc-aminohexanoic acid (Ahx), Fmoc-D-amino acids, HBTU coupling reagents were obtained from Peptides International. 2-Chloromethylquinoline (Sigma Aldrich), sodium cyanoborohydride (Aldrich) and $Re(CO)_5Br$ (Strem Chemicals) were purchased as reagent grade and used without further purification. FluoSpheres aldehyde-sulfate microspheres (0.2 μm) were purchases from Invitrogen. UV-Vis data was obtained from Beckman DU 530 spectrophotometer using quartz cuvettes (10 mm)

2.4.1. Peptide Synthesis

Elongation of peptidyl chains on rink amide MBHA resins (0.1 mmol) was performed using automated (APEX 396 auto-synthesizer) and manual methods using standard

Fmoc deprotection and amino acid coupling cycles.[91] Solid-phase peptide coupling reactions were monitored using the Kaiser test.[92] Repeated Fmoc deprotection throughout the synthesis (15 and 20 minutes periods) was carried out using 20% piperidine solution in *N,N*-dimethylformide (DMF). All amino acid couplings were carried out using 0.05 M or higher concentration of Fmoc-protected amino acid and HBTU, 5 equivalent of *N,N*-diisopropylethylamine (DIPEA) in DMF at 30 and 90 minutes intervals. After each deprotection and coupling step, the resin was washed repeatedly with DMF (3x) and dichloromethane (DCM) (3x). Fmoc-protected aminohexanoic acid (Ahx) was coupled using the same parameters.

Following the Fmoc-deprotection of Ahx linker, the peptidyl resin (0.1 mmol) was reacted with 10-fold excess of 2-(chlorometyl)quinoline in DMF in the presence of DIPEA (2 equiv.) at room temperature for 24 hours. Reaction completion was monitored by RP-HPLC.

Purification of peptides was performed using gradient solvent system consisting of H_2O + 0.1% TFA (solvent A) and CH_3CN + 0.1% TFA (solvent B) at a linear flow rate of 1.5 mL/min and 20 mL/min for analytical and preparative HPLC, respectively. Analytical HPLC was performed using a Grace Vydac Protein/Peptide RP-C18 column (4.6 mm x 250 µm, 5 µm), and preparative HPLC was performed using a Grace Vydac protein/peptide RP-C18 column (22.0 mm x 250 mm, 10 µm). Absorbance was detected at wavelengths of 220 nm and 254 nm using a Waters 2998 Photodiode Array detector. During

purification, fractions were collected, lyophilized, and analyzed by ESI-MS (Waters Micromass Quattro Micro™ API).

2.4.2. Peptide conjugation to FluoSphere Beads

Purified peptides (10 mg, 8 equiv.) were agitated together with aldehyde-functionalized 2 µm FluoSphere beads for 2 hours in methanol (10 mL). The resulting suspension was treated with sodium cyanoborohydride (8 equiv.) and the reaction mixture was allowed to stir overnight. The suspension was transferred to a dialysis tube (molecular cut-off value of 13 KDa) and submerged to 2L de-ionized water (2x) for 4 hours.

2.4.3. Rhenium Coordination

2.4.3.1. Synthesis of $(Et4N)_2[Re(CO)_3Br_3]$

A suspension of Et_4NBr (452 mg, 2.15 mmol) and $Re(CO)_5Br$ (400 mg, 988 µmol) in dry diglyme was heated to 70°C under argon to achieve a clear colourless solution. The reaction mixture was refluxed at 120°C for 4 hours, and heated at 80°C overnight. The reaction mixture was cooled to 50°C and the resulting precipitate was filtered, washed with cold diglyme (3 x 5 mL), diethyl ether (3 x 5 mL) and cold ethanol (2 x 3 mL) to remove excess Et_4N. The solid was dried *in vacuo* (334 mg, 89% yield) and used without further purification.

2.4.3.2. Rhenium coordination

The peptide on solid support was reacted with $(NEt_4)_2[Re(CO)_3Br_3]$ (5 equiv.) in methanol via microwave irradiation (50^0C) for 30 minutes. Resins were washed with DMF (3x) and methanol (3x). The resulting resin was treated with cleavage cocktail and purified using HPLC as outlined in section 2.4.1.

2.4.4. ELISA binding assay using ModFluoSpheres

A 12-well plate coated with 0.1 mg/mL Rhamm was incubated at 4^OC overnight and washed three times with 0.1% TBST. BSA blocking solution was added and incubated for 4 hours at room temperature. 50µL HA (1 mg/mL) or ModFluoSpheres (1 mg/mL) or both in 0.1% TBST were added to the plates at 4^OC and incubated for 2 hours. After incubation, plates received a final wash of 0.1% TBST (3x). Negative control plates were not treated with Rhamm and used to correct for background signals, while positive control plates (with Rhamm) receive only ModSpheres. Each treatment and controls were done in triplicate. 100 µL of 0.1% TBST were added to each plate and fluorescence was recorded for each well.

2.4.5. Cell Uptake Study

MDA-MB-231 cells cultured in FBS were plated in a 12-well tissue culture plate (confluency of 20000 cells per well) one day after seeding. For blocking experiment, antibodies (anti-Rhamm mAb) in serum free media were added and incubated at 37^OC for 10 minutes. Peptides (20 µM) were added and incubated at 37^OC for 10 minutes. Cells were washed with serum free media and mounted using fixing solution consisting

of 0.1M sodium phosphate (pH 7.4) and 2% paraformaldehyde. Cells were photographed using Olympus FluoView FV1000 coupled IX81 Motorized Inverted System Microscope. Tiff images were analyzed using ImageJ (v1.42q) application. Each image was converted to an 8-bit format with threshold values of 7 and 259. Region of interest (ROI) were selected and mean cellular fluorescence was deduced (148 ROIs for each treatment groups, n = 2).

3. Ligand-Based Design: Tubulin-Derived Peptides targeting Rhamm

3.1. Introduction

3.1.1. Microtubules and Rhamm as Tubulin-Binding Proteins

Microtubules are structures which maintain cell morphology and mediate diverse cellular functions such as mitosis, metabolism, locomotion, trafficking of organelles and macromolecules.[93] Most of these functions involve complex interactions between microtubules and a large number of microtubule-associated proteins (MAPs). These interactions regulate polymerization and depolymerization cycles, and the distribution of microtubules in the cell.[94] Microtubules consist of mainly of αβ-tubulin dimers, whose carboxy terminal region contain a highly conserved helical region and a hyper-variable carboxy terminal tail (CTT) sequence composed of highly acidic (negatively charged) residues.[95,96] Also, γ-tubulin, a minor component of microtubules, plays a role in the nucleation of microtubule assembly.

Tubulin exists in different isotopic forms which have been found to be tissue specific due to their differential expression and relative stabilities. Furthermore, the majority of differences between tubulin isotypes are localize within the last 15 residues of the sequences. There are at least seven different isoforms of α-tubulin, β-tubulin has eight isoforms, and γ-tubulin has seven known isoforms.[97] Although the structure of a tubulin

dimer has been obtained by electron crystallography, the three-dimensional structure of CTTs has never been determined due to their high structural heterogeneity.[98,99] These CTTs are found exclusively in the tubulin family and are important functionally because they support the binding of proteins that associate with microtubules.[100,101,102]

In mammalian systems, the carboxy terminus of tubulin undergoes proteolysis with subtilisin (a serine endopeptidase) to modulate microtubule assembly. Subtilisin predominantly cleaves the carboxy-terminal residues of each tubulin subunit, generating the modified tubulin (termed S-tubulin) and releasing short peptides (termed S-peptides) containing the CTT sequence. These S-peptides have been shown to bind to MAPs with high affinity; however, covalent cross-linking experiments have shown that MAPs still bind even with only the last 12 residues (CTT) of α- and β-tubulin.[103] MAPs are positively charged and they bind primarily to the negatively charged CTTs of both α- and β-tubulin; thus the binding to microtubules could be dominated by ionic interactions. Furthermore, β-tubulin derived peptides encompassing the last 12 carboxy-terminal residues showed MAP-stimulated microtubule assembly *in vitro*, while peptides derived directly adjacent to CTT sequences are inactive.[104]

Microtubule-associated motor proteins are a special type of MAP that couples adenosine triphosphate hydrolysis to the generation of force and movement to move cargo along microtubules. Kinesins, a type of microtubule-associated motor protein, are important in the structural organization of the microtubule system in the cell, especially during cell division.[105] Cross-linking experiments indicate direct binding of CTTs to

kinesin's motor domain. Specifically, peptides corresponding to the carboxy terminal 12 amino acid residues of pig β-tubulin competitively interfere with the binding of microtubules to kinesin motors.[106]

Rhamm is one of a number of proteins that is exported to the cell surface by unconventional mechanisms due to its lack of signal peptide for export through the golgi/ER.[107] These unconventionally exported proteins are predicted to be both cell-surface proteins and cytoplasmic proteins, and typically have extracellular functions that are different from their intracellular duties. Aside from being an HA-surface receptor, Rhamm is also reported to localize exclusively in the cytoplasm in a series of human breast cancer and various rodent tumour cell lines. [108] This protein localizes at the perinuclear microtubule network during interphase and may play an important role in the organization of the cytoskeletal network.[109,110] This localization to microtubules is said to be mediated by the carboxy terminus of Rhamm.[111] Protein truncation studies indicate that the carboxy terminal region alone was sufficient to centralize Rhamm to mitotic spindle microtubules.[112] Also, a pull-down assay showed that Rhamm binds to α- and β-tubulin subunits, and this interaction was strongly reduced in the presence of a synthetic peptide mimicking the carboxy terminal region of Rhamm.

3.1.2. Rational Design of Tubulin-derived Peptides

Database searches and pairwise comparisons (Figure 13) between Rhamm and microtubule binding domain of MAPs and kinesins revealed moderate sequence homology (17%-24% as calculated using ClustalX2[113]) to the HA binding domain of

Rhamm; however, MAPs and Rhamm share similar physiochemical properties regarding the amino acid sequence of their tubulin binding site. In other words, both Rhamm and MAPs have a stretch of basic residues which are postulated to bind to tubulins. Furthermore, the secondary structures of the tubulin binding sites of MAPs and hyaluronan binding site of Rhamm has the same degree of helicity and both could be classified as a basic-zipper domain.[114]

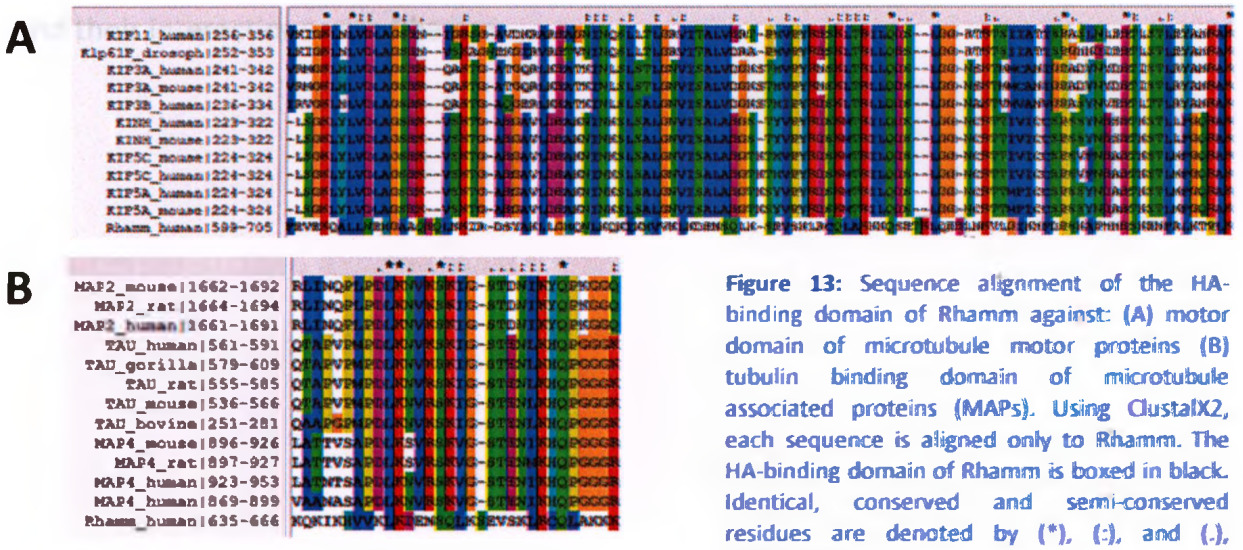

Figure 13: Sequence alignment of the HA-binding domain of Rhamm against: (A) motor domain of microtubule motor proteins (B) tubulin binding domain of microtubule associated proteins (MAPs). Using ClustalX2, each sequence is aligned only to Rhamm. The HA-binding domain of Rhamm is boxed in black. Identical, conserved and semi-conserved residues are denoted by (*), (:), and (.), respectively.

Recently, Rhamm has been reported to use a common binding site to associate with HA in the extracellular surface and microtubules in the cytosol. [115] Since microtubule-associated motor proteins and MAPs show direct binding to CTTs of tubulin, we hypothesize that Rhamm could show direct interaction with synthetic peptides representing the CTTs of different tubulin subtypes. Since HA interacts with Rhamm mainly through ionic interactions between its negatively charged groups and the positively charged groups on Rhamm, molecules possessing an analogous distribution of negative charges can in principle serve as HA mimics. For instance, the Glu and Asp

residues on tubulin CTTs may mimic the carboxylates on HA. Thus, the binding of synthetic CTTs to the HA binding domain of Rhamm might utilize the same charged side chain thought to be important for HA binding.

We investigated the use of known intracellular protein fragments (i.e. CTTs of tubulin) as extracellular ligands for the cell surface receptor Rhamm. Herein, we describe the evaluation of different carboxy-terminal tubulin-derived synthetic peptide analogues and their interactions with Rhamm.

3.2. Results and Discussion

3.2.1. Initial Studies

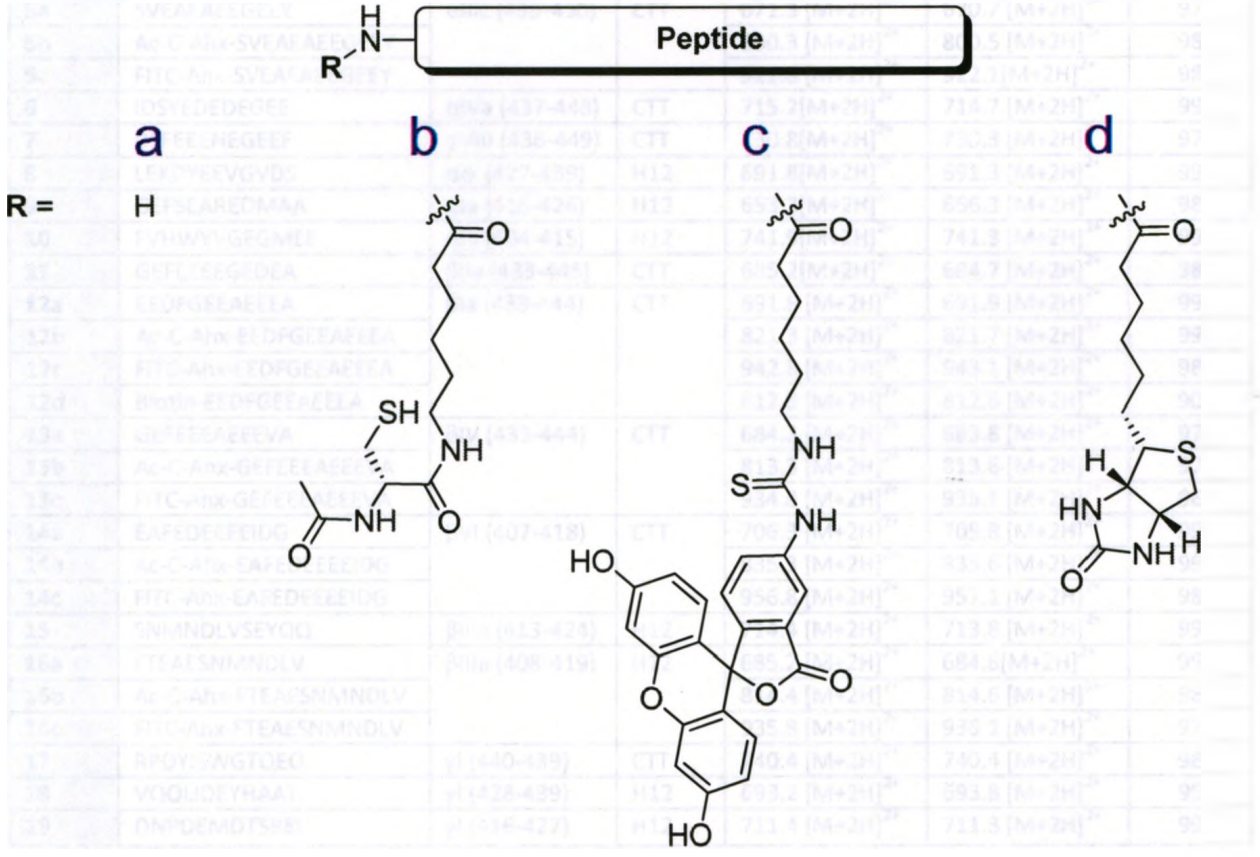

Figure 14: General structure of derivatized CTTs used for evaluation. The figure shows the general structure of unmodified tubulin-derived peptides (a) and peptides conjugated to N-acetyl cysteine (b), FITC (c), and biotin (d).

A six carbon linker was used to increase the distance between the peptide and an additional peptide modification. Derivatized peptides were prepared with either biotin, fluorescein or cysteine modified N-terminus (Figure 14). Table 2 describes all peptides prepared for this study.

Table 2: Analysis of synthesized tubulin-derived peptides using ESI-MS and RP HPLC.

Compd	Sequences	Tubulin Fragment	Type	Calculated M/Z*	Observed M/Z	Purity (%)†
3	DSADGEDEGEEY	αIa (438-449)	CTT	658.2[M+2H]$^{2+}$	657.7 [M+2H]$^{2+}$	98
4a	VEGEGEEEGEEY	αIa (439-451)	CTT	677.7 [M+2H]$^{2+}$	677.6 [M+2H]$^{2+}$	98
4b	Ac-C-Ahx-VEGEGEEEGEEY			807.3 [M+2H]$^{2+}$	807.6 [M+2H]$^{2+}$	98
4c	FITC-Ahx-VEGEGEEEGEEY			928.8 [M+2H]$^{2+}$	927.9 [M+2H]$^{2+}$	98
4d	Biotin-VEGEGEEEGEEY			798.3 [M+2H]$^{2+}$	798.1 [M+2H]$^{2+}$	94
5a	SVEAEAEEGEEY	αIIIc (439-450)	CTT	671.3 [M+2H]$^{2+}$	670.7 [M+2H]$^{2+}$	97
5b	Ac-C-Ahx-SVEAEAEEGEEY			800.3 [M+2H]$^{2+}$	800.5 [M+2H]$^{2+}$	98
5c	FITC-Ahx-SVEAEAEEGEEY			921.8 [M+2H]$^{2+}$	922.1[M+2H]$^{2+}$	98
6	IDSYEDEDEGEE	αIVa (437-448)	CTT	715.2[M+2H]$^{2+}$	714.7 [M+2H]$^{2+}$	99
7	DSFEEENEGEEF	αVIII (438-449)	CTT	730.8[M+2H]$^{2+}$	730.3 [M+2H]$^{2+}$	97
8	LEKDYEEVGVDS	αIa (427-439)	H12	691.8[M+2H]$^{2+}$	691.3 [M+2H]$^{2+}$	99
9	GEFSEAREDMAA	αIa (416-426)	H12	653.3[M+2H]$^{2+}$	656.3 [M+2H]$^{2+}$	98
10	FVHWYVGEGMEE	αIa (404-415)	H12	741.9[M+2H]$^{2+}$	741.3 [M+2H]$^{2+}$	99
11	GEFEEEEGEDEA	βIIa (433-445)	CTT	685.2[M+2H]$^{2+}$	684.7 [M+2H]$^{2+}$	98
12a	EEDFGEEAEEEA	βIa (433-444)	CTT	691.8 [M+2H]$^{2+}$	691.9 [M+2H]$^{2+}$	99
12b	Ac-C-Ahx-EEDFGEEAEEEA			821.3 [M+2H]$^{2+}$	821.7 [M+2H]$^{2+}$	99
12c	FITC-Ahx-EEDFGEEAEEEA			942.8 [M+2H]$^{2+}$	943.1 [M+2H]$^{2+}$	98
12d	Biotin-EEDFGEEAEEEA			812.3 [M+2H]$^{2+}$	812.6 [M+2H]$^{2+}$	90
13a	GEFEEEAEEEVA	βIV (433-444)	CTT	684.3 [M+2H]$^{2+}$	683.8 [M+2H]$^{2+}$	97
13b	Ac-C-Ahx-GEFEEEAEEEVA			813.3 [M+2H]$^{2+}$	813.6 [M+2H]$^{2+}$	97
13c	FITC-Ahx-GEFEEEAEEEVA			934.8 [M+2H]$^{2+}$	935.1 [M+2H]$^{2+}$	96
14a	EAFEDEEEEIDG	βVI (407-418)	CTT	706.3 [M+2H]$^{2+}$	705.8 [M+2H]$^{2+}$	99
14b	Ac-C-Ahx-EAFEDEEEEIDG			835.3 [M+2H]$^{2+}$	835.6 [M+2H]$^{2+}$	99
14c	FITC-Ahx-EAFEDEEEEIDG			956.8 [M+2H]$^{2+}$	957.1 [M+2H]$^{2+}$	98
15	SNMNDLVSEYQQ	βIIIa (413-424)	H12	714.4 [M+2H]$^{2+}$	713.8 [M+2H]$^{2+}$	99
16a	FTEAESNMNDLV	βIIIa (408-419)	H12	685.2 [M+2H]$^{2+}$	684.8[M+2H]$^{2+}$	99
16b	Ac-C-Ahx-FTEAESNMNDLV			814.4 [M+2H]$^{2+}$	814.6 [M+2H]$^{2+}$	98
16c	FITC-Ahx-FTEAESNMNDLV			935.8 [M+2H]$^{2+}$	936.1 [M+2H]$^{2+}$	97
17	RPDYISWGTQEQ	γI (440-439)	CTT	740.4 [M+2H]$^{2+}$	740.4 [M+2H]$^{2+}$	98
18	VQQLIDEYHAAT	γI (428-439)	H12	693.2 [M+2H]$^{2+}$	693.8 [M+2H]$^{2+}$	95
19	DNPDEMDTSREI	γI (416-427)	H12	711.4 [M+2H]$^{2+}$	711.3 [M+2H]$^{2+}$	99

Using enzyme-linked immunosorbent assay (ELISA), the affinity of Rhamm to synthetic CTTs corresponding to α1a- and β$_I$a-tubulin were measured (Figure 15A). Biotin-conjugated CTTs (VEGEGEEEGEEY **4d** and EEDFGEEAEEEA **12d**) were incubated with the immobilized HA-binding domain of Rhamm (Rhamm-CT), washed to eliminate unbound peptides, and the presence of bound peptides were detected by the addition of streptavidin-coupled alkaline phosphatase and a colorimetric phosphatase substrate. As

* The *m/z* calculated and observed values are based on the prominent observed signals as determined by ESI.
† Percent purity determined by RP HPLC with detection at 220 nm.

expected, minimal color development corresponding to plates which receive no peptide or no Rhamm treatment was observed. Results show that both α1a- (VEGEGEEEGEEY, **4d**) and β1a-CTT (EEDFGEEAEEEA, **12d**) displays affinity to Rhamm (*p = 0.001*). Results also indicate that αIa-CTT shows a slightly higher affinity to Rhamm compared to βIa-CTT (*p = 0.01*).

To examine the affinity of αIa- and βIa-CTT to the HA-binding domain of Rhamm, surface plasmon resonance (SPR) binding assay was utilized. To utilize this technique, peptides were conjugated to N-acetyl cysteine were synthesized (VEGEGEEEGEEY **4b** and EEDFGEEAEEEA **12b**), and their thiol functionality was used for immobilization to the sensor plate. For this experiment, Rhamm-CT was passed across a peptide-derivatized surface, and the real time association and dissociation interactions of each peptide to Rhamm-CT were detected and reported as sensograms (Figure 15B). Sensorgram indicates that **4b** (VEGEGEEGEEY) showed higher binding compared to **12b** (EEDFGEEAEEEA). This result is good correlation to the results obtained by ELISA.

Equilibrium dissociation constants (K_D) were obtained from the resulting sensograms. Each sensograms was globally fitted to a 1:1 bimolecular kinetic model (Figure 15C) to obtain the association rate constant (K_{ON}) and dissociation constant (K_{OFF}). The equilibrium dissociation constant (K_D) is given the ratio K_{OFF}/K_{ON}. Using data from different Rhamm concentrations, α1a- (VEGEGEEEGEEY, **4b**) and β1a-CTT (EEDFGEEAEEEA, **12b**) had average calculated K_D of 24 nM and 32 nM, respectively. Data

are consistent with our previous reports that the carboxy terminus of Rhamm contains the tubulin binding domain of Rhamm.[114]

A

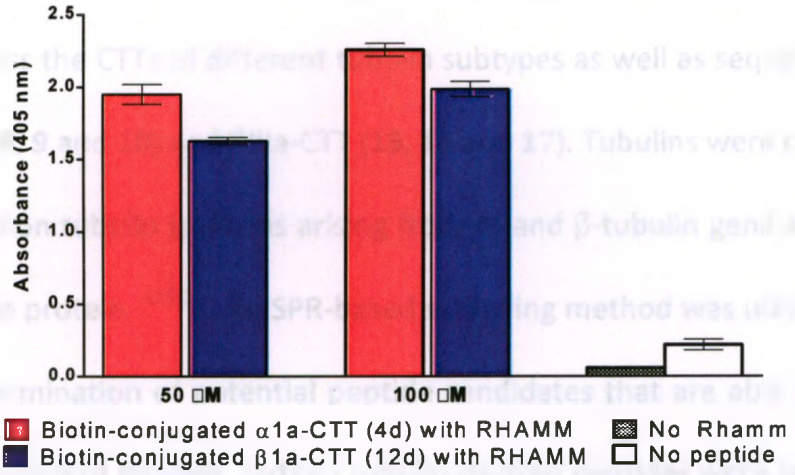

B

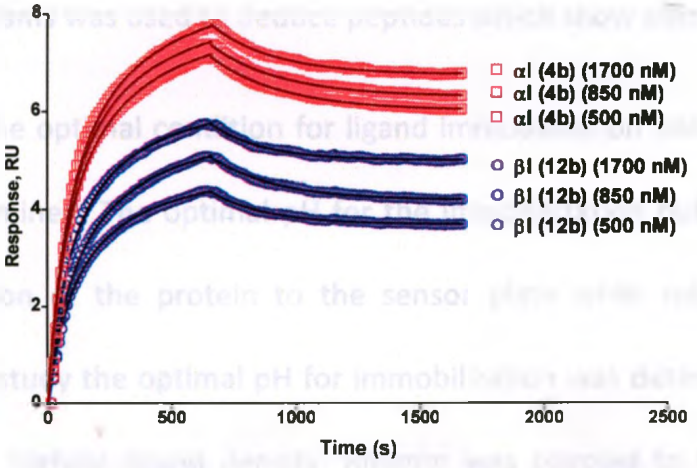

C

Sequence	Compd	Subtype	[Conc.] (nM)	K_{ON} (nM^{-1} sec^{-1})	K_{OFF} (sec^{-1}) (10^{-4})	K_D (nM)	Ave. K_D (nM)
VEGEGEEEGEEY	4b	α1a	500	7052	1.664	23.5	24 ± 1.5
			850	4412	1.168	26.4	
			1700	2795	0.695	24.7	
EEDFGEEAEEEA	12b	β1a	500	7409	2.522	34.0	32 ± 2.5
			850	4056	1.316	32.5	
			1700	2384	0.696	29.2	

Figure 15: (A) Binding of biotin-conjugated CTTs (**4d** and **12d**) to Rhamm using ELISA (n = 3). **(B)** Sensograms depicting the interaction of CTTs (**4b** and **12b**) and Rhamm. An N-terminal acylated Cys spaced by aminohexanoic acid linker was added to each peptide sequence to permit attachment to the SPR sensor plate. Different concentrations (500, 850, and 1700 nM; traces from top to bottom) of Rhamm was flowed over functionalized SPR sensor plate. Black lines represent the global fit of the sensograms to a 1:1 interaction kinetic model **(C)** (Table 3) Kinetic analysis of CTTs (**4b** and **12b**) interacting with Rhamm. The equilibrium dissociation constant, K_D, was calculated from K_{OFF}/K_{ON}.

3.2.2. Screening of tubulin-derived peptides

Based on the promising results from the initial α1a- and β1a-CTT peptides, we then proceeded to evaluate sixteen tubulin derived peptides. Sequences of synthesized peptides encompass the CTTs of different tubulin subtypes as well as sequences directly flanking α1a- (i.e. **8**, **9** and **10**) and βIIIa-CTT (**15**, **16** and **17**). Tubulins were chosen based on the most common tubulin isoforms arising from α- and β-tubulin gene and the most acidic region of the protein. [116,117] An SPR-based screening method was utilized for rapid and accurate determination of potential peptide candidates that are able to recognize the HA-binding domain of Rhamm. Sixteen tubulin-derived peptides were screened, and the resulting sensograms was used to deduce peptides which show affinity to Rhamm.

Prior to screening, the optimal condition for ligand immobilization and analyte binding condition was determined. The optimal pH for the immobilization buffer balances the electrostatic attraction of the protein to the sensor plate while minimizing protein deactivation. In this study the optimal pH for immobilization was determined to be the pH that yielded the highest ligand density. Rhamm was coupled to the sensor plate using sodium bicarbonate buffer of varying pH, at a flow rate of 30 µL/mL and with fixed concentration of EDAC and sulfo-NHS. The Rhamm ligand density for each pH immobilization condition was determined from the average SPR response of six measurements and the maximum ligand immobilization occurred at pH 9.7 (Figure 16A). Ligand immobilization was slightly lower than pH 10.1 due in part to loss of net charge on Rhamm at its isoelectric point.

A

Buffer Ph	Rhamm Concentration (µg/mL)	Ligand Density (RU)
10.1	30	1445.1 ± 31.4
9.7	30	1547.8 ± 29.0
9.1	30	1499.5 ± 34.4
7.0	30	1475.4 ± 13.7
9.7	0	27.22 ± 3.57[‡]

B

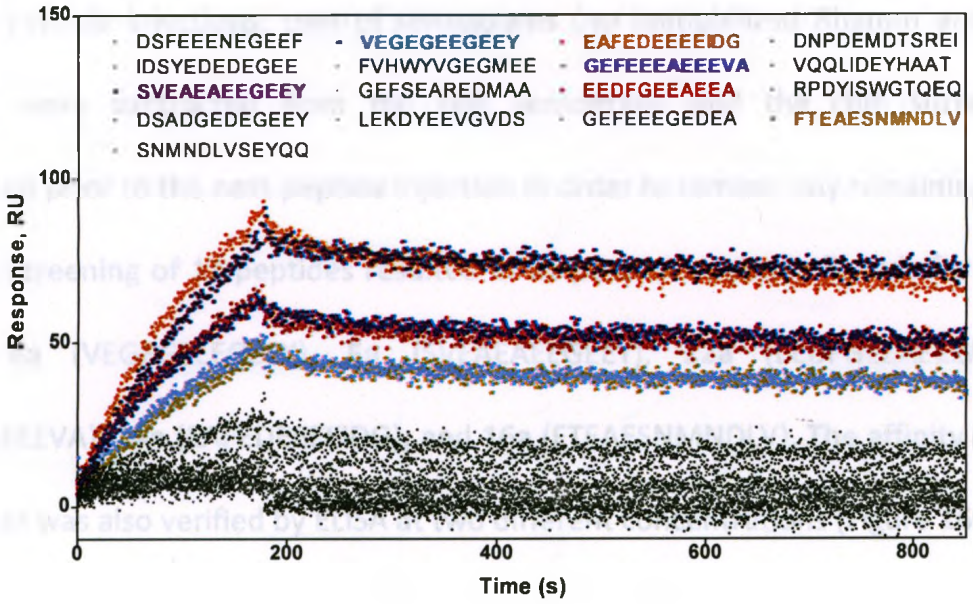

C

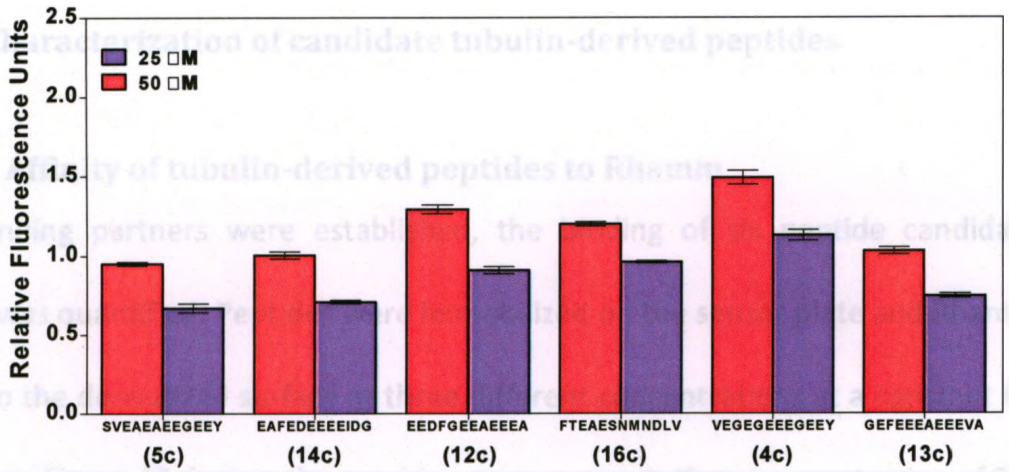

Figure 16: (A) (Table 4) pH dependence of Rhamm-CT immobilization to a SPR sensor plate. Rhamm-CT protein was immobilized in sodium bicarbonate buffer, pH 7.0-10.1, at a flow rate of 30 µL/mL. With Rhamm pI = 10.1, sodium bicarbonate buffer (pH 9.7) for control was used. Ligand density was determined from the average SPR response of six measurements. Proteins were coupled to the sensor plate using EDAC (100 mM) and sulfo-NHS (25 mM). (B) SPR screening of purified tubulin-derived peptides against Rhamm. Shown are sensograms generated by the interaction of 16 tubulin-derived peptides at a concentration of 10 µM. Screening generated 6 peptides (colored traces) which show high affinity to Rhamm. Black traces represent low affinity peptides. (C) Binding of fluorescein-labelled peptides to Rhamm ELISA binding assay (n = 3). Binding studies was performed at 25 µM and 50 µM concentrations of the peptide. Negative control (no immobilized Rhamm) was subtracted for each measurements.

[‡] Sensograms generated using this ligand density were used a control sensogram for each peptide screening.

After immobilization of Rhamm on the SPR sensor chip, injection of a series of tubulin derived peptides was carried out. Association of the peptides with Rhamm proceeded for 3 minutes and the dissociation in analyte free buffer was carried out for 10 minutes. Figure 16B shows the experimental sensograms obtained at a concentration of 10 µM. For each peptide injections, control sensograms (no immobilized Rhamm and buffer injection) were subtracted from the test sensogram, and the chip surface was regenerated prior to the next peptide injection in order to remove any remaining bound peptides. Screening of 17 peptides resulted in six potential peptide ligands for Rhamm namely: **4a** (VEGEGEEEGEEY), **5a** (SVEAEAEEGEEY), **12a** (EEDFGEEAEEEA), **13a** (GEFEEEAEEEVA), **14a** (EAFEDEEEEIDG), and **16a** (FTEAESNMNDLV). The affinity of these six peptides was also verified by ELISA at two different concentrations (Figure 16C).

3.2.3. Characterization of candidate tubulin-derived peptides

3.2.3.1. Affinity of tubulin-derived peptides to Rhamm

Since binding partners were established, the binding of six peptide candidates to Rhamm was quantified. Peptides were immobilized on the sensor plate and Rhamm was flowed to the derivatized surface at three different concentrations at a constant flow of 100 µL/mL. Figure 17 depicts the resulting sensograms at three concentration of Rhamm (500, 750 and 1000 nM). Again, each sensograms has been corrected by subtracting each curve from a reference sensogram (data achieved from sensograms without immobilized peptide) due to refractive index differences between running buffer and sample solution.

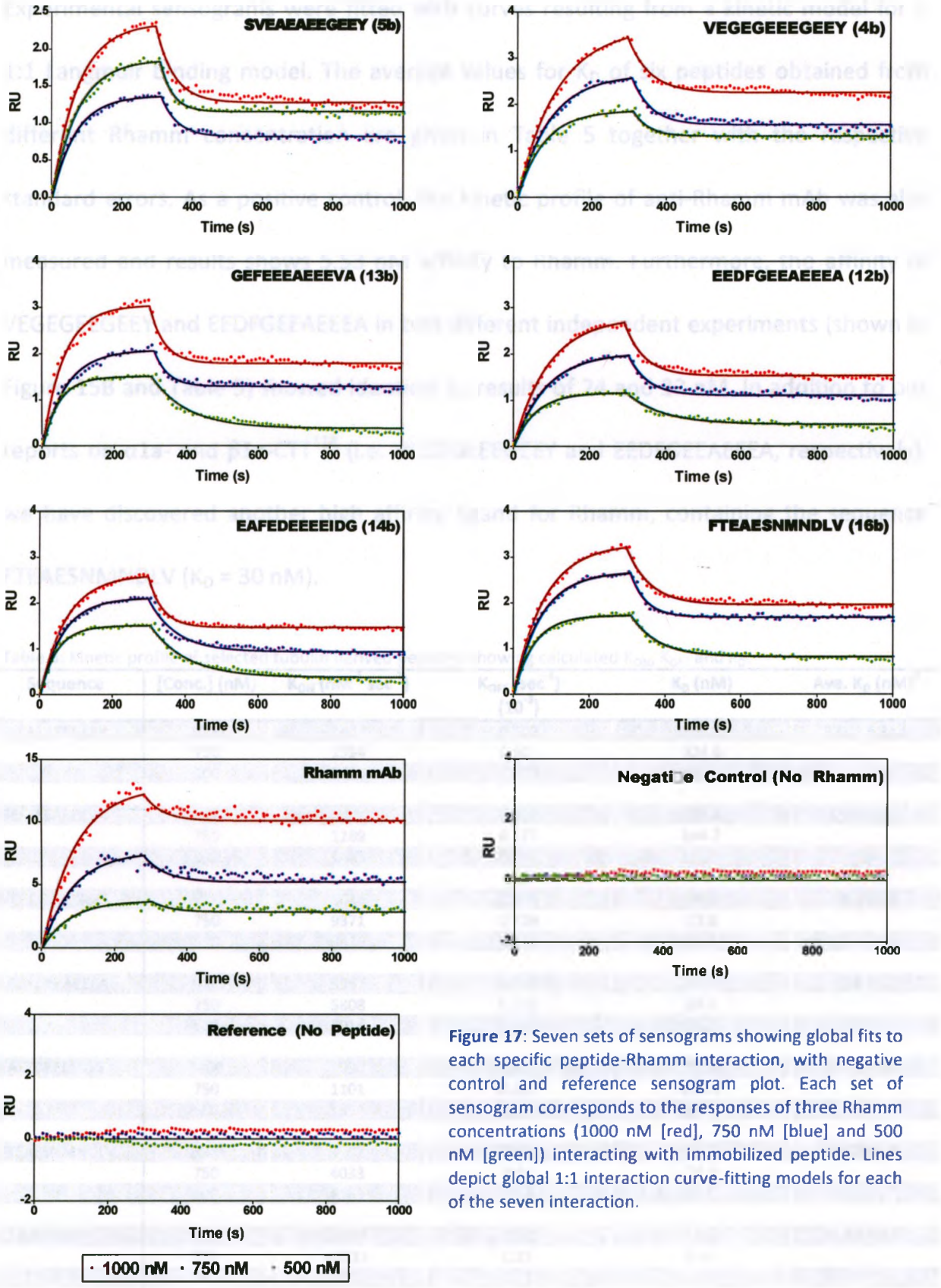

Figure 17: Seven sets of sensograms showing global fits to each specific peptide-Rhamm interaction, with negative control and reference sensogram plot. Each set of sensogram corresponds to the responses of three Rhamm concentrations (1000 nM [red], 750 nM [blue] and 500 nM [green]) interacting with immobilized peptide. Lines depict global 1:1 interaction curve-fitting models for each of the seven interaction.

Experimental sensograms were fitted with curves resulting from a kinetic model for a 1:1 Langmuir binding model. The average values for K_D of six peptides obtained from different Rhamm concentration are given in Table 5 together with the respective standard errors. As a positive control, the kinetic profile of anti-Rhamm mAb was also measured and results shows 5.53 nM affinity to Rhamm. Furthermore, the affinity of VEGEGEEGEEY and EEDFGEEAEEEA in two different independent experiments (shown in Figure 15B and Table 5) showed identical K_D results of 24 and 32 nM. In addition to our reports on α1a- and β1a-CTT[118] (i.e. VEGEGEEEGEEY and EEDFGEEAEEEA, respectively), we have discovered another high affinity ligand for Rhamm, containing the sequence FTEAESNMNDLV (K_D = 30 nM).

Table 5: Kinetic profile of selected tubulin derived peptides showing calculated K_{ON}, K_{OFF} and K_D.

Sequence	[Conc.] (nM)	K_{ON} (nM^{-1} sec^{-1})	K_{OFF} (sec^{-1}) (10^{-3})	K_D (nM)	Ave. K_D (nM)[§]
SVEAEAEEGEEY	1000	1404	0.502	358.2	331.1 ± 24.5
	750	1594	0.517	324.6	
	500	1620	0.503	310.4	
GEFEEEAEEEVA	1000	855	0.102	119.8	130 ± 12.9
	750	1189	0.172	144.7	
	500	1485	0.187	126.0	
VEGEGEEEGEEY	1000	5046	0.124	24.5	24.2 ± 0.4
	750	9371	0.224	23.8	
	500	9436	0.234	24.4	
EEDFGEEAEEEA	1000	5347	0.173	32.4	32.6 ± 1.1
	750	5808	0.196	33.8	
	500	7014	0.222	31.7	
EAFEDEEEEIDG	1000	1090	0.219	201.4	211.3 ± 8.6
	750	1101	0.237	215.4	
	500	1594	0.346	217.0	
FTEAESNMNDLV	1000	3202	0.10	31.9	30.2 ± 1.5
	750	4033	0.11	29.0	
	500	4189	0.12	29.6	
Rhamm mAb	1000	37484	0.22	5.96	5.53 ± 0.4
	750	42913	0.23	5.45	
	500	45172	0.23	5.18	

[§] Errors are standard deviation of the three measurement

As shown in Figure 16C, ELISA results show peptides **4c** (VEGEGEEEGEEY), **12c** (EEDFGEEAEEEA), and **16c** (FTEAESNMNDLV) showed the highest relative binding affinity in all concentrations, thus verifying SPR results. It is possible that the fluorophore modification has an effect on the ligand-Rhamm interaction or on non-specific binding, thus SPR and ELISA results might not exactly match.

3.2.3.2. Specificity of tubulin-derived peptides to the HA binding domain of Rhamm

A competitive ELISA was done to determine the selectivity of the peptides to the HA binding domain of Rhamm. In this assay, fluorescein-labelled peptides were used and the effectiveness of unlabelled HA to block the binding of peptides to Rhamm was evaluated. Fluorescein-labelled peptides (**4c**, **5c**, **12c**, **13c**, **14c** and **16c**) were added to ELISA plates containing immobilized Rhamm, followed by the addition of varying concentration of HA, which is the natural ligand of Rhamm. Thus, a decrease in observed fluorescence is seen as HA displaces the fluorescein-labelled peptides if they compete for the same binding site. Figure 18A shows competitive displacement of peptide binding to Rhamm by HA, and a concentration dependent decrease in fluorescence is observed for all six ligands as the HA competitor concentration increases.

An alternative competition experiment was devised to further assess the peptide ligands since the presence of the label can influence the physical properties of the compound and the resulting binding potential. Using ELISA, unlabelled peptides (**4a**, **5a**, **12a**, **13a**,

14a and **16a**) were used to compete with dye-labelled HA. This assay eliminates confounding results arising from the interaction between the dye label and protein or a change in affinity caused by the addition of a bulky dye to the peptide ligand. As shown in Figure 18B, displacement of labelled-HA by non-fluorescent peptides derived from tubulin is readily observed by decrease of the fluorescence signal. Ligands **16a** or **16b** (FTEAESNMNDLV) and **12a** or **12c** (EEDFGEEAEEEA) appear especially able to compete for the binding with HA consistently, thus reinforcing our notion that further modification at the amino terminus of the peptide has little effect on the binding to Rhamm. However, fluorescein-labelled α1a-CTT (**4c**), which contains the sequence VEGEGEEEGEEY, seemed better at competing with HA compared to unmodified peptide (**4a**).

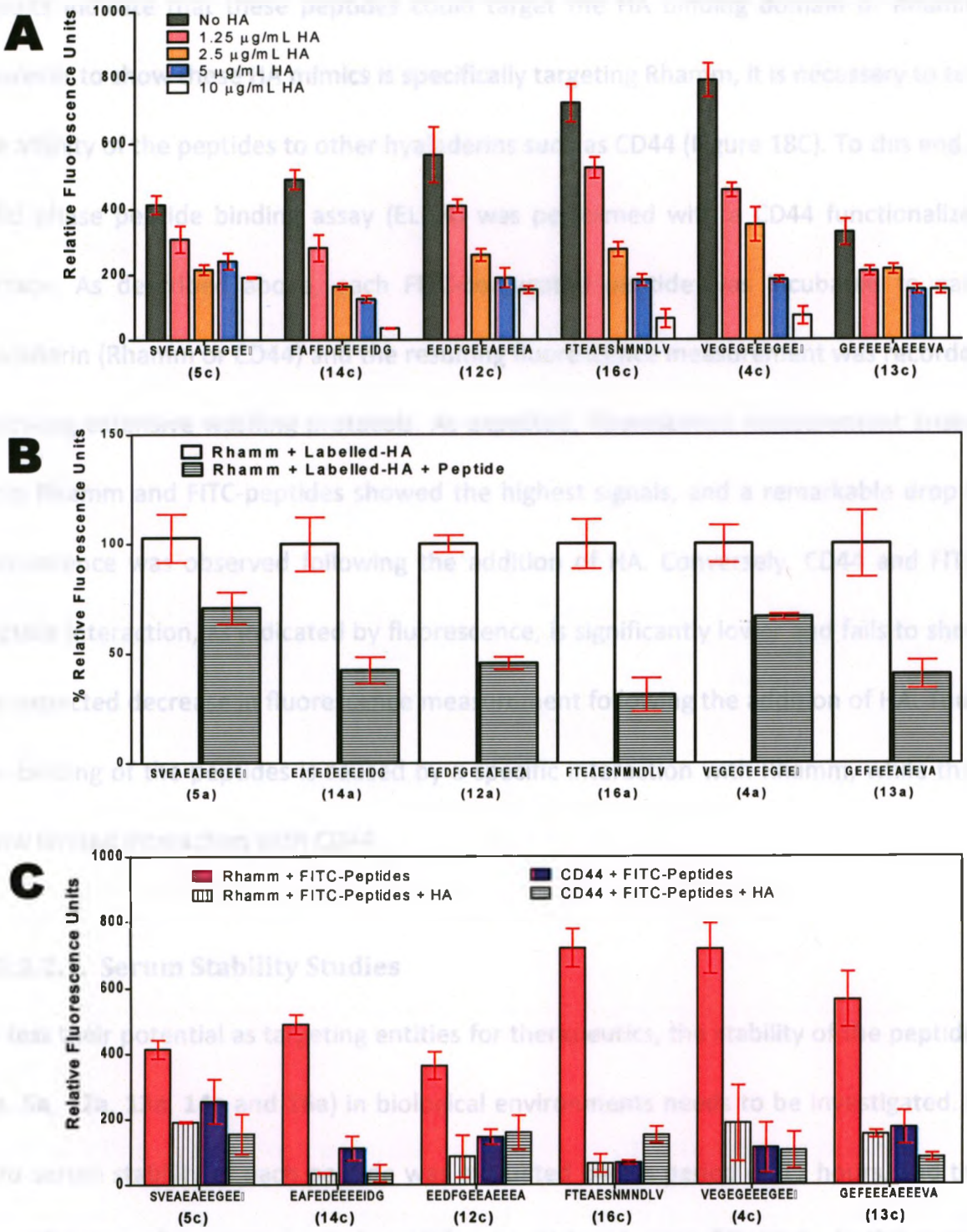

Figure 18: (A) Shows competitive displacement of six selected fluorescein-labelled peptides by HA, (B) Competitive displacement of dye-labelled HA by non-labelled tubulin-derived peptides using solid phase binding assay, and (C) shows ELISA binding assay of FITC-conjugated peptides and purified CD44. Negative control (no immobilized Rhamm or CD44) was subtracted for each measurement. For figures B and C, 10 µg/mL concentration of the peptides and HA was used in all cases.

Results indicate that these peptides could target the HA binding domain of Rhamm. However to show these HA mimics is specifically targeting Rhamm, it is necessary to test the affinity of the peptides to other hyaladerins such as CD44 (Figure 18C). To this end, a solid phase peptide binding assay (ELISA) was performed with a CD44 functionalized surface. As described above, each FITC-conjugated peptide was incubated to each hyaladerin (Rhamm or CD44) and the resulting fluorescence measurement was recorded following extensive washing protocols. As expected, fluorescence measurement arising from Rhamm and FITC-peptides showed the highest signals, and a remarkable drop in fluorescence was observed following the addition of HA. Conversely, CD44 and FITC-peptide interaction, as indicated by fluorescence, is significantly lower and fails to show the expected decrease in fluorescence measurement following the addition of HA. Thus, the binding of the peptides is caused by a specific interaction with Rhamm, while they show limited interaction with CD44.

3.2.3.2.1. Serum Stability Studies

To test their potential as targeting entities for therapeutics, the stability of the peptides (**4a**, **5a**, **12a**, **13a**, **14a** and **16a**) in biological environments needs to be investigated. *In vitro* serum stability of each peptide was evaluated over a period of 11 hours, and the quantification of remaining intact peptide was deduced using RP-HPLC. In this assay, the peptides are subjected to fetal bovine serum at 37^{O}C, and aliquots were taken at 30 minute intervals. At each time point, the reaction was stopped by precipitating serum protein with trifluoroacetic acid (TFA), and centrifuged to obtain the peptides for further

analysis. Unmodified tubulin derived peptides showed serum stability with a reasonable half-life of approximately 2-4 hours (Figure 19).

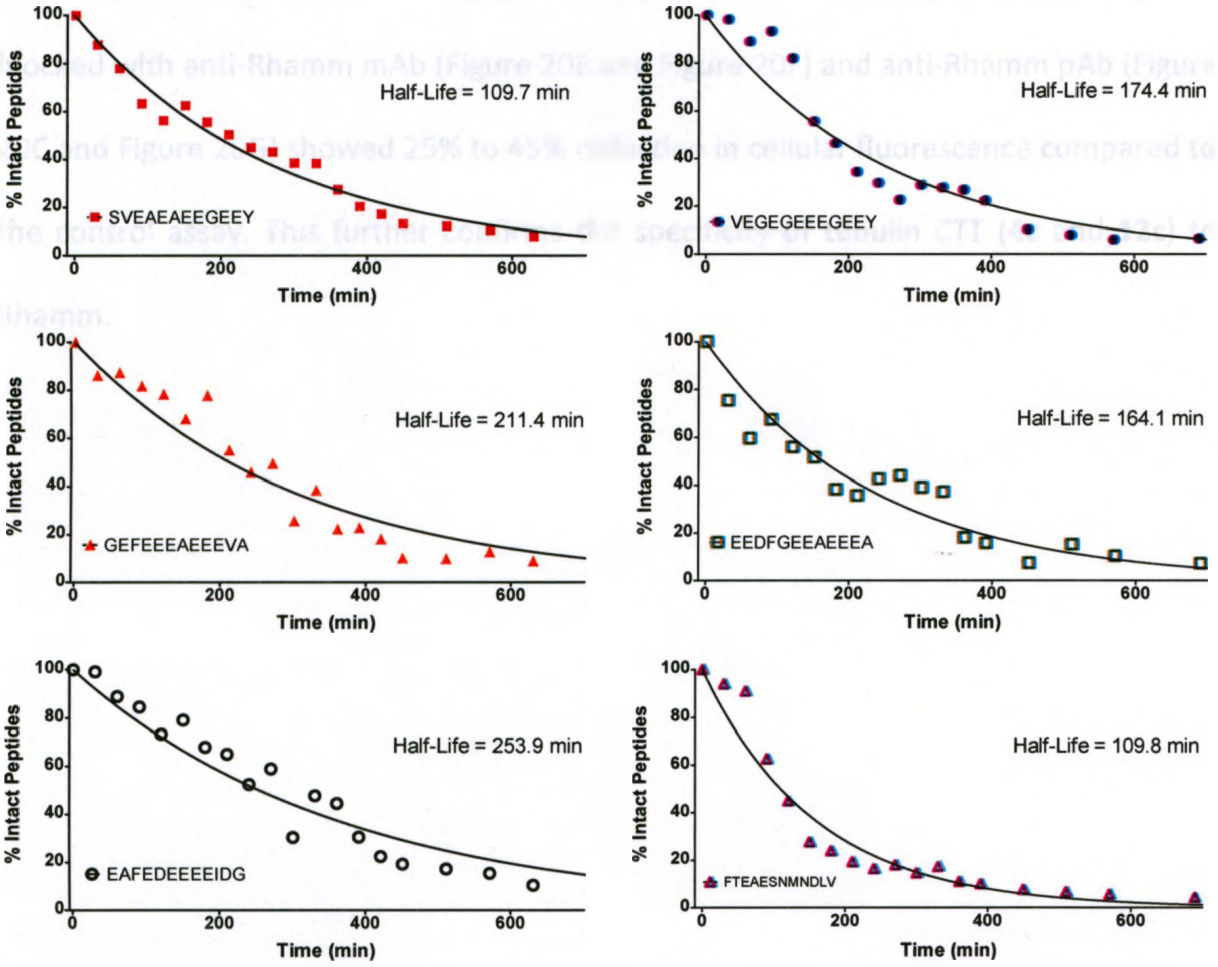

Figure 19: Serum stability study of six tubulin-derived peptides under physiological conditions in fetal bovine serum. The percentage of intact peptides at 30 minute increments for 11 hours is plotted as a function of time. Data were fitted to a first order exponential decay curve.

3.2.3.2.2. Tubulin-derived peptides as imaging probes for breast cancer

To determine the specificity of tubulin derived peptides to Rhamm expressing cells and its potential as targeting entity, a cellular fluorescence assay was performed using MDA-MB-231 (a breast cancer cell line) cells treated with anti-Rhamm antibody. MDA-MB-231 breast tumour cell line shows high expression of Rhamm receptors,[114] thus this cell line was an ideal choice for evaluation of the specificities of tubulin CTTs. MDA-MB-231 cells

were incubated with FITC-conjugated tubulin CTT (**4c** and **12c**) and cellular uptake of the probe was measured. Probe uptake in cells treated with non-specific antibody (i.e. IgG antibody) showed high uptake of probe (Figure 20A and Figure 20E); however, cells blocked with anti-Rhamm mAb (Figure 20B and Figure 20F) and anti-Rhamm pAb (Figure 20C and Figure 20G) showed 25% to 45% reduction in cellular fluorescence compared to the control assay. This further confirms the specificity of tubulin CTT (**4c** and **12c**) to Rhamm.

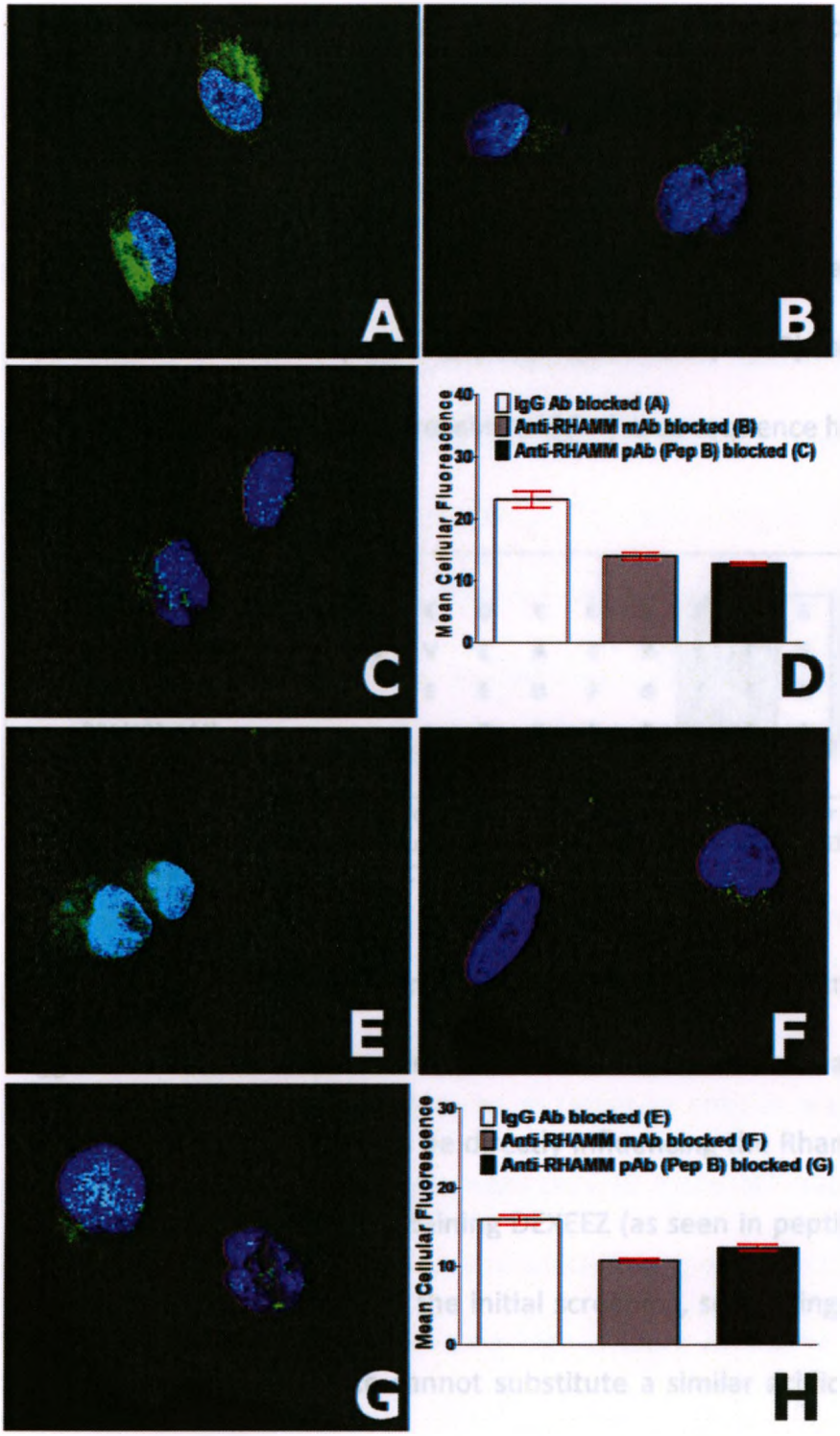

Figure 20: Visualization and quantification of uptake of FITC-conjugated α1a-and β1a-tubulin CTT in breast tumour cells (MDA-MB-231) using fluorescence imaging. Nuclei are shown in blue (DAPI) while fluorescein- conjugated peptides are shown in green. Cells (A), (B) and (C) were incubated with FITC-conjugated α1a-CTT, while cells (E), (F) and (G) were incubated with FITC-conjugated β1a-CTT. Prior to the addition of FITC-conjugated peptides, cells were incubated with antibody blocked with different antibodies specific for the HA binding region of Rhamm. Cells blocked with anti-mouse IgG (A) and (E) serves as positive control since the antibody shows no binding affinity to Rhamm. In (B) and (F), cells were treated with anti-Rhamm mAb. Anti-Rhamm (Pep B) pAb were added to (C) and (H). Quantification of cellular uptake of FITC-labelled peptides representing α1a- (D) and β1a-CTT (E) in MDA-MB-231 breast cancer cell line. ROI corresponding to cell bodies (121 ROI, n = 3) were selected. Mean fluorescence of each ROI was then calculated using 8-bit acquired data. Data were analyzed using one-way ANOVA.

3.2.3.2.3. Common Rhamm binding domain

The described results shown in this report suggest the presence of a common site for the HA binding domain of Rhamm at the variable carboxy terminal moieties of tubulin. A

recurring hexapeptide motif was noted in most peptide candidates, and peptides sharing this acidic carboxy-terminal segment interacted with Rhamm. The motif, EEXEEZ (where X is A or G, and Z is Y or E), is present in synthetic αIa (**4a**), αIIIc (**5a**), βIa (**12b**), and βIV-CTT (**13a**) (Figure 21). Our present results are in agreement with the previous reports that the short sequence EEGEE (Paschal *et al.*, 1989) could be involved in tubulin and MAP binding, a family of proteins which shares sequence homology to Rhamm.[119]

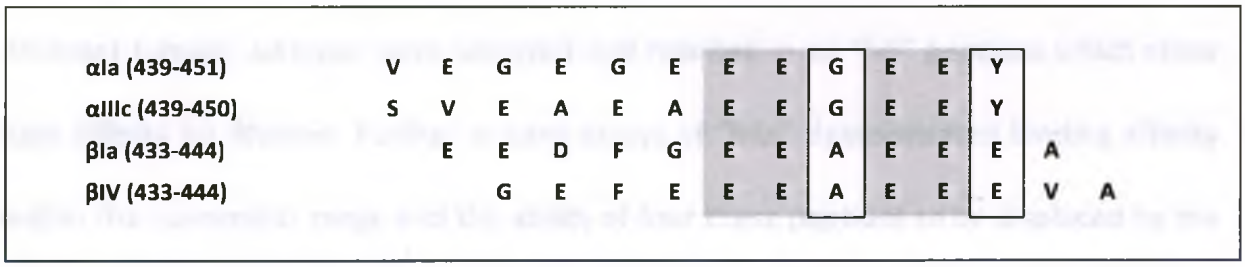

Figure 21: Sequence alignment of the four candidate tubulin CTTs as hyaluronan mimics. Identical sequences are shown in grey while semi-conserved sequences are boxed. Hexapeptide motif, EEXEEZ (where X is A or G, and Z is Y or E), could be the Rhamm binding region. CTTs were aligned with ClustalX2.

Despite the role of acidic functional groups in HA and Rhamm interaction, results also suggest that the random occurrence or an increase of these acidic residues within the CTT region does not appear to be directly influencing the Rhamm-tubulin interaction. It is surprising that peptides containing DEXEEZ (as seen in peptides **2** and **6**) and EEXEDZ (e.g. peptide **11**) motifs failed the initial screening, suggesting that Asp residues within the first and fifth sequence cannot substitute a similar acidic Glu residues within this motif. This might suggest that the CTT interaction with Rhamm is mediated by both electrostatic forces and conformational effects.

3.3. Conclusion

Using bioinformatics and prior literature, a connection between Rhamm and tubulin associated proteins was established. Due to moderate homology between the tubulin binding domain of MAPs and HA-binding domain of Rhamm, further investigation was performed to determine which peptide fragments of tubulin interacts with Rhamm. In this study, the specific interaction between Rhamm and novel ligands were deduced. Using SPR screening, synthetic peptides corresponding to the carboxy terminus of different tubulin subtypes were analyzed and resulted in six "hit" peptides which show high affinity for Rhamm. Further *in vitro* assays of "hits" demonstrated binding affinity within the nanomolar range and the ability of four these peptides to be displaced by the endogenous HA demonstrated specificity to the hyaluronan binding domain of Rhamm. Also, the greater affinity of these peptides to Rhamm compared to another hyaladerin (i.e. CD44) further confirms specificity.

The potential of these small peptides as targeting entities was explored using stability studies and a cell based assay. Peptides showed moderate stability (approximately 110-250 minutes half-life) in bovine serum, which is long enough to facilitate *in vivo* imaging. Interestingly, tumour cells expressing high amount of Rhamm showed high uptake of fluorescein-conjugated probes, and this uptake is effectively blocked by anti-Rhamm. This study represents a promising proof of concept for determining novel peptide candidates using a combination of rational approach and SPR screening.

3.4. Experimental

3.4.1. Materials

All solvents were used without further purification, and purchased from VWR, Fisher Scientific, or Sigma Aldrich. Fmoc-Rink amide MBHA (100-200 mesh) resin, Fmoc amino acids and HBTU coupling reagent (2-(1*H*-benzotriazole 1-yl)-1,1,3,3-tetramethyluronium hexafluorophosphate) for peptide synthesis were obtained from Peptides International. EDAC (*N*-(3-dimethylaminopropyl)-*N*'-ethylcarbodiimide hydrochloride), sulfo-NHS (*N*-hydroxysulfosuccinimide sodium salt) and fluorescein isothiocyanate isomer I (FITC) were purchased from Sigma Aldrich. NHS-Biotin was obtained from Nova BioChem.

3.4.2. Peptide Synthesis

Elongation of peptidyl resins and purification of peptides were carried out as outlined in section **2.4.1.** Acylation of the amino terminus was done (15 and 10 minutes) using 10% acetic anhydride in DMF following Fmoc deprotection. FITC coupling was carried out using FITC fluorescent dye (4 equiv.) and DIPEA (2 equiv.) in DMF for 4 hours.

Full deprotection of cysteine-containing peptides was accomplished using a solution of 94% v/v trifluoroacetic acid (TFA), 1% v/v triisopropylsilane (TIPS), 2.5% v/v H_2O and 2.5% v/v 1,2-ethanedithiol (EDT) for 1-1.5 hours. Full deprotection of all other peptides was done using a solution of 88% v/v TFA, 5% v/v water, 5% m/v phenol, 2% v/v TIPS for 2-4 hours. The filtrate was collected, precipitated using cold tert-butyl methyl ether and

pelleted via centrifugation at 3000 rpm and -5^{0}C for 10 minutes. Pellets were then dissolved in distilled-deionized water and lyophilized yielding solid powders.

3.4.3. ELISA binding assay (biotin-conjugated peptides)

A 96-well plate coated with Rhamm (100 µg/mL) was incubated at 4^{O}C for 1 hour. Plates were washed three times with 200 µL 0.1% TBST. BSA with 0.1% TBST was added and plates were incubated at 4^{O}C for 4 hours. Biotin-conjugated peptides (50 µL of 50 µM or 100 µM) or HA (50 µL of 20 µg/mL) were added to the wells. Control plates received 50 µL 0.1% TBST. Plates were washed three times with TBST. AP-conjugated streptavidin goat anti-mouse IgG (100 µL of 1 mg/mL) were added at room temperature followed by 1 hour incubation. Wells were washed three times with TBST. 100 µL of p-nitrophenyl phosphate (PNPP) (1 tablet in 20 mL APase buffer) was added at room temperature and absorbance at 405 nm was recorded for each well.

3.4.4. Competitive ELISA experiment using a fluorescein-conjugated peptides

ELISA was carried out to test the ability of FITC-labeled tubulin-derived peptides compete with HA for binding site with RHAMM. Recombinant Rhamm (100 µL, 10 µg/mL in 0.05M PBS, pH = 9) was immobilized on 96-well ELISA plates (final concentration of 1 µg/well) and incubated overnight at 4^{O}C. resulting in final amount of protein 1 ug/well. Plates were washed three times with (0.05%) PBS-Tween-20 buffer (200 µL/well), washed with blocking buffer (5% 200 µL/well, PBS-Tween-20)/well), and incubated for 1 hour at room temperature. Following three washes as described above, FITC-labeled tubulin derived peptides (final concentration of 1 µg/mL) and HA (100

µL/well, M.W. 220 kDa, 10 µg/mL in PBS, serial dilutions have been made for HA = 1:1, 1:2, 1:4, 1:8, 1:16) were added to plates and incubated overnight at 4^{O}C. Plates were washed as described above, and absorbance was measured at 485/535 nm.

3.4.5. SPR binding assay of peptides to immobilized Rhamm

ProteON XPR36 system was used for the selection and ranking of different tubulin derived peptides against Rhamm. For immobilization of Rhamm, the ProteON GLC sensor chip surfaces were activated by amine coupling using 100 mM EDAC and 24 mM sulfo-NHS. Rhamm (30 µg/mL in sodium bicarbonate buffer, pH 9.7) was injected at a flow of 30 µl/min. A buffer sample was injected on a different sensor plate for use as a reference. Ethanolamine HCl (1M, pH 8.5) was then injected to deactivate any remaining surface groups. Peptides (10 µM in PBS-T, 2% DMSO) were injected to a Rhamm functionalized surface at 50 µL/min for 3 minutes followed by a 10 minute dissociation (i.e. injection of PBS-T buffer) period. The surfaces were regenerated using two injections of 30 µL of 1M NaCl prior to the injection of the next peptide. In all experiments, reference subtraction was performed using data obtained from reference plate (No Rhamm) and Rhamm functionalized plate.

3.4.6. SPR binding assay of Rhamm to immobilized peptides

After peptide screening, GWC SPRimager®II system was used to determine binding kinetic constants. Thiol containing peptides (Figure 14b, Table 2) were immobilized on a maleimide-functionalized gold-plated chip. For binding studies, a series of concentrations of Rhamm (in milliQ water) were injected over the immobilized peptides.

After a 15 min dissociation phase, the sensor chip surface was regenerated for the next peptide sample injection, via treatment with two 1 min pulse injections of regenerating buffer (2 M NaCl in HBS-EP, pH 7.4) at 100 mL/min. Baseline returned to the initial value after the regeneration step, confirming the removal of all bound analytes. Data were analyzed and the corresponding dissociation constants (K_D) were obtained via non-linear regression fitting to a Langmuir binding model.[120] In all experiments, reference subtraction was performed using data obtained from reference plate (no peptide) and peptide functionalized plate.

3.4.7. Serum Stability Study

The stability of tubulin CTTs in serum was evaluated for up to 11 hours. Each peptides were mixed with pre-heated (37^{O}C, pH 7.3 ± 0.1) fetal bovine serum (FBS), (final sample volume of 3 mL and peptide concentration of 15 µM). The initial time is recorded, and at each 30 minute time point, 40 µL aliquots were taken from the reaction mixture and passed through C18 reverse-phase (C18 Sep-Pak©) cartridge. Peptides were eluted from the cartridge using 3 mL ethanol (70% v/v) with 0.1% TFA, lyophilized, and analyzed using analytical RP-HPLC (Grace Vydac Protein/Peptide RP-C18 column 4.6 x 250 mm, 5 µm). Employed mobile phase of this system were 0.1% TFA in water (eluent A) and 0.1% TFA in CH3CN (eluent B). Linear gradient of 10-95% of eluent B at a flow rate of 1.5 ml/min over 20 minutes was used for each peptide sample. Percent intact peptides were detected using Waters 2998 Photodiode array detector set at 220 and 254 nm,

and identified using ESI-MS. Half-life of peptides were determined using GraphPad Prism version 5.01.

3.4.8. Cell Uptake Study

Cell uptake studies and quantification of cellular fluorescence were carried out according to protocols written on **2.4.5**. For blocking experiment, antibodies (IgG antibody, anti-Rhamm (Pep B) pAb and anti-Rhamm mAb) in serum free media were added and incubated at 37^{O}C for 10 minutes.

4. Library-Based Approach: One-bead One-Compound Library for Hyaluronan Mimetic Peptides

4.1. Design and Screening of OBOC Library

Hyaluronan is a glycosaminoglycan implicated in development, cellular repair and disease processes.[15] HA binds to cell-surface receptors, such as CD44 and Rhamm, which results in its uptake and signalling cascade which ultimately lead to cell migration and invasion.[121] As discussed in Chapter 1, the over-expression of Rhamm and its resulting interaction with HA has been implicated in the pathology of cancers. HA mimicking peptides may serve as antagonists that could block the Rhamm-HA interaction thus limiting the transforming potential of Rhamm. Furthermore, these peptides could also be useful for imaging probe development and drug targeting.

Another method of discovering novel high affinity peptide sequences for Rhamm involves the use of a combinatorial peptide library. Using split-mix synthesis method, a library of 8-mer peptides that mimic the binding capability of HA to Rhamm was developed. The employed library consists of beads charged with random peptides consisting of D-amino acids, thus offering proteolysis resistance to the resulting peptide candidate. Thus, the beads generated represent a collection of peptides which arises from random combination of D-amino acids. In this study, the aforementioned synthetic peptide library was screened against Rhamm, thus allowing *de novo* discovery of new candidates for HA mimetics.

4.2. Results and Discussion

4.2.1. Screening of OBOC Library

An eight amino acid library was synthesized on 90 µm TentaGel beads and screened using Rhamm. The library contains random sequences consisting of nineteen D-amino acids (excluding cysteine). The library was screened *en masse* (approximately 1/3 of the library) to identify candidates which bind to Rhamm using an assay which separates beads based on their affinity for Rhamm (Figure 22).

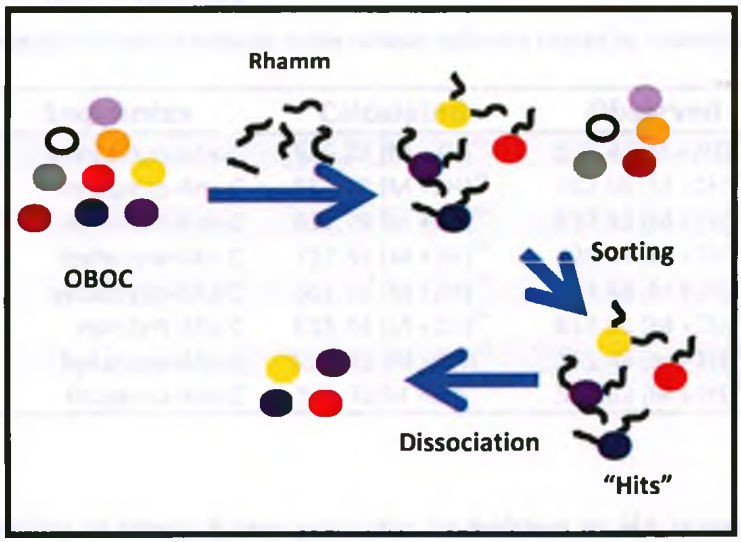

Figure 22: Screening of combinatorial peptide library

Beads containing bound Rhamm were identified and sorted. The peptide sequence for each bead was elucidated by MALDI-TOF mass spectrometry, and re-synthesized for testing in biological assay. Table 6 summarizes the resulting characterization of synthesized 15 "hit" peptides. Lower case letters denotes amino acids with D-configuration.

Table 6: Sequences of HA-mimetic peptides.

Compound	Sequences**	Calculated	Observed	Purity
20a	lpmvamgh	428.2 $[M+2H]^{2+}$	429.1 $[M+2H]^{2+}$	99
21	rpdyranq	510.2 $[M+2H]^{2+}$	510.7 $[M+2H]^{2+}$	97
22a	evgqpnfp	452.7 $[M+2H]^{2+}$	453.2 $[M+2H]^{2+}$	99
23a	erfhedpe	529.8 $[M+2H]^{2+}$	530.4 $[M+2H]^{2+}$	97
24a	fpyfwyew	619.3 $[M+2H]^{2+}$	619.2 $[M+2H]^{2+}$	98
25	yenykdqf	553.3 $[M+2H]^{2+}$	553.7 $[M+2H]^{2+}$	99
26	yedqmyee	553.2 $[M+2H]^{2+}$	554.1 $[M+2H]^{2+}$	95
27a	yedkmyee	553.2 $[M+2H]^{2+}$	554.2 $[M+2H]^{2+}$	99
28	qddlehwr	549.3 $[M+2H]^{2+}$	550.5 $[M+2H]^{2+}$	80
29	kfpsqnne	482.2 $[M+2H]^{2+}$	482.7 $[M+2H]^{2+}$	98
30a	nprntrrt	564.3 $[M+2H]^{2+}$	564.6 $[M+2H]^{2+}$	98
31	ksynrnpe	504.3 $[M+2H]^{2+}$	504.9 $[M+2H]^{2+}$	98
32a	hplaqqea	447.2 $[M+2H]^{2+}$	448.3 $[M+2H]^{2+}$	99
33	vymkrded	527.7 $[M+2H]^{2+}$	528.3 $[M+2H]^{2+}$	94
34a	fhqygnsa	461.7 $[M+2H]^{2+}$	462.2 $[M+2H]^{2+}$	98

4.2.2. Affinity of "Hit" Peptides

Table 7: HA-mimetic peptides containing cysteine in the carboxy-terminus spaced by aminohexanoic acid linker moiety.

Compound	Sequences	Calculated	Observed	Purity
20b	lpmvamgh-Ahx-C	536.27 $[M+2H]^{2+}$	536.43$[M+2H]^{2+}$	98
22b	evgqpnfp-Ahx-C	552.78 $[M+2H]^{2+}$	552.66 $[M+2H]^{2+}$	97
23b	erfhedpe-Ahx-C	637.79 $[M+2H]^{2+}$	637.98 $[M+2H]^{2+}$	98
24b	fpyfwyew-Ahc-C	727.33 $[M+2H]^{2+}$	725.87 $[M+2H]^{2+}$	95
27b	yedkmyee-Ahx-C	661.28 $[M+2H]^{2+}$	661.48 $[M+2H]^{2+}$	97
30b	nprntrrt-Ahx-C	615.84 $[M+2H]^{2+}$	614.61 $[M+2H]^{2+}$	96
32b	hplaqqea-Ahx-C	555. 29 $[M+2H]^{2+}$	555.46 $[M+2H]^{2+}$	98
34b	fhqygnsa-Ahx-C	569.76$[M+2H]^{2+}$	568.62 $[M+2H]^{2+}$	98

To validate the ability of these 8-mer peptides to behave as HA mimics, eight peptides (Table 7) were synthesized containing cysteine residue in the carboxy terminus spaced by aminohexanoic acid linker. Since peptides are conjugated to Tentagel beads via the C-terminus, the amino terminus of the peptide is exposed and potentially could be interacting with the protein during screening, thus additional modification (i.e. attachment of different moieties for further characterization) is placed on the carboxy-

** Lowercase letters represent D-configuration of amino acids

terminus. The resulting cysteine-conjugated peptides were immobilized onto a surface plasmon resonance (SPR) sensor plate and their affinity for Rhamm was determined.

Compd	K_D (nM)
20b	414
22b	158
23b	124
24b	608
27b	101
30b	764
32b	134
34b	414

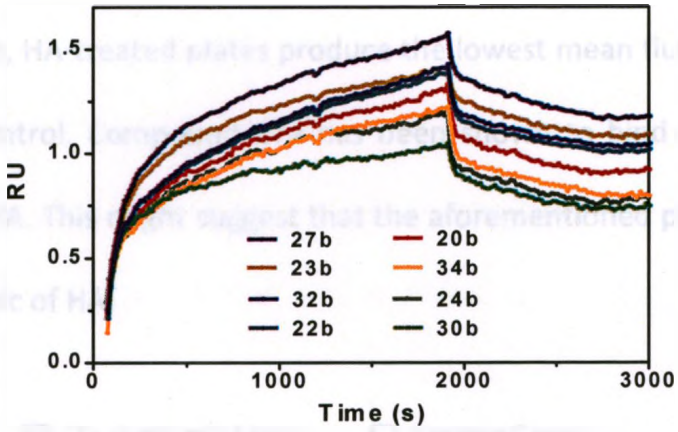

Figure 23: Dissociation constants of selected peptides and their corresponding SPR sensogram.

Experimental sensograms were fitted to a 1:1 Langmuir model to calculate dissociation constants (K_D) for each peptide (Figure 23). Compound **27b**, containing the sequence yedkmyee, showed the highest affinity to binding affinity to Rhamm and had a calculated K_D of 101 nM.

4.2.3. Specificity of "Hit" Peptides

Using SPPS, compound **27a**, which showed the highest binding affinity to Rhamm, was synthesized and the binding affinity to Rhamm was examined using ELISA (Figure 24). In this assay, GST-Rhamm was immobilized, and was followed by the addition of analytes (**27a** or HA) onto each ELISA plate. To examine the binding affinity, HA-conjugated fluorescent beads were added to compete with the binding of each analyte to Rhamm. After repeated washing, mean fluorescence at 505 nm was recorded. Positive control

group, which produces the highest fluorescence counts upon addition of HA-conjugated fluorogenic beads, contains only Rhamm; therefore, peptides that compete with HA-conjugated fluorescent beads would produce a lower mean fluorescence. Since HA is the natural ligand of Rhamm, HA-treated plates produce the lowest mean fluorescence, thus serving as negative control. Compound **27a** has been shown to bind directly to Rhamm and compete with HA. This might suggest that the aforementioned peptide **27a** is capable of acting as a mimic of HA.

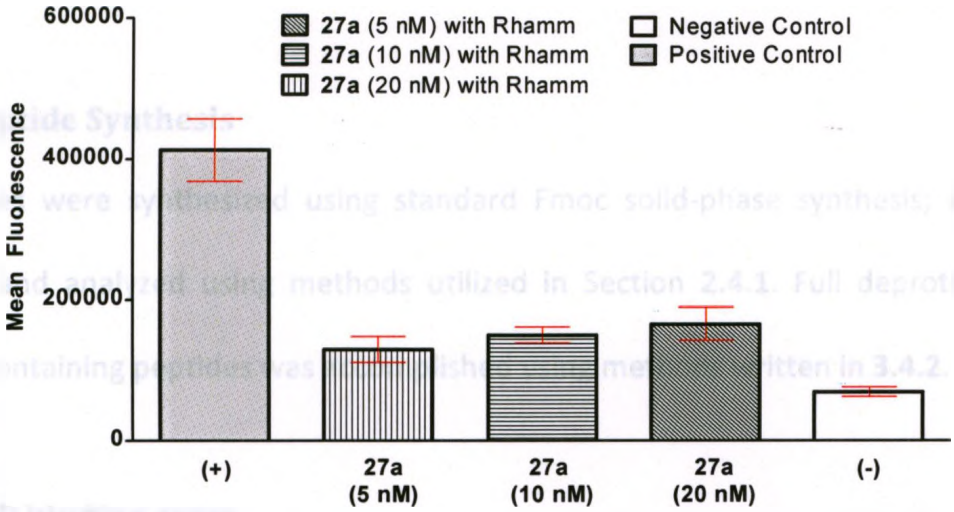

Figure 24: Competitive binding assay of **27a** using ELISA. In each assay, GST-Rhamm bound to a 96-well plate was used as the primary protein. HA-conjugated fluorescent beads were used as competitor and fluorogenic substrate to monitor binding assay. Positive control plates were treated with HA-conjugated fluorescent beads, while negative control plates were treated with both HA and HA-conjugated fluorescent beads. Background (no immobilized Rhamm) was subtracted for each treatment group. Data are the mean of four experiments, analyzed using ANOVA (all data are statistically significant compared to positive and negative control groups, $p<0.01$), and error bars shown are the standard error of the mean. $P<0.05$ was considered significant.

4.3. Conclusion

Elucidation of novel targeting entities for Rhamm using a library-based method yielded 17 potential ligands for Rhamm. Eight peptides were selected from the pool of hit peptides and their binding affinities to Rhamm was calculated using SPR. Peptides showed moderate binding affinities ranging from 0.1-0.7 μM. Furthermore, compound

27 which had calculated K_D of 101 nM showed specificity to the HA binding domain of Rhamm.

4.4. Experimental

Tentagel beads (90 µm, 0.5 mmol/g), Fmoc-rink amide MBHA, Fmoc D- and L-amino acids, and HBTU coupling reagents were purchased from Peptides international. All solvents were purchased from Sigma Aldrich and/or Fisher used without further purification.

4.4.1. Peptide Synthesis

All peptides were synthesized using standard Fmoc solid-phase synthesis; and then prepared and analyzed using methods utilized in Section **2.4.1**. Full deprotection of cysteine-containing peptides was accomplished using methods written in **3.4.2.**

4.4.2. SPR binding assay

Protocols and calculations were carried out using protocols outlined in section **3.4.5**.

4.4.3. Competitive ELISA experiment using fluorescent HA-beads

A 12-well plate coated with 0.1 mg/mL Rhamm was incubated at $4^{O}C$ overnight and washed three times with 0.1% TBST. BSA blocking solution was added and incubated for 4 hours at room temperature. Then, 50µL HA (1 mg/mL) or peptides was added (5 nM, 10nM, or 20 nM) in 0. 1% TBST to the corresponding wells at $4^{O}C$ and incubated for 2 hours. Negative control wells were not treated with Rhamm. Positive control plates

(with immobilized Rhamm) were treated only with HA fluorescent beads. 100 µL of 0.1% TBST was added to each plate and fluorescence was recorded for each well.

5. Synthesis and Characterization of Rhenium *fac* Tricarbonyl Complexes containing *Bis*-(1-Methylbenzimidazol-2-yl) Ligands

5.1. Introduction

Recently, rhenium (I) complexes containing the *fac*-$M(CO)_3^+$ moieties were highlighted for their potential as surrogates for *fac*-$^{99m}Tc(CO)_3^+$ complexes, which are fundamental in development of radioactive products for diagnostic applications. The $M(CO)_3^+$ core (M = Re/Tc) is chemically inert due to its low-spin d^6 M(I) center, and limited facial coordination sites about the metal due to the other three facially disposed carbonyl donors.

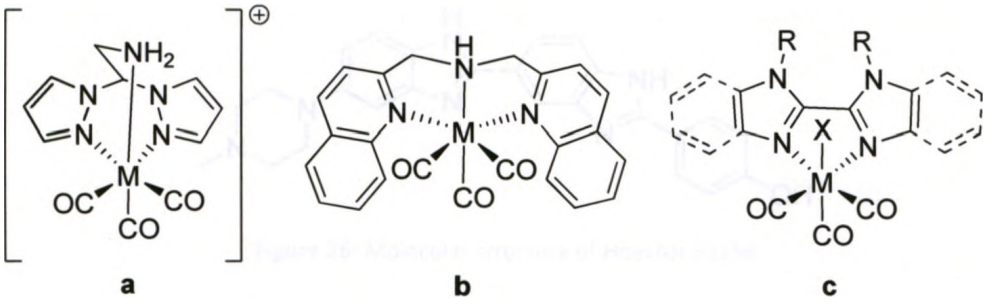

Figure 25: Examples of $Re(CO)_3^+$ chelators.

It has been shown that $^{99m}Tc/Re(CO)_3^+$ chelators containing *N*-heterocyclic donors produces complexes that have high *in vivo* and *in vitro* stability.[122,123] For example, bis(pyrazolyl)ethylamine $^{99m}Tc(CO)_3^+$ complexes (Figure 25a) has been used to monitor myocardial perfusion.[124] Furthermore, bis-(quinolin-2-ylmethyl)amine $^{99m}Tc(CO)_3^+$ complexes (Figure 25b) has been conjugated to the primary amine of bioactive molecules such as fMLF (a peptide containing the sequence N-formyl derivatized Met-

Leu-Phe), a peptide that binds to the formyl peptide receptor which is over-expressed in leucocytes.[125,126]

Bibenzimidazoles have received much attention because of its potential to act as an antiviral agent[127], fluorogenic agent[128] and are effective chelating agents for transition metal ions. [129,130,131] For instance, Hoechst 33258 is a widely used fluorescent probe of chromosomal DNA structure (Figure 26).[128] Also, bibenzimidazoles tend to be very robust and remain stable under thermal and chemical stresses.[132] Bibenzimidazoles are also easily derivatized to attain the desired spectral properties for use as luminescent compounds.[133,134]

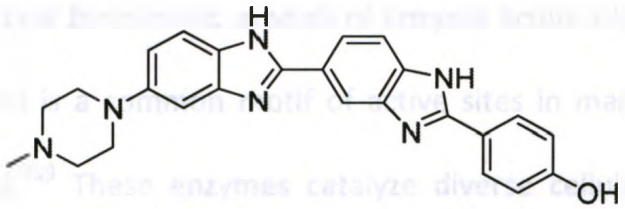

Figure 26: Molecular structure of Hoechst 33258.

Rhenium 2,2'-biimidazole and 2,2'-bibenzimidazole rhenium tricarbonyl complexes (Figure 25c) are important precursors for the construction of luminescent molecular and supramolecular assemblies.[135,136] However, to date, no reports were published which utilizes 2,2'-bibenzimidazole rhenium tricarbonyl complexes for molecular imaging.

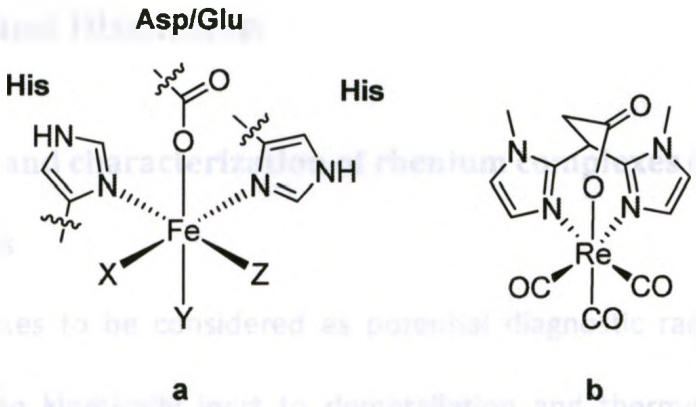

Figure 27: (a) Model of 2-His-1-carboxylate facial triad, a common active site motif in non-heme iron(II) enzymes. (b) An example of 2-his-1-carboxylate facial triad ligand (i.e. 3,3-bis(imidazol-2-yl)propionic acid) coordinated to rhenium tricarbonyl core.

The histidine imidazole moiety is essential for the coordination of metals in metalloproteins; therefore complexes containing ligands consisting of imidazole derivatives are important biomimetic models of enzyme active sites. [137,138] The 2-His-1-carboxylate facial triad is a common motif of active sites in many non-heme iron (II) enzymes (Figure 27a).[139] These enzymes catalyze diverse cellular processes such as metabolism of amino, nucleic and fatty acids. Tripodal N,N,O-ligands, such as 3,3-bis(1-methylimidazol-2-yl)propionic acid (Figure 27b), mimic this binding geometry and also allows for facial coordination of rhenium tricarbonyl core.

With the aim of further exploring novel Re(I) complexes for molecular imaging, bi- and tridentate ligands with a functionalized bis-(1methylbenzimidazol-2-yl) moiety was synthesized and complexation with rhenium tricarbonyl core was studied using spectroscopic techniques such as UV/Vis, NMR and mass spectrometry.

5.2. Results and Discussion

5.2.1. Synthesis and characterization of rhenium complexes containing bidentate ligands

For metal complexes to be considered as potential diagnostic radiopharmaceuticals, complexes must be kinetically inert to demetallation and thermodynamically stable towards hydrolysis at physiological pH. To this end, multidentate ligands that forms 5- and 6-membered chelate rings upon coordination to a metal are most commonly utilized.

To confirm the possibility of using rhenium coordinated bibenzimidazole compounds for molecular imaging, compound **35,**[141] a previously reported chelator, was synthesized by reacting 1-methylbenzimidazole (2 equiv.) and nBuLi (one equiv.) at -78°C (Scheme 3).

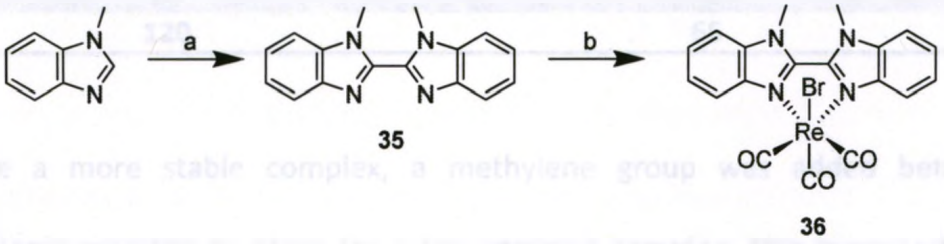

Scheme 3: Synthesis of **36**. (a) nBuLi in hexanes (0.5 equiv.), THF, -78°C. (b) $Re(CO)_5Br$, toluene, 80°C.

The resulting ligand **35** was reacted to $(Et_4N)_2[Re(CO)_3Br_3]$ to create rhenium complex **36**. Spectroscopic data for **36** is identical to previously reported values, and the reported crystal structure of this complex indicates that the carbonyl ligands assume facial coordination at the rhenium center, while the bromide and bis-benzimidazole ligands coordinates defines the other face of the complex. [140,141] The bibenzimidazole ligand is

bent around the rhenium center with an angle of 168^{O} and the N-Re-N angle of 74^{O} suggests distorted octahedral complex, thus it is postulated that the rhenium-bibenzimidazole complex **36** is greatly strained making it less stable in biological systems.[140,142,143]

To test the stability of the complex, **36** was incubated with a coordinating solvent, acetonitrile at 40^{O}C, and the resulting reaction mixture was analyzed using RP-HPLC and mass spectrometry. Results indicate that the $Re(CO)_3^+$ core dissociates from the bis-benzimidazole **36** and forms $[Re(CO)_3(H_2O)(CH_3CN)_2]^+$ complex in acetonitrile as early as 30 minutes (Table 8). This result further supports the postulate that the complex might be unstable in biological systems.

Table 8: Percentage of intact complex **36** after incubation with acetonitrile at 40^{O}C at 30 minutes increment for 2 hours.

Elapse Time (min)	% Remaining[††]
30	85
60	79
90	70
120	65

To create a more stable complex, a methylene group was added between the benzimidazole moieties to allow for a less strained complex. This increased flexibility may allow the ligands to adjust to the steric demands of the metal core and hence contribute to the overall stability of the metal complexes. Thus, in an attempt to demonstrate the possibility of increasing the flexibility of **35**, chelator **37** was proposed and synthesized using a modified literature method.[144] Ligand **37** was synthesized by

[††] Data were obtained as ratio of integration of diode-array chromatograph of peak corresponding to **36** at different time points compared to time 0.

reacting 1,2-phenyldiamine and diethyl malonate at elevated temperature using microwave irradiation (48% yield). Next, ligand **37** was reacted with $(Et_4N)_2[Re(CO)_3Br_3]$ in methanol to afford complex **38** and the product was characterized using NMR and mass spectrometry.

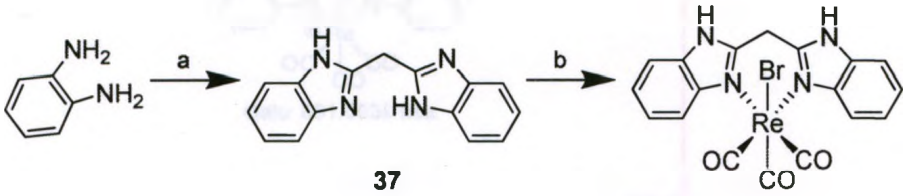

Scheme 4: Synthesis of rhenium tricarbonyl bis-(benzimidazol-2-yl)methane bromide complex (compound **38**). (**a**) diethyl malonate, HCl (6M), reflux for 24 hours; (**b**) $(Et4N)_2[Re(CO)_3Br_3]$, DCM, RT.

Again, the complex was solubilised in acetonitrile at 40^{O}C and the thermal decomposition of **38** was analyzed using RP-HPLC and mass spectrometry. Since the bromide ligand is labile in the presence of coordinating solvents, solvent coordinated complex is observed. LC-MS analysis showed acetonitrile substitution of bromide atoms in complex **38** (observed $[M]^+$ = 561.79 m/z, calculated $[M]^+$ = 561.09 m/z) (Figure 28), but showed no evidence of $Re(CO)_3^+$ core dissociation even after 2 hours of incubation in acetonitrile at 40^{O}C. Mass spectrum of complex also contains both ^{185}Re and ^{187}Re isotopic ratio of 2:3, respectively. Thus, the introduction of a methylene group within the bis-benzimidazole ligand (i.e. ligand **37**) allows for more flexibility and forms a much more stable 6-membered chelate ring upon coordination to $Re(CO)_3^+$ core.

However, the utility of this complex as a viable $Re(CO)_3^+$ core chelator could be hampered by the low yields of the complex since the N-H of the ligand could also coordinate with the metal complex. Analysis of the reaction mixture using RP-HPLC and

mass spectrometry indicates the formation of multiple products showing identical mass and each contains the expected ^{187}Re and ^{185}Re isotopic ratio.

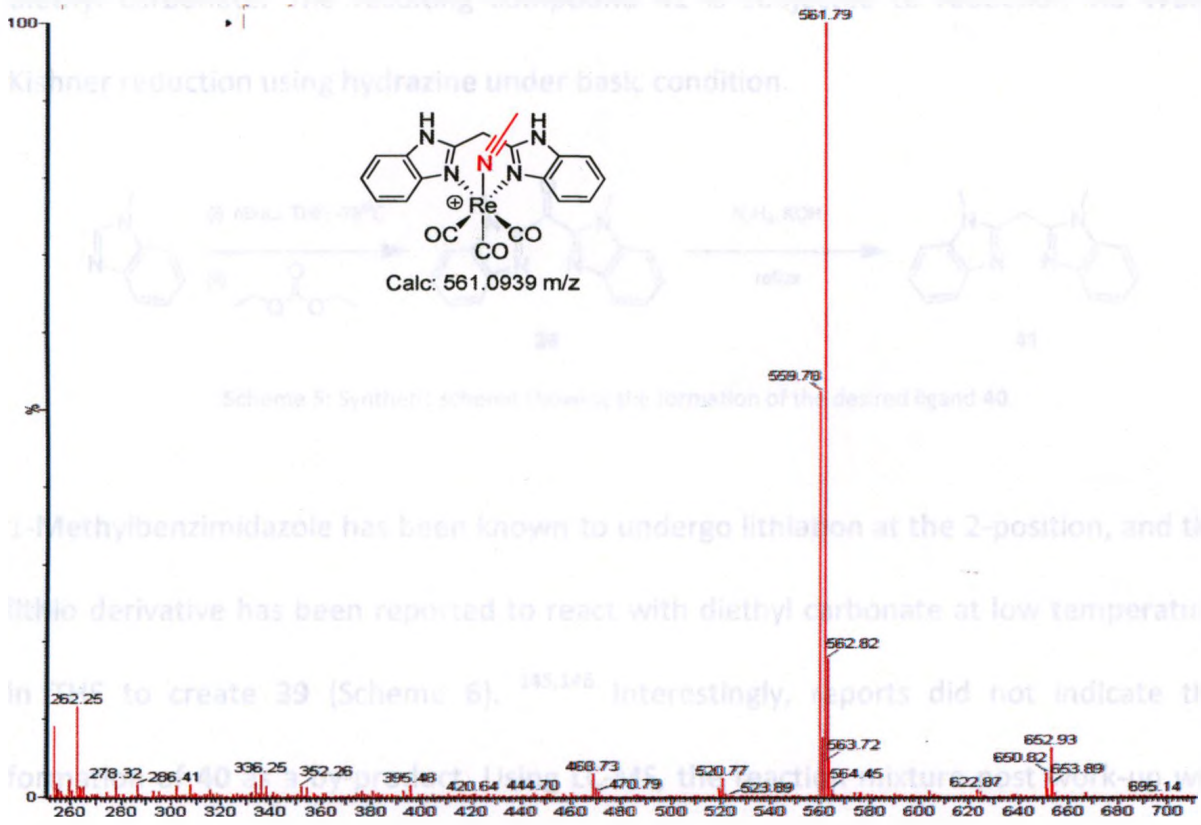

Figure 28: Mass spectrum of complex **38** after incubation in acetonitrile at 40°C.

To prevent linkage isomers, the N-H of the ligand was methylated to create bis-1-methylbenzimidazole rhenium tricarbonyl complex (Figure 29). However, methylation of ligand **37** proved difficult, thus a new synthetic scheme was designed in order to develop the desired ligand (Scheme 5).

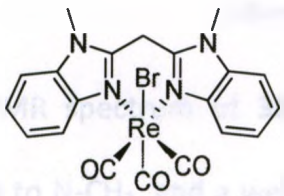

46

Figure 29: N-methylated rhenium tricarbonyl bis-(benzimidazol-2-ly)methane chelator bromide complex (**46**).

This reaction includes the formation of an intermediate **39** using a reaction which generates the anion of 1-methylbenzimidazole, which is immediately reacted with diethyl carbonate. The resulting compound **41** is subjected to reduction via Wolff-Kishner reduction using hydrazine under basic condition.

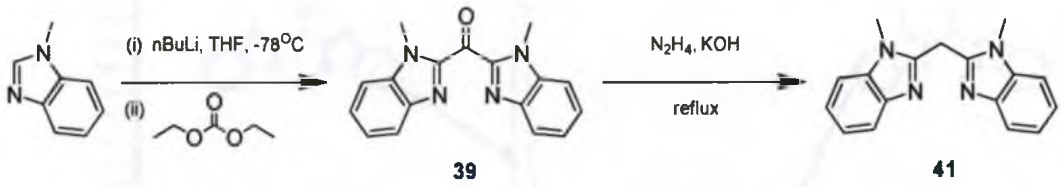

Scheme 5: Synthetic scheme showing the formation of the desired ligand **40**.

1-Methylbenzimidazole has been known to undergo lithiation at the 2-position, and the lithio derivative has been reported to react with diethyl carbonate at low temperature in THF to create **39** (Scheme 6). [145,146] Interestingly, reports did not indicate the formation of **40** as a by-product. Using LC-MS, the reaction mixture post work-up was analyzed, and it showed 5:1 ratio of alcohol **40** to ketone **39** (Figure 30A). Products were purified using silica gel chromatography and were fully characterized by NMR (Figure 30B) and mass spectrometry.

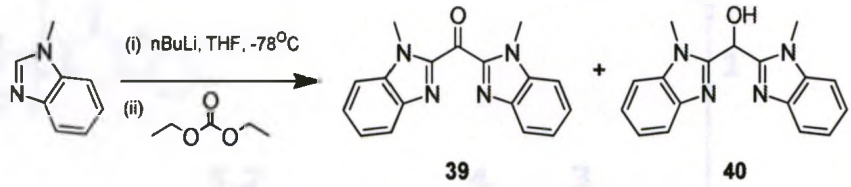

Scheme 6: Synthesis of **39** and side-product **40**.

The ^{1}H NMR spectrum of **39** and **40** both has a sharp singlet at around δ4 ppm assignable to N-CH_3, and a well resolved AA'BB' pattern of two sets of multiplets in the aromatic region integrating to 2:2:2:2. The simplicity and well resolved peaks establishes

the high symmetry of ligands. However, **40** showed a singlet at δ7.08 ppm corresponding to CH-OH proton, which is absent in **39**.

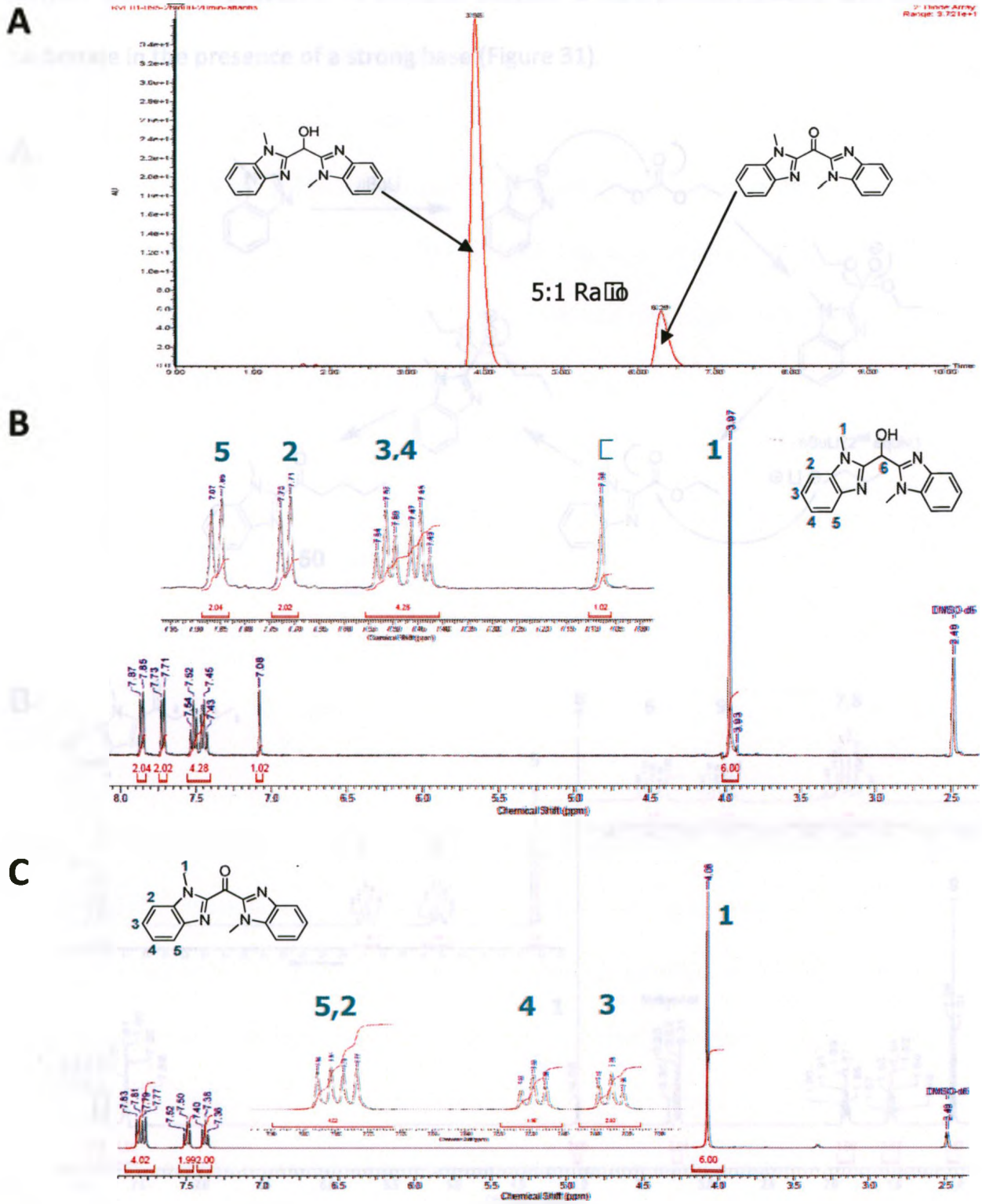

Figure 30: (A) HPLC chromatogram of a reaction mixture (post work-up) showing the ratio (5:1) of products formed. ^{1}H NMR of purified alcohol **39 (B)** and purified ketone **38 (C)**.

Compound **50** was also detected in the aforementioned reaction. This by-product is postulated to form when a second equivalent of nBuLi reacts with an intermediate formed from the reaction of equimolar amount 1-methylbenzimidazole and diethyl carbonate in the presence of a strong base (Figure 31).

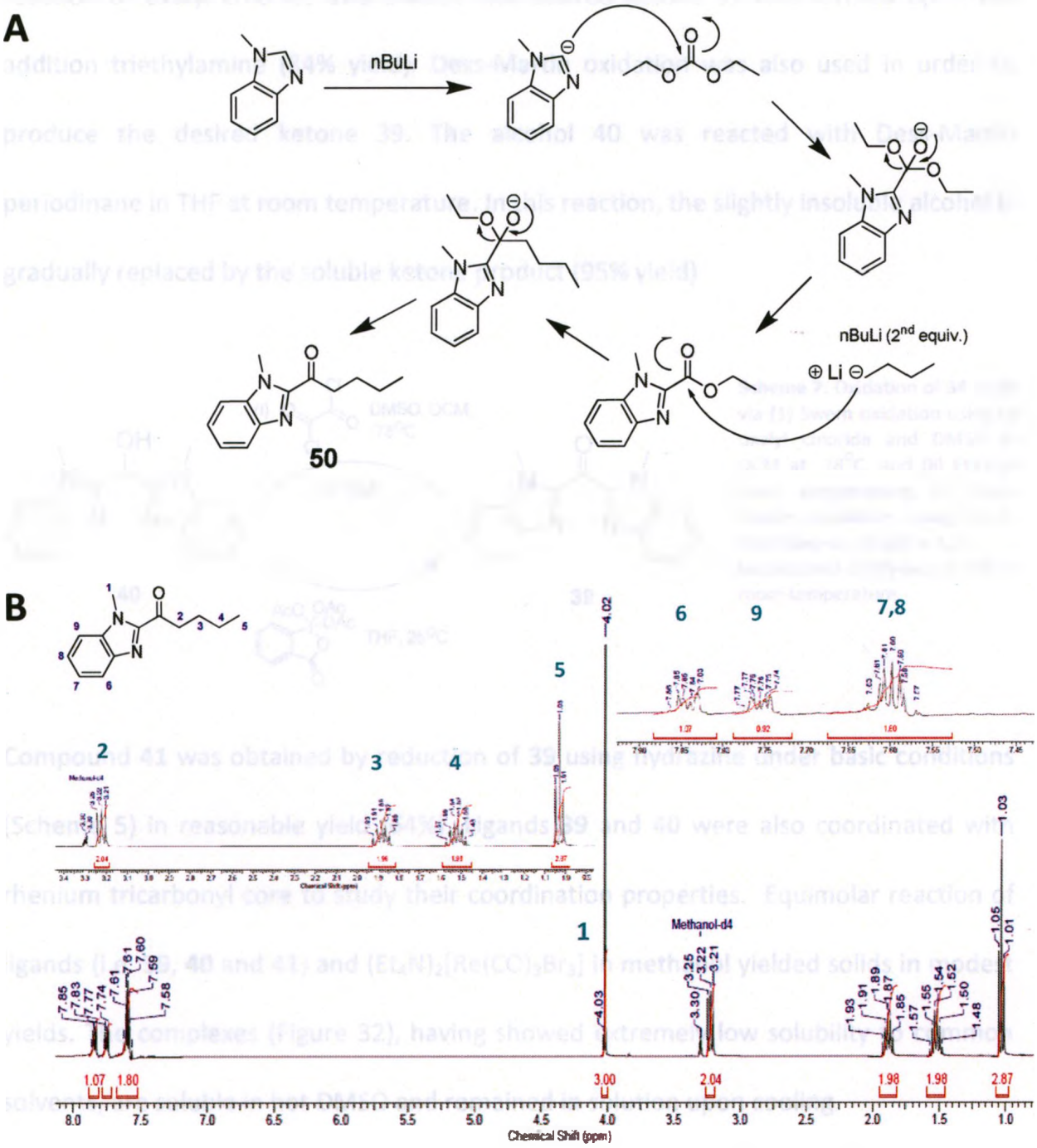

Figure 31: (A) Proposed mechanism of the formation of by-product **50**. (B) ^{1}**H** NMR of compound **50**.

Due to the low yield of 39 from the aforementioned reaction, compound 39 was also prepared by oxidation of 40. This was done using two different methods: (1) Swern and (2) Dess-Martin oxidation (Scheme 7). Using Swern oxidation, 40 was reacted at low temperature with dimethylchlorosulfonium chloride, which is formed from the initial reaction of oxalyl chloride and DMSO. The desired ketone 39 was formed upon the addition triethylamine (84% yield). Dess-Martin oxidation was also used in order to produce the desired ketone 39. The alcohol 40 was reacted with Dess-Martin periodinane in THF at room temperature. In this reaction, the slightly insoluble alcohol is gradually replaced by the soluble ketone product (95% yield).

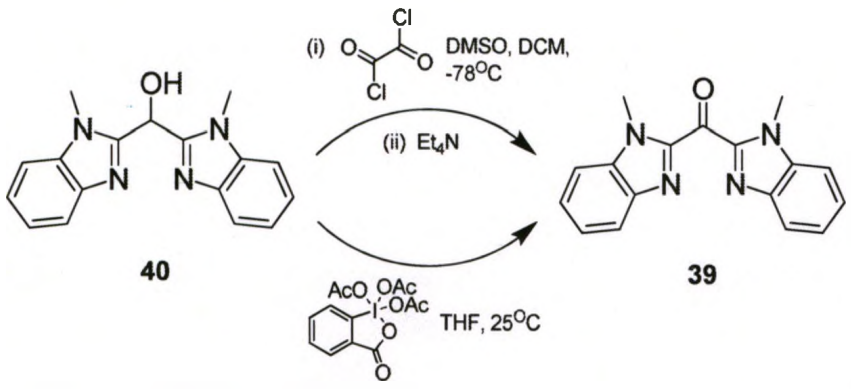

Scheme 7: Oxidation of **34** to **35** via (1) Swern oxidation using (i) oxalyl chloride and DMSO in DCM at -78°C, and (ii) Et_3N at room temperature; (2) Dess-Martin oxidation using 1,1,1-triacetoxy-1,1-dihydro-1,2-benziodoxol-3(*1H*)-one in THF at room temperature.

Compound **41** was obtained by reduction of **39** using hydrazine under basic conditions (Scheme 5) in reasonable yield (64%). Ligands **39** and **40** were also coordinated with rhenium tricarbonyl core to study their coordination properties. Equimolar reaction of ligands (i.e. **39**, **40** and **41**) and $(Et_4N)_2[Re(CO)_3Br_3]$ in methanol yielded solids in modest yields. The complexes (Figure 32), having showed extremely low solubility to common solvents, are soluble in hot DMSO and remained in solution upon cooling.

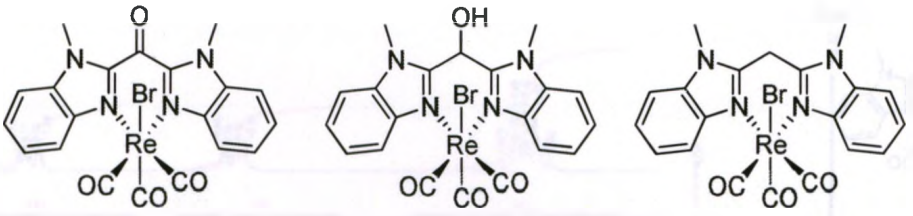

45 **46** **47**

Figure 32: Structures of rhenium complexes showing bidentate ligands

The ^{1}H-NMR (d_6-DMSO) of complex **45**, **46** and **47** showed bidentate coordination of respective ligands (Figure 33). ^{1}H-NMR data showed similar spectrum in the aromatic region compared to ligands but shifted slightly downfield. These observations clearly demonstrate that the metal complex in DMSO was highly symmetric as the two benzimidazole moieties were equivalent.

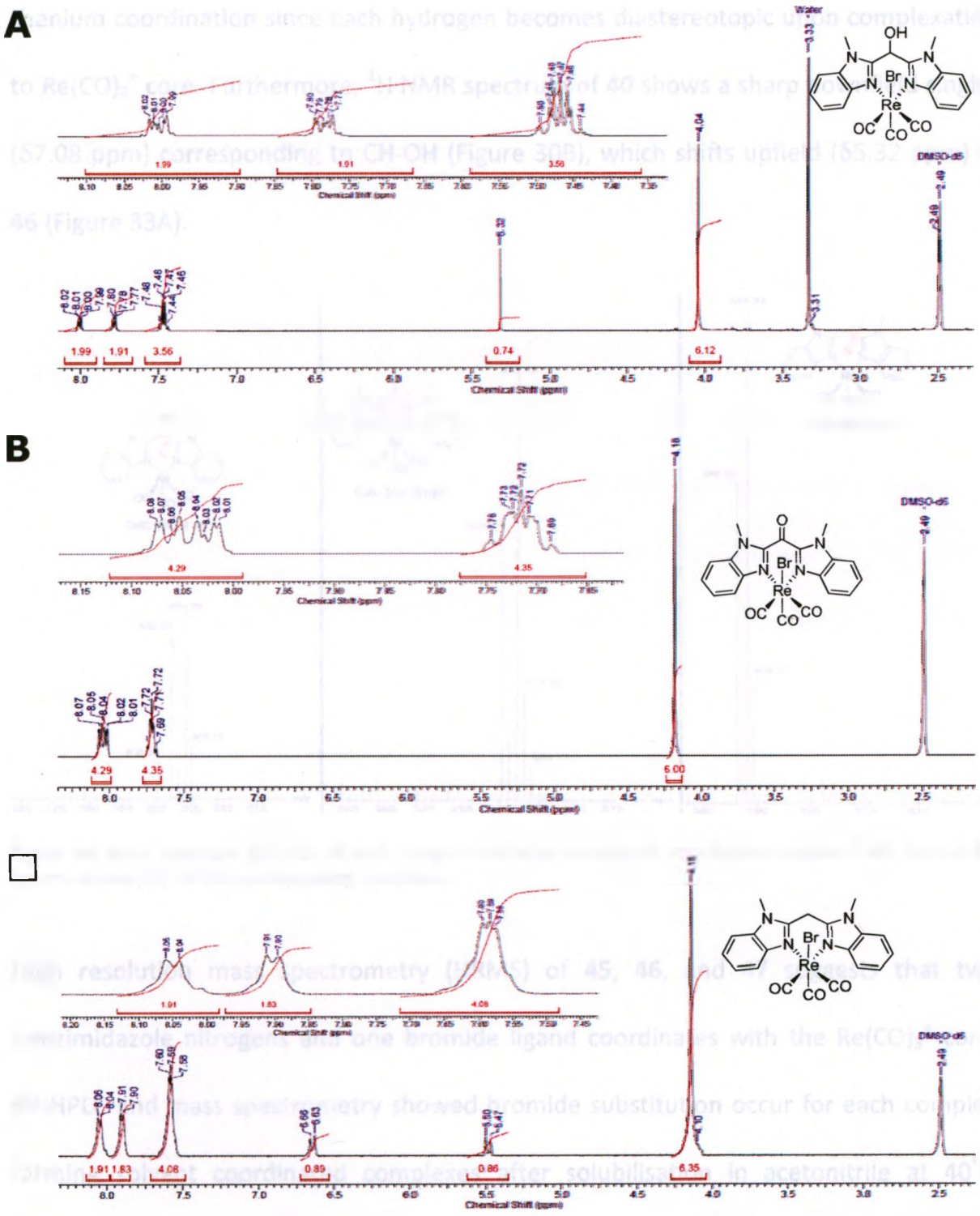

Figure 33: ^{1}H NMR of rhenium complexes containing bidentate bis-(1-methylbenzimidazol-2-yl) ligands.

The appearance of the two doublets (δ6.64 ppm and δ5.48 ppm, $J_{H,H}$ = 12 Hz) for each of the hydrogen on the methylene bridge of compound **47** (Figure 33C) is indicative of

rhenium coordination since each hydrogen becomes diastereotopic upon complexation to $Re(CO)_3^+$ core. Furthermore, ^1H NMR spectrum of **40** shows a sharp downfield singlet (δ7.08 ppm) corresponding to C**H**-OH (Figure 30B), which shifts upfield (δ5.32 ppm) in **46** (Figure 33A).

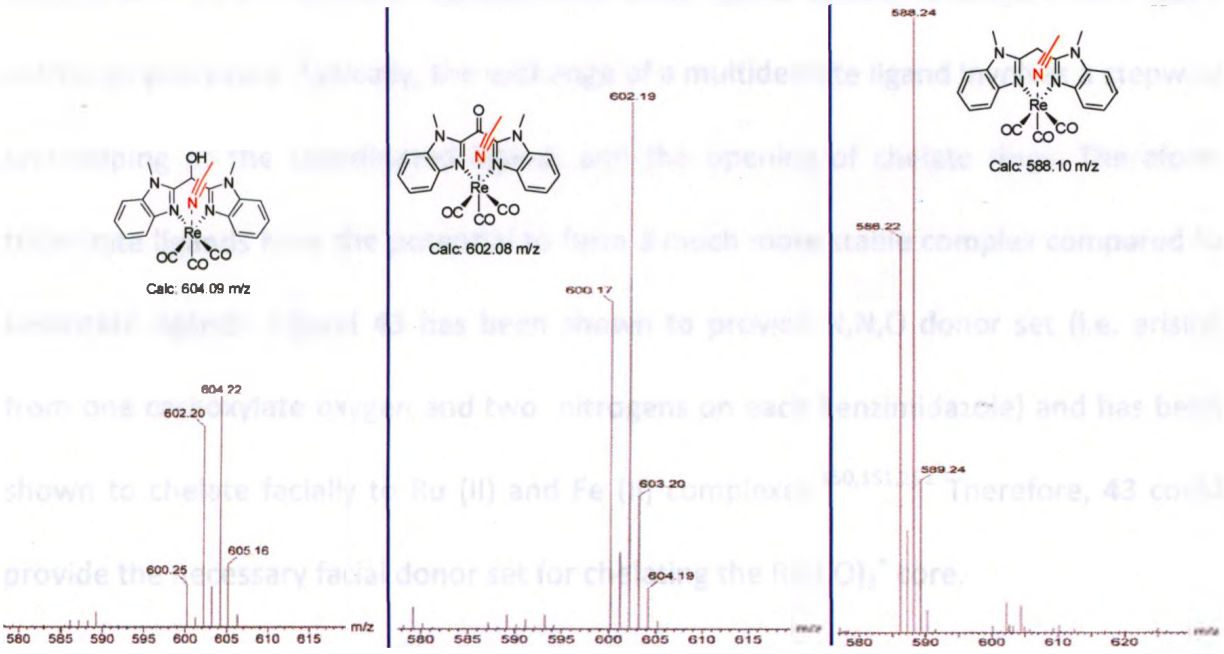

Figure 34: Mass spectrum (ESI-MS) of each complex indicating acetonitrile coordinated species of **45**, **46** and **47**. Spectra shows $[M]^+$ of the corresponding complexes.

High resolution mass spectrometry (HRMS) of **45**, **46**, and **47** suggests that two benzimidazole nitrogens and one bromide ligand coordinates with the $Re(CO)_3^+$ core. RP-HPLC and mass spectrometry showed bromide substitution occur for each complex forming solvent coordinated complexes after solubilisation in acetonitrile at 40^oC (Figure 34). Also, results indicate that for each complex, ligand **39**, **40** and **41** remained bound to the $Re(CO)_3^+$ core and are unable to be substituted with acetonitrile. Thus the addition of the methylene bridge between the two benzimidazole rings has resulted in an improved stability towards ligand exchange.

5.2.2. Synthesis and characterization of rhenium complexes containing tridentate ligands

As a general rule, the chelate effect predicts that stability of complexes increases with increasing number of chelate rings around a metal core.[147,148,149] Multidentate ligands tend to form a more stable complexes since these ligands tend to undergo slower ligand exchange processes. Typically, the exchange of a multidentate ligand involves a stepwise unwrapping of the coordinated ligand, and the opening of chelate rings. Therefore, tridentate ligands have the potential to form a much more stable complex compared to bidentate ligands. Ligand **43** has been shown to provide N,N,O donor set (i.e. arising from one carboxylate oxygen and two nitrogens on each benzimidazole) and has been shown to chelate facially to Ru (II) and Fe (II) complexes.[150,151,152] Therefore, **43** could provide the necessary facial donor set for chelating the $Re(CO)_3^+$ core.

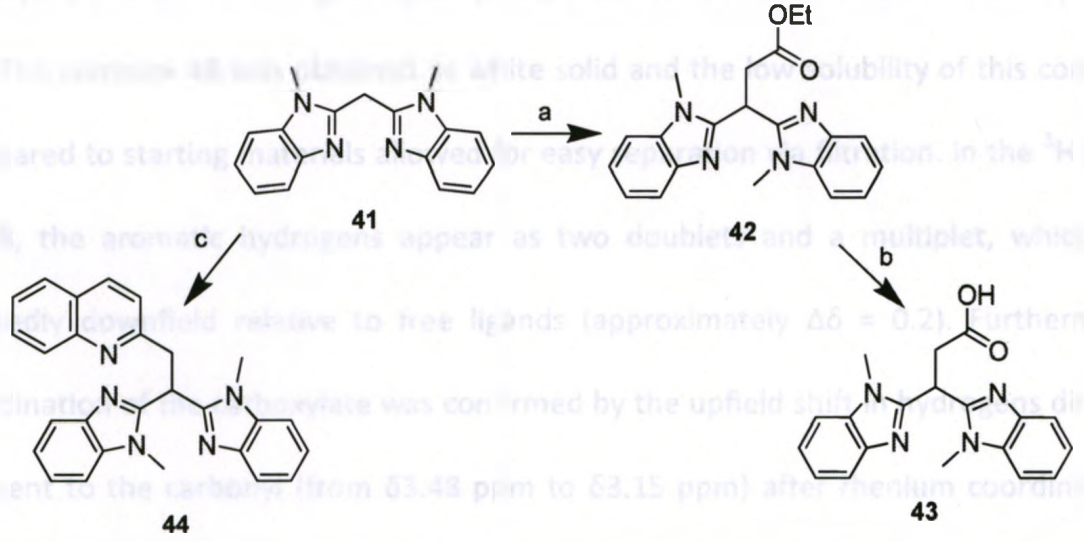

Scheme 8: Synthesis of tridentate rhenium chelators **43** and **44**. **(a)** (i) *n*BuLi in hexanes, THF, -78°C; (ii) ethyl bromoacetate; (b) (i) NaOH (2M) in THF, RT; (ii) 2M HCl, RT; **(c)** (i) *n*BuLi in hexanes, THF, -78°C; (ii) 2-(chloromethyl)quinoline.

Lithiation of **41** at the bridging methylene group with *n*-butyllithium at -78^{O}C in THF and subsequent addition of ethyl bromoacetate resulted in the clean formation of **42**. Subsequently, the ester functionality of **42** was hydrolyzed in THF with excess potassium hydroxide to give **43** after work-up. Products and intermediates were characterized by mass spectrometry and NMR spectroscopy.

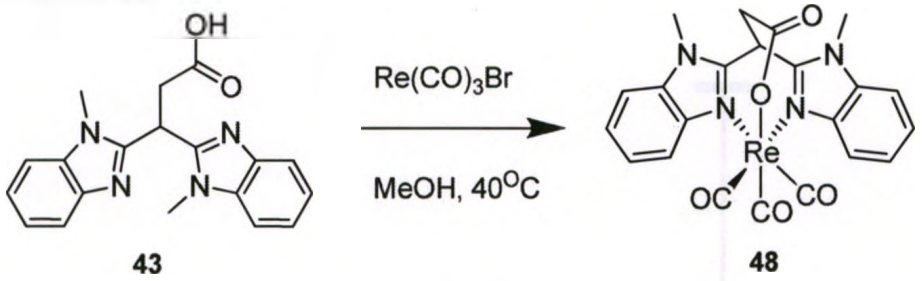

43 **48**

Figure 35: Synthesis of complex **47**.

Rhenium coordination of ligand **43** was carried out in dry methanol heated to 40^{O}C using $Re(CO)_5Br$, and the resulting complex precipitated out of solution after 1 hour (Figure 35). The complex **48** was obtained as white solid and the low solubility of this complex compared to starting materials allowed for easy separation via filtration. In the ^{1}H NMR of **48**, the aromatic hydrogens appear as two doublets and a multiplet, which are markedly downfield relative to free ligands (approximately $\Delta\delta$ = 0.2). Furthermore, coordination of the carboxylate was confirmed by the upfield shift in hydrogens directly adjacent to the carbonyl (from δ3.48 ppm to δ3.15 ppm) after rhenium coordination. Also the hydrogen at the methylene bridge which appears as triplet at δ5.53 ppm in the free ligand, is shifted to δ5.27 ppm in the complex.

The stability of the complex was also examined in acetonitrile at elevated temperature. Again, using LC-MS the reaction mixture was analyzed for the formation of acetonitrile coordinated species. Results indicate the absence of the acetonitrile coordinated species and only showed the presence of the complex (calculated for ^{187}Re $[M+H]^+$ = 606.1 m/z, observed $[M+H]^+$ = 606.6 m/z) (Figure 36), thus indicating tridentate chelation of ligand **43**.

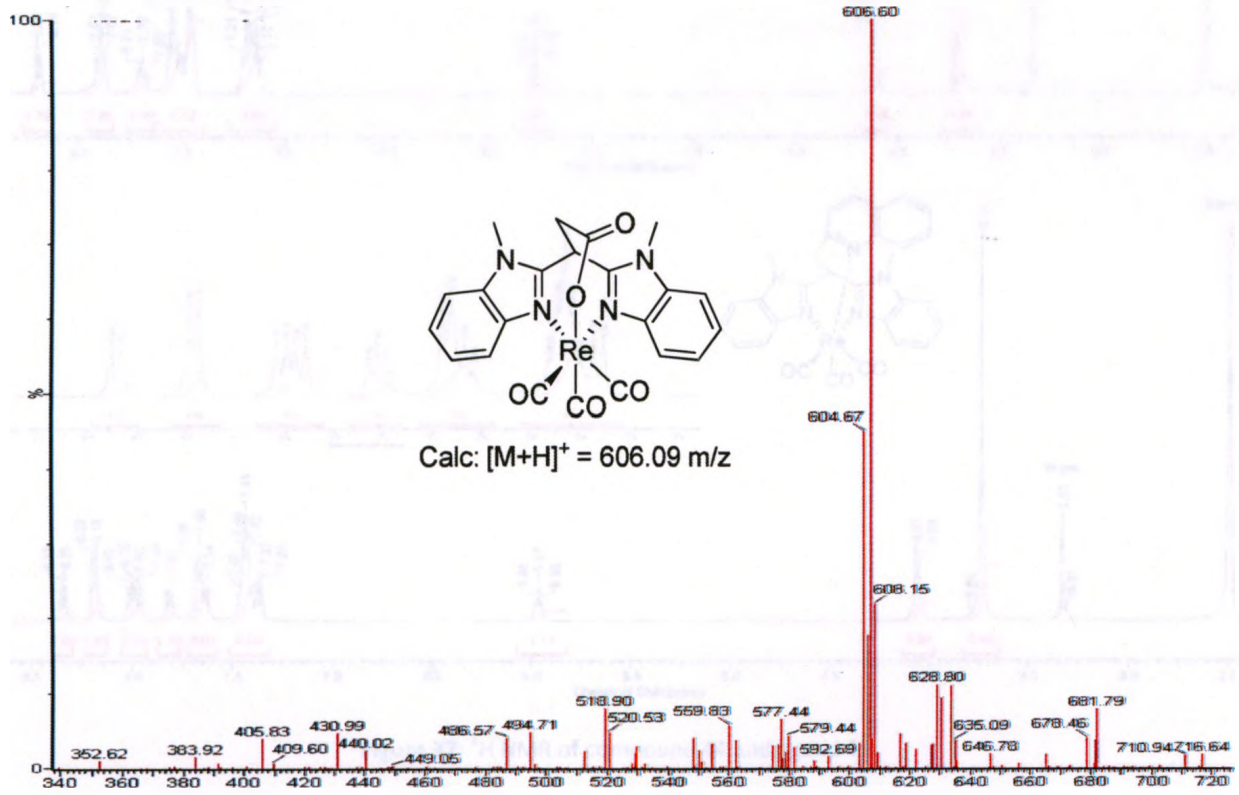

Figure 36: Mass spectrum (ESI-MS) of complex **47** indicating tridentate ligand chelation after solubilisation of the complex in acetonitrile at 40°C.

To test whether the bulky third arm has significant effects in the stability of the rhenium tricarbonyl complex, **44** was designed, synthesized and rhenium coordinated with $Re(CO)_3^+$ core. To this end, compound **41** was reacted with *n*-butyllithium at -78°C in THF, and the resulting anion was reacted with 2-(chloromethyl)quinoline to afford ligand

44. Ligand **44** was reacted with $Re(CO)_5Cl$ to give the desired complex **49**, which was characterized by NMR and mass spectrometry.

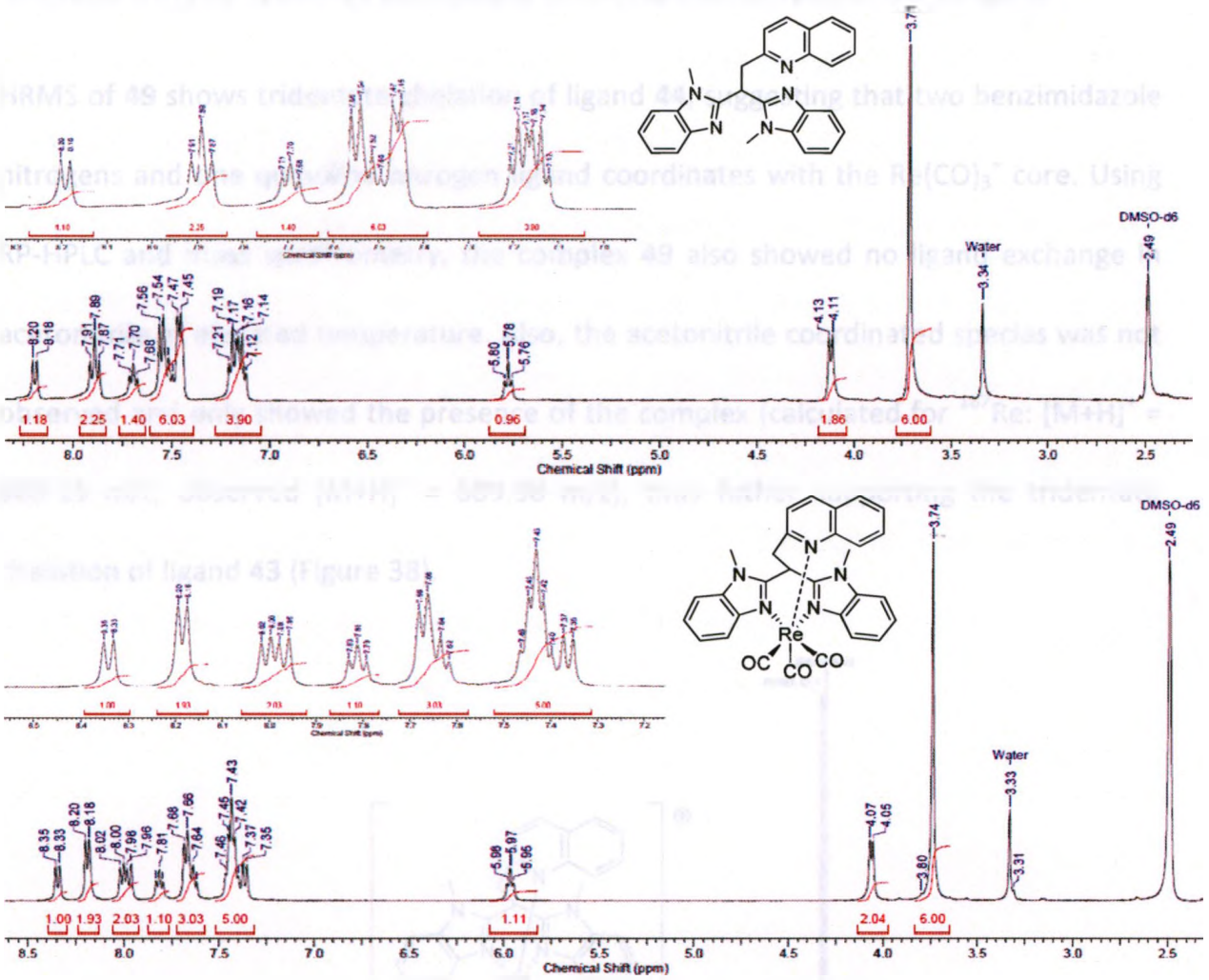

Figure 37: ^{1}H NMR of compound **44** and ligand **49**.

In the ^{1}H NMR of **49** (Figure 37), the aromatic hydrogens are slightly shifted downfield relative to free ligands. The coordination of the quinoline arm was confirmed by the minor shift in the aliphatic hydrogens directly adjacent to quinoline nitrogen, from δ4.12 ppm in free ligand to δ4.07 ppm after rhenium coordination. Furthermore, the hydrogen at the methylene bridge which appears as triplet at δ5.78 ppm in the free ligand, is shifted to δ5.97 ppm in the complex. From the ^{1}H NMR of complex **48** and **49**, it is

observed that the hydrogen at the methylene bridge for both complexes are shifted downfield compared to free ligand, while the $—CH_2—$ group which connects the third chelating arm and appear as doublet are shifted upfield compared to free ligand.

HRMS of **49** shows tridentate chelation of ligand **44**, suggesting that two benzimidazole nitrogens and one quinoline nitrogen ligand coordinates with the $Re(CO)_3^+$ core. Using RP-HPLC and mass spectrometry, the complex **49** also showed no ligand exchange in acetonitrile at elevated temperature. Also, the acetonitrile coordinated species was not observed and only showed the presence of the complex (calculated for ^{187}Re: $[M+H]^+$ = 689.15 m/z, observed $[M+H]^+$ = 689.98 m/z), thus futher supporting the tridentate chelation of ligand **43** (Figure 38).

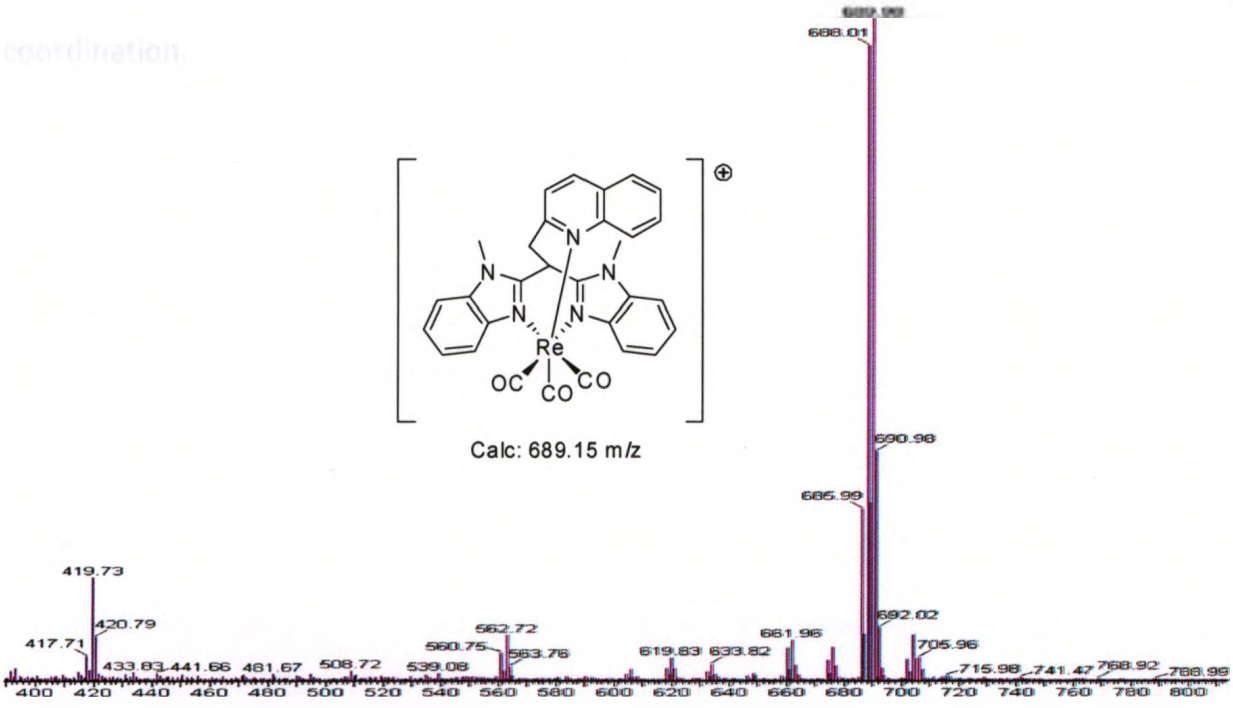

Figure 38: Mass spectrum (ESI-MS) of complex **49** suggesting tridentate ligand chelation after solubilisation of the complex in acetonitrile at 40°C.

5.2.3. UV-Vis Absorption Studies of Bis-1-methylbenzimidazole complexes.

The spectra of the complexes containing ligands **39**, **40**, **41**, **43** and **44** were recorded in DMSO because of their lack of solubility in other solvents (Figure 39). The absorption spectra of ligands **40**, **41**, **43** and **44** show intense band at approximately 280-285 nm, which are attributed to π-π* transitions. With the exception of slight variation in absorption bands, the absorption maxima for ligands **40**, **41**, **43** and **44** are unaffected by coordination to $Re(CO)_3^+$. The extensive conjugation is absent for compounds **40**, **41**, **43** and **44** due to the methylene spacer, thus the absorption maximum for each ligand is blue-shifted compared to **39.** The absorption of **39** show intense band at 344 nm and on the basis of the similarity of the spectra to those of related ligands, this band maybe assigned to π-π* transitions. Also, ligand **39** show pronounced red shift upon coordination.

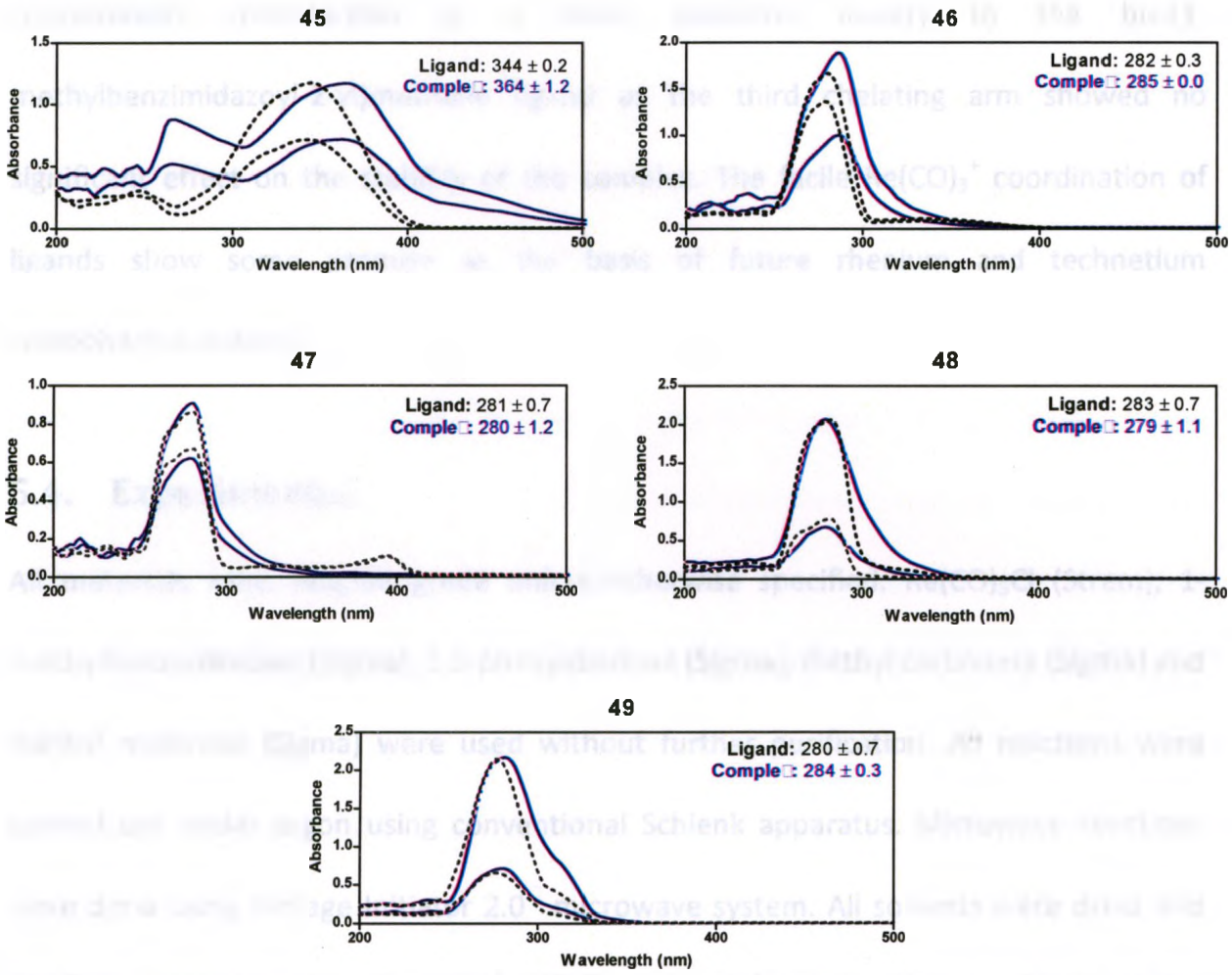

Figure 39: UV-Vis absorption spectra of rhenium complexes and their corresponding ligands in DMSO. Black dotted lines represent absorption of ligands while blue solid lines represent absorption of complexes.

5.3. Conclusion

In conclusion, the tricarbonyl rhenium complexes incorporating bi- and tridentate bis(1-methylbenzimidazol-2-yl) ligands have been obtained and characterized spectroscopically. The introduction of a methylene group between the bis-2,2'-benzimidazole moiety increase the stability of the resulting rhenium tricarbonyl complex. HPLC studies of the rhenium tricarbonyl complex containing bis-(2,2'-benzimidazol-2-yl) showed no thermal decomposition in acetonitrile. UV/vis studies indicate increase red shifting of π-conjugated ligands (i.e. **39**) upon rhenium

coordination. Introduction of a bulky quinoline moiety to the bis-(1-methylbenzimidazoyl-2-yl)methane ligand as the third chelating arm showed no significant effect on the stability of the complex. The facile $Re(CO)_3^+$ coordination of ligands show some promise as the basis of future rhenium and technetium radiopharmaceuticals.

5.4. Experimental

All materials were reagent grade unless otherwise specified. $Re(CO)_5Cl$ (Strem), 1-methylbenzimidazole (Sigma), 1,2-phenyldiamine (Sigma), diethyl carbonate (Sigma) and diethyl malonate (Sigma) were used without further purification. All reactions were carried out under argon using conventional Schlenk apparatus. Microwave reactions were done using Biotage Initiator 2.0□ microwave system. All solvents were dried and distilled prior to use. Analytical HPLC was performed using a Grace Vydac protein/peptide RP-C18 column (4.6 mm x 250 mm, 5 μm) using a gradient system of (1) H_2O + 0.1% of TFA and (2) CH_3CN + 0.1% of TFA. Analytical TLC was carried out on EMD silica gel 60 F_{254} plates, and column chromatography was performed using Merck silica gel 60 (230-400 mesh). ^1H and ^{13}C NMR data were obtained using a Varian Mercury 400. UV-Vis absorption studies were done using Beckman DU 530□ spectrophotometer and 10mm quartz cuvettes. Mass spectra were obtained using Finnigan MAT 8200 (EI-HRMS) and Micromass LCT (ESI-MS). For compounds containing rhenium, both ^{185}Re and ^{187}Re peaks were observed, and ^{187}Re mass is reported.

5.4.1. Synthesis of Ligands

Synthesis of bis-2,2-1-methylbenzimidazole (35)

To a solution 1-methylbenzimidazole (0.5 g, 3.78 mmol) in dry THF (30 mL) at -78^{O}C was added nBuLi (2.5 M, 0.76 mL, 1.9 mmol). The reaction mixture was allowed to warm to room temperature and stirred for 24 hours. Reaction mixture was quenched 1M HCl, followed by evaporation of volatiles. Solution was made basic with 2M NaOH and the resulting precipitate was filtered. Crude product was purified using silica chromatography (eluent $CHCl_3$) to give 0.37 g of **35** (70% yield). ^{1}H NMR (400 MHz, $CDCl_3$, 25^{O}C): δ = 7.88-7.86 (m, 2H, $H_{benzimid}$), 7.50-7.48 (m, 2H, $H_{benzimid}$), 7.40-7.36 (m, 4H, $H_{benzimid}$), 4.33 (s, 6H, N-CH_3) ppm. ^{13}C NMR (400 MHz, DMSO-d_6, 25^{O}C): δ = 142.56, 141.5, 136.22, 123.96, 122.87, 120.32, 110.09, 32.45 ppm. ESI-MS: $[M+H]^+$ = 263.28 m/z (calc: 263.14 m/z).

Synthesis of bis-(benzimidazol-2-yl)methane (37)

1,2-Phenyldiamine (1.07 g, 9.89 mmol) and diethyl malonate (0.79 g, 4.93 mmol) in 6M HCl (20 mL) was heated to 80^{O}C via microwave irradiation for 3 hours. At this temperature, the reaction mixture turned clear yellow. The reaction mixture was then heated to 100^{O}C for 5 hours. The solution was cooled and the resulting precipitate was filtered. The crude material was dissolved in hot H_2O containing charcoal; subsequently, the charcoal was filtered while the solution is hot. The solution was cooled to 0^{O}C, the precipitate was filtered and recrystallized in ethanol:water (8:2) to afford beige crystals (0.58 g, 48%). ^{1}H NMR (400 MHz, DMSO-d_6, 25^{O}C): δ = 7.50-748 (m, 4H, $H_{benzimid}$), 7.14-

7.12 (m, 4H, $H_{benzimid}$), 4.47 (s, 2H, Ar-CH_2-Ar) ppm. ESI-MS: $[M+H]^+$ = 249.17 m/z (calc: 249.11 m/z).

Synthesis of bis-(1-methylbenzimidazol-2-yl)alcohol (40)

To a solution 1-methylbenzimidazole (0.41 g, 3.1 mmol) in dry THF (20 mL) at -78^{O}C was added nBuLi (2.5 M, 1.2 mL, 3.1 mmol). The color of the solution became bright red on the addition of the base. The solution was stirred for 1 hour. Subsequently, diethyl carbonate (180 µL, 1.5 mmol) was added and the reaction was stirred for 30 minutes. The reaction mixture was allowed to warm to room temperature and was stirred overnight. The reaction was quenched with 1M HCl (20 mL) and volatiles were evaporated. The resulting aqueous solution was extracted with DCM (3 x 50 mL) and was made basic with 5N aqueous ammonia until a precipitate appeared. The product was filtered and washed with H_2O and hexanes. Recrystallization in ethyl acetate:hexane afforded white crystals (9:1) (0.25 g, 58%). ^{1}H NMR (400 MHz, DMSO-d_6, 25^{O}C): δ = 7.97-7.85 (m, 2H, $H_{benzimid}$), 7.73-7.71 (m, 2H, $H_{benzimid}$), 7.54-7.43 (m, 4H, $H_{benzimid}$), 7.08 (s, 1H, C**H**-OH), 3.97 (s, 6H, N-CH_3) ppm. ^{13}C NMR (400 MHz, DMSO-d_6, 25^{O}C): δ = 150.56, 134.65, 134.15, 124.62, 116.45, 111. 73, 109.07, 61.22, 31.16 ppm. ESI-MS: $[M+H]^+$ = 293.15 m/z (calc: 293.13 m/z). EI-HRMS: 292.1332 m/z (calc: 292.1324 m/z).

Synthesis of bis-(1-methylbenzimidazol-2-yl)ketone (39)

Swern Oxidation: To a solution of oxalyl chloride (0.53 g, 4.1 mmol) in DCM at -78^{O}C, DMSO (0.32 g, 4.1 mmol) was added and the solution was stirred for 30 minutes. The resulting solution was added to a slurry of **39** (0.12 g, 0.41 mmol) in DCM (30 mL) at -78^{O}C. The reaction was stirred at room temperature for 4 hours, followed by the

addition of triethylamine in excess. Then, 1M HCl (20 mL) was added to quench the reaction. Volatites were evaporated, basified with 5N aqueous ammonia until precipitate appeared. The product was filtered, washed with H_2O (3 x 20 mL) and hexanes (3 x 20 mL). This product was purified using column chromatography (silica; eluent ethyl acetate/hexane, 1:1) to give 0.10 g of **39** (84%).

Dess-Martin Oxidation: DMP (0.72 g, 1.70 mmol) was added to a slurry of **39** (0.5 g, 1.71 mmol) in dry THF (30 mL) and the reaction was stirred for 48 hours. Over time the reaction turned clear yellow. The reaction completion was monitored by TLC (1:1 hexane:ethylacetate with 1% Et_3N). Then, H_2O (30 mL) was added to quench the reaction, volatiles were evaporated and extracted with DCM (3 x 20 mL). The organic layers were pooled, dried with $MgSO_4$, and purified using silica column chromatography (DCM:MeOH, 9.5:0.5) (0.47 g, 95%). ^{1}H NMR (400 MHz, d_6-DMSO, 25^{O}C): δ = 7.82 (m, 2H, $H_{benzimid}$), 7.78 (m, 2H, $H_{benzimid}$), 7.50 (m, 2H, $H_{benzimid}$), 7.38 (m, 2H, $H_{benzimid}$), 4.08 (s, 6H, N-CH_3) ppm. ^{13}C NMR (400 MHz, $CDCl_3$, 25^{O}C): δ = 178.91, 146.82, 142.41, 136.77, 126.23, 123.73, 122.92, 110.21, 32.03 ppm. ESI-MS: $[M+H]^+$ = 291.24 m/z (calc: 291.12 m/z). EI-HRMS: 290.1172 m/z (calc: 290.1168 m/z).

Synthesis of bis-(1-methylbenzimidazol-2-yl)methane (41)

A solution of hydrazine hydrate (15 mL), **38** (0.18 g, 0.62 mmol), and KOH (0.103 g, 1.80 mmol) was heated to 80^{O}C for 3 hours, then the temperature was raised to 120^{O}C and stirred overnight. The reaction mixture was extracted with DCM (3 x 50 mL). The organic layer was died with $MgSO_4$, filtered and volatiles were evaporated. The crude product was purified using column chromatography (silica; eluent ethyl acetate/methanol,

9.5:0.5) which gave a white solid (0.11 g, 64%). ^{1}H NMR (400 MHz, d_6-DMSO, 25^{O}C): δ = 7.55-7.51 (m, 4H, $H_{benzimid}$), 7.24-7.14 (m, 4H, $H_{benzimid}$), 4.68 (s, 2H, Ar-CH_2-Ar), 3.83 (s, 6H, N-CH_3) ppm. ^{13}C NMR (400 MHz, $CDCl_3$, 25^{O}C): δ = 149.12, 142.24, 136.11, 122.71, 122.14, 119.42, 109.30, 30.44, 28.58 ppm. ESI-MS: $[M+H]^+$ = 277.31 m/z (calc: 277.14 m/z). EI-HRMS: 276.1381 m/z (calc: 276.1375 m/z).

Synthesis of 3,3-bis(1-methylbenzimidazol-2-yl)propanoic acid (43)

Synthesis of 42: To a solution of **40** (0.20 g, 0.72 mmol) in THF (30 mL) at -78^{O}C was added nBuLi (2.5 M, 288 µL, 0.72 mmol). The reaction mixture was stirred for 1 hour at -78^{O}C, followed by dropwise addition of ethyl bromoacetate (0.122 g, 0.72 mmol). The solution was allowed to warm to room temperature and stirred for 24 hours. The reaction was quenched with H_2O (10 mL), volatiles were evaporated, and extracted with ethyl acetate (3 x 50 mL). The organic layer was dried with magnesium sulphate, filtered and evaporated. The product was purified using silica chromatography (eluent ethyl acetate/methanol 9:1) (0.23 g, 88%). ^{1}H NMR (400 MHz, $CDCl_3$, 25^{O}C): δ = 7.77-7.75 (m, 4H, $H_{benzimid}$), 7.28-7.25 (m, 4H, $H_{benzimid}$), 5.46 (t, 1H, C**H**-CH_2, $J_{H,H}$ = 7.68 Hz), 4.13 (q, 2H, C**H**$_2$-CH_3, $J_{H,H}$ = 7.03 Hz), 3.76 (s, 6H, N-CH_3), 3.60 (d, 2H, CH-C**H**$_2$, $J_{H,H}$ = 7.46 Hz), 1.19 (t, 3H, CH_2-C**H**$_3$, $J_{H,H}$ = 7.25 Hz). ^{13}C NMR (400 MHz, $CDCl_3$, 25^{O}C): δ = 170.75, 151.14, 142.00, 136.41, 122.83, 122.17, 119.71, 109.23, 61.03, 36.18, 35.91, 30.22, 14.03 ppm. EI-HRMS: 362.1746 m/z (calc: 362.1743 m/z).

Synthesis of 43: To a solution of **42** (0.15 g, 0.41 mmol) in THF (15 mL) was added KOH (23 mg, 0.41 mmol) in water (2 mL). The resulting solution was stirred overnight. Reaction was monitored via TLC (eluent ethyl acetate with 1% Et_3N). Subsequently, 1

equiv. of 1M HCl was added. Solvents were evaporated, and the resulting solid product was dissolved in anhydrous ethanol. Filtrate was collect and recrystallization from EtOH/H_2O (95:5) gave white crystals (0.12 g, 88%). ^{1}H NMR (400 MHz, d_6-DMSO, 25^{O}C): δ = 7.71-7.67 (m, 4H, $H_{benzimid}$), 7.40-7.31 (m, 4H, $H_{benzimid}$), 5.53 (t, 1H, C**H**-CH_2, $J_{H,H}$ = 7.42 Hz), 3.94 (s, 6H, N-CH_3), 3.48 (d, 2H, CH-C**H**$_2$, $J_{H,H}$ = 7.42 Hz) ppm. ^{13}C NMR (400 MHz, CD_3CN, 25^{O}C): δ = 171.59, 148.65, 135.04, 133.75, 125.08, 124.96, 116.12, 111.49, 36.02, 32.73, 30.71 ppm. ESI-MS: $[M+H]^+$ = 335.31 m/z (calc: 335.15 m/z).

Synthesis of 3,3-bis(1-methylbenzimidazol-2-yl)-2-methylquinoline (44)

To a solution of **40** (0.11 g, 0.4 mmol) in THF (30 mL) at -78^{O}C was added nBuLi (2.5 M, 160 µL, 0.4 mmol). The reaction mixture was stirred for 1 hour at -78^{O}C, followed by dropwise addition of 2-(chloromethyl)quinoline (0.18 g, 1.2 mmol). The solution was allowed to warm to room temperature and stirred for 24 hours. The reaction was quenched with H_2O (10 mL), volatiles were evaporated, and extracted with ethyl acetate (3 x 50 mL). The organic layer was dried with $MgSO_4$, filtered and evaporated. The product was purified using silica chromatography (eluent $CHCl_3$) which affords white solid (0.14 g, 84%). ^{1}H NMR (400 MHz, d_6-DMSO, 25^{O}C): δ = 8.20-8.18 (m, 1H, ArH), 7.92-7.91-7.87 (m, 1H, ArH), 7.71-7.68 (m, 1H, ArH), 7.56-7.45 (m, 6H, Ar), 7.21-7.12 (m, 4H, ArH), 5.78 (t, 1H, C**H**-CH_2, $J_{H,H}$ = 7.82 Hz), 4.12 (d, 2H, C**H**-CH_2, $J_{H,H}$ = 7.82 Hz), 3.71 (s, 6H, N-CH_3) ppm. ^{13}C NMR (400 MHz, CD_3OH, 25^{O}C): δ = 159.07, 152.81, 148.22, 142.19, 137.81, 136.59, 130.58, 128.69, 128.45, 127.93, 127.11, 123.84, 123.22, 122.81, 119.45, 110.37, 41.10, 38.37, 30.43 ppm. ESI-MS: $[M+H]^+$ = 418.34 m/z (calc: 418.20 m/z).

5.4.2. Synthesis of Complexes

Synthesis of rhenium tricarbonyl bis-(1-methylbenzimidazol-2-yl) bromide (36) and rhenium tricarbonyl bis-(benzimidazol-2-yl)methane bromide (38)

General procedure: $(Et_4N)_2[Re(CO)_3Br_3]$ (1 equiv.) was added to a solution of dry methanol (20 mL) containing **34** or **37**. Methanol was evaporated and the resulting solid was slurried in $CHCl_3$. Precipitate was filtered and washed with DCM (4 x 20 mL) and hexanes (4 X 20 mL). Sollids was dried and recrystallized in 10% methanol in $CHCl_3$.

Compound 36: (75% yield) ^{1}H NMR (400 MHz, DMSO-d_6, 25^{O}C): δ = 8.04-8.02 (m, 2H, $H_{benzimid}$), 7.93-7.91 (m, 2H, $H_{benzimid}$), 7.69-7.64 (m, 4H, $H_{benzimid}$) 4.47 (s, 6H, N-CH_3) ppm. ^{13}C NMR (400 MHz, d_6-DMSO, 25^{O}C): δ = 189.58, 183.08, 146.48, 140.39, 136.43, 125.80, 117.60, 112.92, 35.32 ppm. EI-HRMS: 611.9550 m/z (calc: 611.9807 m/z).

Compound 38: (88% yield) ^{1}H NMR (400 MHz, d_6-DMSO, 25^{O}C): δ = 7.97-7.95 (m, 2H, $H_{benzimid}$), 7.67-7.66 (m, 2H, $H_{benzimid}$), 7.45-7.40 (m, 4H, $H_{benzimid}$), 5.32 (d, 1H, Ar-C**H**$_2$-Ar, $J_{H,H}$ = 12 Hz), 4.66 (d, 1H, Ar-C**H**$_2$-Ar, $J_{H,H}$ = 12 Hz) ppm. EI-HRMS: 597.9724 m/z (calc: 597.9650 m/z)

Synthesis of rhenium tricarbonyl bis-(1-methylbenzimidazol-2-yl)ketone bromide (45), rhenium tricarbonyl bis-(1-methylbenzimidazol-2-yl)alcohol bromide (46) and rhenium tricarbonyl bis-(1-methylbenzimidazol-2-yl)methane bromide (47)

General procedure: Equimolar $(Et_4N)_2[Re(CO)_3Br_3]$ was added to a hot (40^{O}C) solution of dry methanol (20 mL) containing **38**, **39** or **40**. A precipitate appeared after 20 minutes and the reaction mixture was stirred for another 2 hours. The precipitate was filtered

and washed with hot methanol (4 x 20 mL), H_20 (4 X 20 mL) and $CHCl_3$ (4 x 20 mL). The resulting solid was dried and recrystallized in DMSO.

Compound 45: (65% yield) ^{1}H NMR (400 MHz, DMSO-d_6, 25^{O}C): δ = 8.08-8.03 (m, 4H, $H_{benzimid}$), 7.75-7.69 (m, 4H, $H_{benzimid}$), 4.18 (s, 6H, N-CH_3) ppm. ^{13}C NMR (400 MHz, DMSO-d_6, 25^{O}C): δ = 199.30, 198.21, 177.62, 154.12, 147.12, 147.01, 137.73, 134.96, 127.53, 117.47, 35.64 ppm. EI-HRMS: 639.9664 m/z (calc: 639.9756 m/z)

Compound 46: (60% yield) ^{1}H NMR (400 MHz, DMSO-d_6, 25^{O}C): δ = 8.02-7.99 (m, 2H, $H_{benzimid}$), 7.80-7.77 (m, 2H, $H_{benzimid}$), 7.50-7.44 (m, 4H, $H_{benzimid}$), 5.32 (s, 1H, C**H**-OH), 4.04 (s, 6H, N-CH_3) ppm. ^{13}C NMR (400 MHz, DMSO-d_6, 25^{O}C): δ = 197.38, 196.96, 146.84, 145.89, 137.88, 135.29, 124.40, 121.43, 121.09, 69.82, 29.44 ppm. EI-HRMS: 642.0206 m/z (calc: 641.9912 m/z)

Compound 47: (71% yield) ^{1}H NMR (400 MHz, DMSO-d_6, 25^{O}C): δ = 8.06-8.04 (m, 2H, $H_{benzimid}$), 7.91-7.58 (m, 2H, $H_{benzimid}$), 7.60-7.58 (m, 4H, $H_{benzimid}$), 6.64 (d, 1H, Ar-C**H**$_2$-Ar, $J_{H,H}$ = 12 Hz), 5.48 (d, 1H, Ar-C**H**$_2$-Ar, $J_{H,H}$ = 12 Hz), 4.15 (s, 6H, N-CH_3) ppm. ^{13}C NMR (400 MHz, d_6-DMSO, 25^{O}C): δ = 198.34, 198.07, 146.67, 140.40, 134.10, 124.64, 123.37, 119.79, 113.20, 33.23, 29.86 ppm. EI-HRMS: 626.0641 m/z (calc: 625.9963 m/z).

Synthesis of rhenium tricarbonyl 3,3-bis(1-methylbenzimidazol-2-yl)propanoic acid (48) and rhenium tricarbonyl 3,3-bis(1-methylbenzimidazol-2-yl)-2-methylquinoline (49)

General procedure: Equimolar $Re(CO)_5Br$ and **42** or **43** in dry methanol refluxed for 2 hours. The resulting precipitate was filtered and washed with hot methanol (4 x 20 mL),

H_20 (4 X 20 mL) and $CHCl_3$ (4 x 20 mL). The resulting solid was dried and recrystallized in DMSO.

Compound 48: (85% yield) ^{1}H NMR (400 MHz, DMSO-d_6, 25^{O}C): δ = 7.94-7.92 (m, 2H, $H_{benzimid}$), 7.84-7.82 (m, 2H, $H_{benzimid}$), 7.57-7.50 (m, 4H, $H_{benzimid}$), 5.27 (t, 1H, C**H**-CH_2, $J_{H,H}$ = 7.51), 4.12 (s, 6H, N-CH_3), 3.27 (d, 2H, CH-C**H**$_2$, $J_{H,H}$ = 7.51) ppm. ^{13}C NMR (400 MHz, DMSO-d_6, 25^{O}C): δ = 198.21, 196.99, 186.77, 144.96, 140.12, 134.90, 124.29, 118.47, 118.47, 110.96, 45.29, 33.56, 30.99 ppm. ESI-MS: $[M+H]^+$ = 605.28 m/z (calc: 605.08 m/z). EI-HRMS: 604.0627 m/z (calc: 604.0756 m/z).

Compound 49: (79% yield) ^{1}H NMR (400 MHz, DMSO-d_6, 25^{O}C): δ = 8.35-8.33 (m, 1H, ArH), 8.20-8.18 (m, 2H, ArH), 8.02-7.96 (m, 2H, ArH), 7.83-7.79 (m, 1H, ArH), 7.68-7.62 (m, 3H, ArH), 7.46-7.35 (m, 5H, ArH), 5.98 (t, 1H, C**H**-CH_2, $J_{H,H}$ = 6.64 Hz), 4.07 (d, 2H, CH-C**H**$_2$, $J_{H,H}$ = 7.03 Hz), 3.74 (s, 6H, N-CH_3) ppm. ESI-MS: $[M+H]^+$ = 689.98 m/z (calc: 689.14 m/z).

6. References

[1] Zacarro, L.; Del Gatto, A.; Pedone, C.; Saviano, M. (2009) Peptides for tumour therapy and diagnosis: current status and future directions. *Curr. Med. Chem.* **16**(7), 780-795.

[2] Cai, W.; Niu, G.; Chen, X. (2008) Imaging of integrins as biomarkers for tumor angiogenesis. *Curr. Pharm. Des.*, **14**, 2943.

[3] Horton, M. A. (1997) The αvβ3 integrin "vironectin receptor." *Int. J. Biochem. Cell Biol.*, **29**, 721.

[4] Chen, X.; Conti, P. S.; Moats, R. A. (2004) In vivo near-infrared fluorescence imaging of integrin alphavbeta3 in brain tumor xenografts. *Cancer Res.*, **64**, 8009.

[5] Schottelius, M.; Wester, H. J.; Reubi, J. C.; Senekowitsch-Schmidtke, R.; Schwaiger, M. (2002) Improvement of pharmacokinetics of radioiodinated Tyr3-octreotide by conjugation with carbohydrates. *Bioconjug. Chem.*, **13**, 1021.

[6] Meisetschlager, G.; Poethko, T.; Stahl, A.; Wolf, I.; Scheidhauer, K.; Schottelius, M.; Herz, M.; Wester, H. J.; Schwaiger, M. (2006) Gluc-Lys([18F]FP)-TOCA PET in patients with SSTR-positive tumors: biodistribution and diagnostic evaluation compared with [111In]DTPA-octreotide. *J. Nucl. Med.*, **47**, 566.

[7] Laurent, T. C.; and Fraser, J. R. E. (1992) Hyaluronan. *FASEB J.* **6**, 2397-2404.

[8] Fraser, J. R. E.; Laurent, T. C.; and Laurent, U. B. G. (1997) Hyaluronan: Its nature, distribution, functions and turnover. *J. Intern. Med.* **242**, 27-33.

[9] Naot, D.; Sionov, R.V.; and Ish-Shalom, D. (1997) CD44: Structure, function, and association with the malignant process. *Adv. Cancer Res.* **71**, 241-319.

[10] Naor, D.; Nedvetzki, S.; Golan, I.; Melnik, L.; and Faitelson, Y. (2002) CD44 in cancer. *Crit. Rev. Clin. Lab. Sci.* **39**, 527-579.

[11] Sohara, Y.; Ishiguro, N.; Machida, K.; Hisashi, K.; Thant, A. A.; Takeshi, S.; Matsuda, S.; Kimata, K.; Iwata, H. Hamaguchi, M. (2001) Hyaluronan activates cell motility of v-Src-transformed cells via Ras-mitogen-activated protein kinase amd phosphoinositide 3-kinase-Akt in a tumor-specific manner. *Mol. Biol. Cell.* **12**, 1859-1868.

[12] Bourguignon, L. Y.; Zhu, H.; Shao, L.; and Chen, Y. W. (2000) CD44 interaction with tiam1 promotes Rac1 signalling and hyaluronic acid-mediated breast tumor cell migration. *J. Biol. Chem.* **275**, 1829-1838.

[13] Bourguignon, L. Y.; Singleton, P. A.; Zhu, H.; and Diedrich, F. (2003) Hyaluronan-mediated CD44 interaction with RhoGEF and Rho kinase promotes Grb2-associated binder-1 phosphorylation and phosphatodylinositol 3-kinase signalling leading to cytokine (macrophage-colony stimulating factor) production and breast tumor progression. *J.Biol. Chem.* **278**, 29420-29434.

[14] Bourguinon L. Y.; Peyrollier, K.; Gilad, E.; and Brightman, A. (2007) Hyaluronan-CD44 interaction with neural Wiskott-Aldrich syndrome protein (N-WASP) promotes actin polymerization and ErbB2 activation leading to beta-catenin nuclear translocation, transcriptional up-regulation, and cell migration in ovarian tumor cells. *J. Biol. Chem.* **282**, 1265-1280.

[15] Turley, E. A.; Austen L.; Vandeligt, K.; and Clary, C. (1991) Hyaluronan and a cell-associated hyaluronan binding protein regulate the locomotion of ras-transformed cells. *J. Cell. Biol.* **112**, 1041-1047.

[16] Hall, C. L.; Wang, C.; Lange L. A.; and Turley, E. A. (1994) Hyaluronan and the hyaluronan receptor RHAMM promote focal adhesion turnover and the transient tyrosine kinase activity. *J. Cell Biol.* **126** (2), 575-588.

[17] Gust, K. M.; Hofer, M. D.; Perner, S.R.; Chinnaiyan, A. M.; Varambally, S.; Moller, P.; Rinnab, L.; Rubin, M. A.; Greiner, J.; Schmitt, M.; Kuefer, R.; and Ringhoffer, M. (2009) Rhamm (CD168) is overexpressed at the protein level and may constitute an immunogenic antigen in advanced prostate cancer disease. *Neoplasia.* **11**(9), 956-963

[18] Wang, C.; Thor, A.D.; Moore, D.H. 2nd; Zhao, Y.; Kerschmann, R. Stern, R.; Watson, P.H.; and Turley, E. A. (1998) The overexpression of RHAMM, a hyaluronan-binding protein that regulates ras signalling, correlates with overexpression of mitogen-activated protein kinase and is a significant parameter in breast cancer progression. *Clin. Cancer Res.* **4**(3), 567-576.

[19] Greiner, J.; Ringhoffer, M.; Taniguchi, M.; Schmitt, A.; Kirchner, D.; Krähn, G.; Heilmann, V.; Gschwend, J.; Bergmann, L. Döhner, H.; and Schmitt, M. (2002) Receptor for hyaluronan acid-mediated motility (RHAMM) is a new immunogenic leukemia-associated antigen in acute and chromic myeloid leukemia. *Exp Hematol.* **30**(9), 1029-1035.

[20] Assmann, V.; Marshall, J. F.; Fieber, C.; Hofmann, M.; I.R.; and Hart, I.R. (1998) The human hyaluronan receptor RHAMM is expressed as an intracellular protein in breast cancer. *J. Cell Sci.* **111**, 1685-1694

[21] Hall C. L. and Turley, E. A. (1995) Hyaluronan: Rhamm mediated cell locomotion and signalling in tumorigenesis. *J. Neurooncol.* **26**(3), 221-229

[22] Sherman, L; Sleeman, J.; Herrlich, P.; and Ponta, H. (1994) Hyaluronate receptors: Key players in growth, differentiation, migration, and tumor progression. *Curr. Opin. Cell Biol.* **6**, 726-733.

[23] Mohapatra, S.; Yang, X.; Wright, J. A.; Turley, E. A.; and Greenberg, A. H. (1996) Soluble hyaluronan receptor induces mitotic arrest by suppressing cdc2 and cyclin B1 expression. *J. Exp. Med.* **183**, 1663-1668.

[24] Yang, B. H.; Yang B. L.; Savani, R.C.; and Turley, E.A. (1994) Identification of a common hyaluronan binding motif in the hyaluronan binding proteins RHAMM, CD44, and link protein. *EMBO J.* **13**, 286-295

[25] Ziebell, M.R. and Prestwich G.D. (2004) Interactions of peptide mimics of hyaluronic acid with the receptor for hyaluronan mediated motility (RHAMM). *J. Comput. Aided Mol. Des.* **18**, 597-614.

[26] Yang, B.; Zhang, L.; and Turley, E. A. (1993) Identification of two hyaluronan-binding domains in the hyaluronan receptor RHAMM. *J. Biol. Chem.* **268**, 8617-8623.

[27] Ziebell, M. R.; Glenn, P. D. (2004) Interactions of peptide mimics of hyaluronic acid with the receptor for hyaluronan mediated motility (Rhamm). *J Comput Aided Mol Des.* **18**, 597-614.

[28] Carlos FGC, Geraldes; Djanashvili, Kristina; Peters, Joop A. (2010) Glycoconjugate probes abd targets for molecular imaging using magnetic resonance. *Future Med. Chem.*, **2** (3), 409-425.

[29] Bertozzi, C. R.; Kiessling, L. L. (2001) Chemical Glycobiology. *Science.* **291**(5512), 2357-2364.

[30] Lee, S.; Xie, J.; Chen, X. (2010) Peptide-based probes for targeted molecular imaging. *Biochemistry*, **49**(7), 1365-1375.

[31] Davis, B. G.; Robinson, M. A. (2002) Drug delivery systems based on sugar-macromolecule conjugates. *Curr. Opin. Drug Discov. Devel.* **5**(2), 279-288.

[32] Rudin, M.; Weissleder, R. (2003) Molecular imaging in drug discovery and development. *Nat Rev Drug Discov,* **2**, 123-131.

[33] Jorgensen W.L. (2004) The many roles of computation in drug discovery. *Science.,* **303**, 1813 -1817.

[34] Pollock, S.; Safer, H. (2001) Bioinformatics in the drug discovery process. *Ann Rep Med Chem.*, 1 -9

[35] Warren, G.L.; Andrews, C.W.; Capelli A.-M.; Clarke, B.; LaLonde, J.; Lambert, M.H.; Lindvall, M.; Nevins, N.; Semus, S.F.; Senger S. (2006) A critical assessment of docking programs and scoring functions. *J Med Chem* 2006, **49**, 5912-5931.

[36] Sali, A.; Glaeser, R.; Earnest, T.; Baumeister, W. (2003) From words to literature in structural proteomics. *Nature.* **422**, 216-225.

[37] Berman, H.M.; Westbrook, J.; Feng, Z.; Gilliland, G.; Bhat, T.N.; Weissig, H.; Shindyalov, I.N.; Bourne, P.E.(2000) The Protein Data Bank. *Nucl Acids Res.* **28**, 235-242.

[38] Steindl, T.M.; Schuster, D.; Laggner, C.; Langer, T. (2006) Parallel screening: a novel concept in pharmacophore modeling and virtual screening. *J Chem Inf Model.* **46**, 2146-2157.

[39] Kellenberger, E.; Muller, P.; Schalon, C.; Bret, G.; Foata, N.; Rognan, D. (2006) sc-PDB: annnotated database of druggable binding sites from the Protein Data Bank. *J Chem Inf. Model.* **46**, 717-727.

[40] Garcia-Serna, R.; Opatowski, L.; Mestres, J. (2006) FCP: functional coverage of the proteome by structures. *Bioinformatics* **22**, 1792-1793.

[41] Zhang, Q.; Muegge, I. (2006) Scaffold hopping through virtual screening using 2D and 3D similarity descriptors: ranking, voting, and consensus scoring. *J Med Chem.* **49**, 1536-1548.

[42] Song, M.C.; Lim, J. S.; Tong, C. J. (2009) Recent advances in computer-aided drug design. *Briefings in Bioinformatics.* **10**(5), 579-591.

[43] Jones, D.T.; Taylor, W.R.; Thornton, J.M. (1992) A new approach to protein fold recognition. *Nature*. **358**, 86–89.

[44] Miyazawa, S.; Jernigan, R. L. (1985) Estimation of effective interresidue contact energies from protein crystal structures: quasichemical approximation. *Macromolecules* **18**, 534–552.

[45] Betancourt , M.R.; Thirumalai, D. (1999) Pair potentials for protein folding: choice of reference states and sensitivity of predicted native states to variations in the interaction schemes. *Protein Sci* **8**, 361–369.

[46] Schwede, T; Kopp, J.; Guex, N., *et al.* (2003) SWISS-MODEL: an automated protein homology-modeling server. *Nucleic Acids Res.* **31**, 3381–3385

[47] Sutcliffe, M.J.; Haneef, I.; Carney, D., *et al.* (1987) Knowledge based modelling of homologous proteins, Part I: Three-dimensional frameworks derived from the simultaneous superposition of multiple structures. *Protein Eng.* **1**, 377–384.

[48] Bates, P.A.; Kelley, L.A.; MacCallum, R.M., *et al.* (2001) Enhancement of protein modeling by human intervention in applying theautomatic programs 3D-JIGSAW and 3D-PSSM. *Proteins* **5,** 39–46.

[49] Levitt, M. (1992) Accurate modeling of protein conformation by automatic segment matching. *J. Mol. Biol.* **226**, 507–33.

[50] Rarey, M; Kramer, B.; Lengauer, T., et al. (1996) A fast flexible docking method using an incremental construction algorithm. *J Mol Biol* **261**, 470–89.

[51] Boehm, H.J.; Boehringer, M.; Bur, D., *et al.* (2000) Novel inhibitors of DNA gyrase: 3D structure based biased needle screening, hit validation by biophysical methods, and 3D guided optimization. A promising alternative to random screening. *J Med Chem.* **43**, 2664–2674.

[52] Ewing, T.J.; Makino, S.; Skillman, A. G., *et al.* (2001) DOCK 4.0: search strategies for automated molecular docking of flexible molecule databases. *J. Comput. Aided Mol. Des.* **15**, 411–428.

[53] Ziebell, M. R.; Zhai, Z. G.; Luo, B.; Luo, Y.; Turley, E. A.; Prestwich, G. D. (2001) Peptides that mimic glycosaminoglycans: high-affinity ligands for a hyaluronan binding domain. *Biol. Chem.,* **8**(11), 1081-1094.

[54] Ziebell, M.R. and Prestwich G.D. (2004) Interactions of peptide mimics of hyaluronic acid with the receptor for hyaluronan mediated motility (RHAMM). *J. Comput. Aided Mol. Des.,* **18**, 597-614.

[55] Altschul, S. F.; Gish, W.; Miller, W.; Myers, E. W.; Lipman, D. J. (1990). Basic local alignment search tool. *J. Mol. Biol.*, **215**(3), 403–410.

[56] Altschul, S. F., Madden, T. L., Schaffer, A. A.; Zhang, J.; Zhang, Z.; Miller, W. Lipman, D. J. (1997) Gapped BLAST and PSIBLAST: a new generation of protein database search programs. *Nucleic Acids Res.*, **25**(17), 3389–3402.

[57] Tatusov, R. L., Galperin, M. Y., Natale, D. A. and Koonin, E. V. (2000), 'The COG database: a tool for genome-scale analysis of protein functions and evolution, *Nucleic Acids Res.*, **28**(1), 33–36.

[58] Corpet, F.; Servant, F.; Gouzy, J.; Kahn, D. (2000) ProDom and ProDom-CG: toolsfor protein domain analysis and whole genome comparisons. *Nucleic Acids Res.* **28**(1), 267–269.

[59] Bateman, A.; Birney, E.; Durbin, R.; Eddy, S. R.; Howe, K. L.; Sonnhammer, E. L. (2000) The Pfam protein families database. *Nucleic Acids Res.* **28**(1), 263–266.

[60] Schultz, J., Milpetz, F., Bork, P. and Ponting, C. P. (1998), 'SMART, a simple modular architecture research tool: identification of signaling domains', *Proc. Natl Acad. Sci.USA.* **95**(11), pp. 5857–5864.

[61] Attwood, T. K., Croning, M. D., Flower, D. R. *et al.* (2000), 'PRINTS-S: the database formerly known as PRINTS', *Nucleic Acids Res.* **28**(1), 225–227.

[62] Rice D.W.; Eisenberg, D. (1997) A 3D–1D substitution matrix for protein fold recognition that includes predicted secondary structure of the sequence. *J Mol Biol.* **267**, 1026–38.

[63] Harris, C.J.; Stevens, A.P. (2006) Chemogenomics: structuring the drug discovery process to gene families. *Drug Discov. Today*, **11**, 880-888.

[64] Izrailev, S.; Farnum, M.A. (2004) Enzyme classification by ligand binding. *Proteins: Struct., Funct., and Bioinf.* **57**, 711-724.

[65] Francis, G.A.; Fayard, E.; Picard, F.; Auwerx, J. (2003) Nuclear receptors and the control of metabolism. *Annu. Rev. Physiol.* **65**, 261-311.

[66] Jacoby, E. (2006) Chemogenomics: drug discovery's panacea? *Mol BioSystems.* **2**, 218-220.

[67] Houghten, R. A.; S.K.; Pinilla, C.; Blondelle, S. E.; Appel, J. R.; Dooley, C.T.; Cuervo, J. H. (1991) Generation and use of synthetic combinatorial libraries for basic research and drug discovery. *Nature*, **354**, 84-86

[68] Liu, R.; Marik, J.; Lam, K.S. (2002) A novel peptide-based encoding system for "one-bead one-compound" peptidomimetic and small molecule combinatorial libraries. *J Am Chem Soc.* **124**, 7678.

[69] Ellman, J.A. (1996) Design, synthesis, and evaluation of small-molecule libraries. *Account Chem Res.* **29**, 132–143.

[70] Houghten, R. A.; S.K.; Pinilla, C.; Blondelle, S. E.; Appel, J. R.; Dooley, C.T.; Cuervo, J. H. (1991) Generation and use of synthetic combinatorial libraries for basic research and drug discovery. *Nature*, **354**, 84-86

[71] Sasaki, S.; Takagi, M.; Tanaka, Y.; Maeda, M. (1996) A new application of a peptide library to identify selective interaction between small peptides in an attempt to develop recognition molecules towards protein surfaces. *Tetrahedron. Lett.* **37**(1), 85-88.

[72] Lam, K.S.; Hruby, V.J.; Lebl, M.; Knapp, R. J.; Kazmierski, W. M.; Hersh, E. M.; Salmon, S. E. (1993) The chemical synthesis of large random peptide libraries and their use for the discovery of ligands for macromolecular acceptors. *Bioorg. Med. Chem. Lett.* **3**(3), 419–424.

[73] Lam, K.S.; Salmon, S.E.; Hersh, E.M.; Hruby, V.J.; Kazmierski, W.M.; Knapp, R.J. (1991) A new type of synthetic peptide library for identifying ligand binding activity. *Nature*. **354**, 82–84.

[74] Amadei, G. A.; Cho, C.-F.; Lewis, J. D.; Luyt, L.G. (2010) A fast, reproducible and low-cost method for sequence deconvolution of "on-bead" peptides via "on-target" maldi-TOF/TOF mass spectrometry. *J. Mass Spect.* **45**(3), 241-251.

[75] Zuckermann, R.N.; Kerr, J.M.; Siani, M.A.; Banville, S.C.; Santi, D.V. (1992) Identification of highest-affinity ligands by affinity selection from equimolar peptide mixtures generated by robotic synthesis. *Proc Natl Acad Sci USA*. **89**, 4505–4509.

[76] Pinilla, C.; Appel, J.R.; Blanc, P.; Houghten, R. A. (1992) Rapid identification of high affinity peptide ligands using positional scanning synthetic peptide combinatorial libraries. *Biotechniques*. **13**, 901–905.

[77] Balogh, L.; Polyak, A.; Mathe, D.; Kiraly, R.; Thurocy, J. (2008) Absorption, uptake and tissue affinity of high-molecular weight hyaluronan after oral administration in rats and dogs. *J. Agric. Food Chem.* **56**(22), 10582-10593.

[78] Coradini, D.; Zorzet, S.; Rossin, R.; Scarlata, I.; Pellizzaro, C.; Turrin, C.; Bello, M.; Cantoni, S.; Speranza, A.; Sava, G.; Mazzi, U.; Perbellini, A., (2004) Inhibition of hepatocellular carcinomas in vitro and hepatic metastases in vivo in mice by the histone deacetylase inhibitor HA-But. *Clin. Can. Res.* **10**(14), 4822-4830

[79] Udabage, L.; Brownlee, G. R.; Nilsson, S. K.; Brown, T. J., The over-expression of HAS2, Hyal-2 and CD44 is implicated in the invasiveness of breast cancer. *Experimental Cell Research* **2005,** 310, (1), 205-217.

[80] Day, A.J.; Prestwich, G. D. (2001) Hyaluronan binding protein; tying up the giant. *J. Biol. Chem.,* **227**(15), 4585-4588.

[81] Ziebell, M.R. and Prestwich G.D. (2004) Interactions of peptide mimics of hyaluronic acid with the receptor for hyaluronan mediated motility (RHAMM). *J. Comput. Aided Mol. Des.,* **18**, 597-614.

[82] Ziebell, M. R.; Zhao, Z.-G.; Luo, B.; Turley, E. A.; Prestwich, G. D. (2001) Peptides that mimic glycosaminoglycan: high-affinity ligands for hyaluronan binding domain. *Chem. Biol.,* **8**(11), 1081-1094.

[83] Wei, L; Banerjee, S.R., Levadala, M. K.; Babich, J.; Zubieta, J. (2006) Rhenium tricarbonyl complexes with ligands derived from arylpiperazines. *Inorg. Chem. Commun.,* **6**, 1099-1103.

[84] Deutsch, E; Libson, K; Vanderheyden, J-L.; Ketring A.R.; Maxon, H.R. (2009) The chemistry of rhenium and technetium as related to the use of isotopes of these elements in therapeutic and diagnostic nuclear medicine. *Nucl. Med. Biol.,* **13**, 465-477.

[85] Schibli, R.; La Bella, R.; Alberto, R.; Garcia-Garayoa, E.; Ortner, K.; Abram, U.; Schubinger, P.A. (2000) Influence of the denticity of ligand systems on the in vitro and in vivo behaviour of Tc-99m(I)-tricarbonyl complexes: A hint for the future functionalization of biomolecules. *Bioconj. Chem.,* **11**(3), 345-351.

[86] Richer, C.; Domergue, V.; Gervais, M.; Bruneval, P.; Giudicelli, J.F. (2000) Fluospheres for cardiovascular phenotyping genetically modified mice. *J. Cardiovasc. Pharmacol.,* **36**(3), 396-404.

[87] Banergee, S.R.; Babich, J. W.; Zubieta, J. (2006). A new bifunctional amoni acid chelator targeting the glucose transporter. *Inorganica Chimica Acta.,* **359**, 1603-1612.

[88] Kurz, P.; Spingler, B.; Fox, T.; Alberto, R. (2004) [TcI(CN)3(CO)3]2- and [ReI(CN)3(CO)3]2-: Case studies for the binding properties of CN- and CO. *Inorg. Chem.,* **43**(13), 3789-3791.

[89] Schibli, R.; Katti, K. V.; Volkert, W. A.; Barnes, C. L.. (1998) Novel coordination behavior of fac-[ReBr3(CO)3]2- with 1,3,5-triaza-7-phosphaadamantane (PTA). Systematic investigation on stepwise replacement of the halides by PTA ligand. Phase transfer studies and X-ray crystal structure of [NEt4][ReBr2((PTA)(CO)3], [ReBr(PTA)2(CO)3], and [Re(PTA)3(CO)3]PF6. *Inorg. Chem.,* **37**(20), 5306-5312.

[90] Wei, L.; Babich, J. W.; Ouellette, W.; Zubieta, J. (2006) Developing the {M(CO)3}+ core for fluorescence applications: rhenium tricarbonyl core complexes with benzimidazole, quinoline, and tryptophan derivatives. *J. Inorg. Chem.* **45**, 3057-3066.

[91] Chan, W. C.; White, P. D. (2000) *Fmoc Solid Phase Peptide Synthesis;* Chan, W. C., White, P. D.. Eds.; Oxford university Press: New York, pp 41-76.

[92] Kaiser, E.; Colescott, R. L.; Bossinger, C. D.; Cook, P. I. (1970) Color test for detection of free terminal amino groups in the solid phase synthesis of peptides. *Biochem.,* **34**, 595-598.

[93] Goldstein, L. S.; and Philp, A. V. (1999) The road less travelled: emerging principles of kinesin motor utilization. *Annu. Rev. Cell. Dev. Biol.* **15**, 141-183.

[94] Nogales, E. (2001) Structural insights into microtubule function. *Annu. Rev. Biomol. Struct.* **30**, 397-420

[95] Nogales, E.; Wolf, S. G.; and Downing, K.H. (1999) Structure of the alpha beta tubulin dimer by electron crystallography. *Nature.* **391**, 199-203.

[96] Sackett, D. L.; Bhattacharyya, B.; and Wolff, J. (1985) Tubulin subunit carboxyl termini determine polymerization efficiency. *J. Biol chem.* **260**, 43-45.

[97] Luduen R. F., Banerjee, A., and Khan, I. A. (1992) Tubulin structure and biochemistry. *Curr. Opin. Cell Biol.* **4,** 53–57

[98] Lowe, J.; Li, H.; Downing, K. H.; Nogales, E. (2001) Refined structure of αβ-tubulin at 3.5 Å resolution. *J. Mol. Biol.*, **313**(5), 1045-1057.

[99] Nogales, E. ; Wolf, S.G.; Downing, K. H. (1998) Structure of the alpha beta tubulin dimer by electron crystallography. *Nature,* **391**(6663), 199-203.

[100] Ponsting, H.; Little, M.; Khrauhs, E.; and Kempf, T. (1979) Carboxy-terminal amino acid sequence of α-tubulin form porcine brain. *Nature*, **282**, 423-424.

[101] Serano, L.; de la Torre, J.; Maccioni R. B.; and Avila, J. (1984) Controlled proteolysis of tubulin by subtilisin; Localization of the site for MAP2 interaction. *Biochemsitry*, **23**, 4675-4681.

[102] Littauer, U.Z.; Giveon, D.; Thierauf, M.; Ginzburg, I.; Ponstingl, H. (1986) Common and distinct tubulin binding sites for microtubule-associated protein. *Proc. Natl. Acad. Sci. USA,* **83**, 7162-7199.

[103] Chau, M. F.; Radeke, M. J.; de Ines, C.; Barasoain, I.; Kohlstaedt, L. A. (1998) The microtubule-associated protein Tau cross-links two distinct sites on each α and β tubulin monomer via separate domains. *Biochemistr,* **37**, 17692-17703.

[104] Cross, D.; Dominguez, J.; Maccioni, R. B. (1991) MAP-1 AND MAP-2 binding sites at the C-terminus of beta-tubulin. Studies with synthetic tubulin peptides. *Biochemistry,* **30**(17), 4362-4366.

[105] Walczak, C. E.; Vernos, I.; Mitchison, T. J.; Karsenti, E.; Heald, R. (1998) A model for the proposed roles of different microtubule-based motor proteins in establishing spindle bipolarity. *Curr. Biol.*, **8**, 903-913.

[106] Tucker, C.; and Goldstein, L. S. B. (1997) Probing the kinesin-microtuble interaction. *J. Biol. Chem.*, **272**(14), 9481-9488.

[107] Maxwell, C. A.; McCarthy, J.; Turley, E. A. (2008) Cell-surface and mitotic spindle Rhamm: moonlighting or dual oncogenic functions. *J. Cell Sci.*, **121**(7), 925-932.

[108] Hofmann, M.; Fieber, C.; Assmann, V.; Goettlicher, M.; Sleeman, J.; Plug, R.; Howells, N.; von Stein, O.; Ponta, H. Herrlich, P. (1998) Identification of IHABP, a 95 KDa intracellular hyaluronate binding protein. *J. Cell Sci.*, **111,** 1673-1684.

[109] Assmann, V.; Jenkinson, D.; Marshall, J.F.; and Hart, I.R. (1999) The intracellular hyaluronan receptor RHAMM/IHABP interacts with microtubules and actin filaments. *J. Cell. Sci.*, **112**, 3943-3954.

[110] Haddad, A. A.; and Turley, E. A. (2000) RHAMM protein interacts with the cytoskeleton. *Mol. Biol. Cell.,* **11**, 88a

[111] Maxwell, C.A.; and Pilarski L. M. (2000) Affinity of Rhamm isoforms for interphase and mitotic microtubules in suspension cells. *Mol. Biol. Cell.,* **11**, 200a

[112] Tolg, C.; Hamilton, S. J.; Morningstar, L.; Zhang, J.; Esguerra, K. V.; Telmer, P. G.; Luyt, L. G.; Harrison, R.; McCarthy, J. B.; Turley, E. A. (2010) RHAMM promotes interphase microtubule instability and mitotic spindle integrity trough MEK1/ERK1, 2 activity. *J Biol. Chem.*, **285**, 26461-26474.

[113] Larkin, M. A.; Blackshields, G.; Brown, N. P.; Chenna, R.; McGettigan, P. A.; McWilliam, H.; Valentin, F.; Wallace, I. M.; Wilm, A.; Lopez, R.; Thompson, J. D.; Gibson, T. J.; Higgins, D. G. (2007) Clustal W and Clustal X version 2.0. *Bioinformatics*, **23**(21), 2947-2948.

[114] Tolg, C.; Hamilton, S. J.; Morningstar, L.; Zhang, J.; Esguerra, K. V.; Telmer, P. G.; Luyt, L. G.; Harrison, R.; McCarthy, J. B.; Turley, E. A. (2010) RHAMM promotes interphase microtubule instability and mitotic spindle integrity trough MEK1/ERK1, 2 activity. *J Biol. Chem.*, **285**, 26461-26474.

[115] Maxwell, C. A.; Keats, J. J.; Crainie, M.; Sun, X.; Yen, T. Shibuya, E.; Hendzel, M. Chan, G.; and Pilarski, L. M. (2003) RHAMM is a centrosomal protein that interacts with dynein and maintains spindle pole stability. *Mol. Biol. Cell.,* **14**, 2262-2276.

[116] Popodi, E. M.; Hoyle, H. D.; Turner, R. F.; Raff, E. C. (2008) Cooperativity between the β-tubulin carboxy tail and the body of the molecule is required for microtubule function. *Cell Motil. Cytoskeleton,* **65**(12), 955-963.

[117] Nielson, M. G.; Gadagkar, S. R.; Gutzwiller, L. (2010) Tubulin evolution in insects: gene duplication and subfunctionalization provide specialized isoforms in a functionally constrained gene family. *BMC Evol. Biol.,* **10,** 113.

[118] Esguerra, K.V.; Zhang, J.; Cho, C.-F.; Lewis, J.; Turley, E.; Luyt, L. (2010) Tubulin derived peptides as optical imaging probes targeting RHAMM. *J. Nucl. Med,.* **51**(2), 394a

[119] Paschal, B.M.; Obar, R.A.; Vallee, R. B. (1989) Interaction of brain cytoplasmic dynein and MAP2 with a common sequence at the C terminus of tubulin. *Nature*, **30** (6249), 569-572.

[120] Zhang, L; Furst, EM; Kiick, KL. (2006) Manipulation of hydrogelassembly and growth factor delivery via the use of peptide–polysaccharide interactions. *J. Control Release*, **114**, 130–42.

[121] Turley, E. A.; Noble, P. W.; Bourguignon, L. Y. W. (2002) Signaling properties of hyaluronan receptors. *J. Biol Chem.*, **277**(7), 4589-4592.

[122] Schibli, R.; La Bella, R.; Alberto, R.; Garcia-Garayoa, E.; Ortner, K.; Abram, U.; Schubiger, P. A. Influence of the denticity of ligand systems on the in vitro and in vivo behavior of 99mTc-tricarbonyl complexes: a hint for the future functionalization of biomolecules. *Bioconjugate Chem.*, 2000, **11**, 345–351.

[123] Alves, S; Paulo, A.; Correia, J. D. G.; Gano, J; Smith, C. J.; Santos, I. (2005) Pyrazolyl derivatives as bifunctional chelators for labeling tumor-seeking peptides with the fac-[M(CO)3]+ moiety (M = 99mTc, Re): synthesis, characterization and biological behavior. *Bioconj. Chem.*, **16**, 438–449.

[124] Maria, L.; Cunha, S.; Videira, M.; Gano, L. Paulo, A.; Santos, I. C.; Santos, I. (2005) Rhenium and technetium tricarbonyl complexes anchored by pyrazoles-based tripods: novel lead structures for the design of myocardial imaging agents. *Dalton Trans.*, **28**, 3010-3019.

[125] Banerjee, S. R.; Schaffer, P.; Babich, J. W.; Valliant, J. F.; Zubieta, J. (2005) Design and synthesis of site directed maleimide bifunctional chelators for technetium and rhenium. *Dalton Trans.*, **24**, 3886-3897.

[126] Stephenson, K. A.; Banerjee, S. R.; Besanger, T.; Sogbein, O. O.; Levadala, M. K.; Mcfarlane, N.; Lemon, J. A.; Boreham, D. R.; Maresca, K. P.; Brennan, J. D.; Babich, J. W.; Zubieta, J.; Valliant, J. F. (2004) Bridging the gap between in vitro and in vivo imaging; isostrucutural Re and 99mTc complexes for correlating fluorescence and radioimaging studies. *J. Am. Chem. Soc.*, **126**(28), 8598-8599.

[127] Roderick, W. R.; Nordeew, C. W.; Von Esch, A. M.; Appell, R. N. (1972) Bisbenzimidazoles. Potential inhibitors of rhinoviruses. *J Med. Chem.* **15**, 655.

[128] Weisblum, B.; Haenssler, E. (1974) Fluorometric properties of bibenzimidazole derivative Hoeschst 33258, a fluorescent probe specific for at concentration in chromosomal DNA. *Chromosoma.* **46**, 255-260.

[129] Fieselmann, B. F.; Hendrickson, D. N.; Stuckey, G. D. (1978) Synthesis, electron paramagnetic resonance, and magnetic studies of binuclear bis(.eta.5-cyclopentadienyl)titatium(III) compounds with bridging pyrazolate, biimidazolate, and bibenzimidazole anions. *Inorg. Chem.* **17**, 2078-2084.

[130] Boinnard, D.; Cassoux, P.; Petrouleas, V.; Savariault, J.-M.; Tuchageus, J.-P. (1990) Iron(II) complexes of 2,2'-biimidazole and 2,2'-bibenzimidazole as models of the photosynthetic mononuclear non-heme ferrous sites. Synthesis, molecular and crystal structure, and Moessbauer and magnetic studies. *Inorg. Chem.* **29**, 4114-4122.

[131] Mueller, E.; Bernardinelli, G.; Reedijk, J. (1995) 4,4'Bis(2-picolinimino)-2,2'-bibenzimidazoles: a new class of dinucleating ligands which allow for a tuning of the metal-metal distance. Structures and properties of a dicopper(II) complex and of two oxygenation products of a dicopper(I) complex; a tentative coordination chemical modeling of hemocyanon. *Inorg Chem.*, **34**, 5979-6988.

[132] Buckley, A.; Stuetz, D. E.; Serad, G. A. In *Encyclopedia of Polymer Science and Engineering*; Kroschwitz, J. I., Ed.; Wiley: New York, 1988; Vol. 11, pp 572-601.

[133] Machura, B.; Switlicka, A.; Nawrot, I.; Michalik, K. (2010) tricarbonyl rhenium complex of 2,2'-bis(4,5-dimethylimidazole) – synthesis, spectroscopic characterization, x-ray structure and DFT calculations. *Inorg. Chem. Commun.*, **13**, 1317-1320.

[134] Mukhopadhyay, C.; Ghosh, S. Butcher, R. J. (2010) An efficient and versatile synthesis of 2,2'-(alkanediyl)-bis-1H-benzimidazoles employing aqueous fluoroboric acid as catalyst: density functional theory calculations and fluorescence studies. *ARKIVOC*, **iv**, 75-96.

[135] Benkstein, K. D.; Hupp, J. T.; Stern, C. L. (2000) Luminescent mesoporous molecular materials based on neutral tetrametallic rectangles. *Angew. Chem.*, **112**, 3013.

[136] Dinolfo, P. H.; Williams, M. E.; Charlotte, L. S.; Hupp, J. T. (2004) Rhenium-based molecular rectangles as frameworks for ligand-centered mixed valency and optical electron transfers. *J. Am. Chem. Soc.* **126**(40), 12989-13001.

[137] Deschamps, P.; Kulkarni, P. P.; Sarkar, Bibudhendra, S. (2003) The crystal structure of a novel copper(II) complex with asymmetric ligand derived from L-histidine. *Inorg. Chem.* **42**(23), 7366-7368.

[138] Osz, K.; Varnagy, K. Suli-Varha, Sanna, Daniele, S. Micera, G. Sovago, I. (2003) Transition metal complexes of bis(imidazole-2-yl) derivatives of dipeptides. J. *Inorg. Biochem.* **98**, 24.

[139] Hegg, E. L.; Que Jr., L. (1997) The 2-his-1-carboxylate facial triad, an emerging structural motif in mononuclear non-heme iron (II) enzymes. *Eur. J. Biochem.*, **250**, 625-629.

[140] Leirer, M.; Knör, G.;Vogler, A. (1999) Electronic spectra of 1,2-diiminetricarbonylrhenium (I) chloride complexes with imidazole derivatives as ligands. *Inorg. Chim. Acta.* **288**, 150.

[141] Rau, S.; Görls, H. (2004) Solid state structure of a rhenium bibenzimidazole complex. *J. Coord. Chem.* **57**(17) 1587-1590.

[142] Fortin, S.; Beauchamn, A. L. (2001) Preparations, characterization and structures of (biimidazole) dihalobis (triphenylphoshone) rhenium(III) salts: strong ion-pairing and acid-base properties. *Inorg. Chem.* **40**, 105-112.

[143] Baril-Robert, F. Beauchamp, A. L. (2004) Preparation and crystal structure of (2,2'-bibenzimidazole) dihalobis (triphenylphosphine) rhenium (III) halides. *Polyhedron* **23**, 1139-1144.

[144] Miranda, F. S.; Menezes, F. G.; Vicente, J.; Bortoluzzi, A. J.; Zucco, C.; Neves, A.; Goncalves, N. S. Bis-(1H-benzimidazol-2-yl)-methanone: new preparation, crystal structure, vibrational spectroscopy and DFT calculations. *J. Mol. Struct.,* **938**, 1-9

[145] Pozharskii, A. F.; Simonov, A. M. (1963)Direct N-arylation of five-membered terocycles I. *J. Gen. Chem. USSR,* **33**, 172.

[146] Bruijnincx, P. C. A.; Lutz, M.; Spek, A. L.;van Faasen, E. L.; Weckhuysen, B. M.; van Koten, G.; Klein, Gebbink, R. J. M. (2005) Bis(1-methylimidazol-2-yl)propionates and bis(1-methylbenzimidazol-2-yl)-propionates: a new family of biomimetics N,N,O ligands – synthesis, structures and Cu(II) coordination complexes. *Eur. J. Inorg. Chem.*, 779-787.

[147] Hancock, R. D. (1989) Molecular mechanics calculations as a tool in coordination chemistry. *Prog. Inorg. Chem.*, **37**, 187-291.

[148] Hancock, R. D.; Martell, A. E. (1989). Ligand design for selective complexation of metal ions in aqueous solution. *Chem Rev.*, **89**, 1975.

[149] Hancock, R. D. (1992) Chelate ring size and metal ion selection. The basis of selectivity for metal ions in open-chain ligands and macrocycles. *J. Chem. Educ.* **69**, 615.